

Numerical Studies of Disordered Tight-Binding Hamiltonians

R.T. Scalettar

Physics Department, University of California, Davis, CA 95616

Abstract. These are notes used for a set of lectures delivered at the Vietri summer school on Condensed Matter Physics in Fall 2006. They concern the general problem of the interplay of interactions and disorder in two dimensional electronic systems, as realized in the specific context of Quantum Monte Carlo simulations of the Anderson-Hubbard Hamiltonian. I wish to thank the organizers of this school for their hospitality during my visit, and their work in general in providing this educational opportunity for students over the years. It is a pleasure also to acknowledge the collaborators together with whom I have learned much of the physics and numerics presented in these notes: Zhaojun Bai, Andrew Baldwin, George Batrouni, Karim Bouadim, Wenbin Chen, Peter Denteneer, Fred Hébert, Norman Paris, Matt Schram, Nandini Trivedi, Martin Ulmke, Ichitaro Yamazaki and Gergely Zimanyi. This work was supported by the National Science Foundation (NSF-DMR-0312261 and NSF-ITR-0313390), and China Special Funds for Major State Basic Research Projects under contract 2005CB321700.

CONTENTS

| | |
|---|-----------|
| I. Introduction | 2 |
| A. Contents of these notes | 2 |
| B. Brief Overview of Physics | 3 |
| C. Guide to Exercises | 4 |
| II. The Translationally Invariant Hubbard model | 5 |
| A. Noninteracting Limit ($U = 0$) | 6 |
| B. Strong Coupling Limit ($t=0$) | 8 |
| C. Green's Functions for the Hubbard Hamiltonian | 11 |
| D. Exact Diagonalization | 14 |
| E. Mean Field Theory | 18 |
| III. Disorder in the Absence of Interactions | 24 |
| A. The Anderson Transition | 24 |
| B. A Digression into Non-Hermiticity: The Hatano-Nelson Model | 25 |
| IV. Prescription for Determinant Quantum Monte Carlo | 27 |
| A. Basic Formalism | 27 |
| B. Results: Local Moment, Spin Correlation, and Specific Heat | 29 |
| V. DQMC for the Anderson-Hubbard Hamiltonian | 30 |
| A. Interaction driven Anderson Insulator to Metal Transition | 30 |
| B. Effect of Zeeman Field | 34 |
| C. The Role of Particle-Hole Symmetry | 38 |
| D. Interaction driven Band Insulator to Metal Transition | 42 |
| VI. Conclusions | 46 |
| Appendix A: Creation and Destruction Operators and the Hubbard Hamiltonian | 47 |

| | |
|--|-----------|
| Appendix B: Formal Foundation of Classical Monte Carlo | 50 |
| Why Monte Carlo Works: Detailed Balance, Transition Probabilities and All That | 50 |
| Relation to Molecular Dynamics and the Langevin Equation | 54 |
| Error Analysis in Monte Carlo | 55 |
| Appendix C: Determinant Quantum Monte Carlo in Detail | 58 |
| A Useful Analogy: Multidimensional Gaussian Integration | 58 |
| Basic Formalism of Determinant QMC | 59 |
| Subtleties and “Tricks of the Trade” | 60 |
| What Determinant QMC Simulations Can Do and Concluding Remarks | 61 |
| Appendix D: Supplementary Material | 61 |
| Particle-Hole Symmetry | 61 |
| Relation between the Attractive and Repulsive Hubbard Models | 62 |
| Alternates to Determinant QMC | 63 |
| Tutorial One | 63 |
| Tutorial One Solutions | 64 |
| Tutorial Two | 65 |
| Tutorial Two Solutions | 65 |
| Tutorial Three | 66 |

I. INTRODUCTION

A. Contents of these notes

These notes discuss the physics of electrons which move in a disordered potential and which also interact with each other. This is an enormous field, one of the most interesting in condensed matter physics, both for theory and experiment. In order to make it tractable, the focus will be on a specific model- the Hubbard Hamiltonian with random bond and site energies, although a brief foray into an interesting case when the hopping is non-Hermitian will be taken. A particular computational method, “determinant Quantum Monte Carlo” [1], will be described in detail and will provide the bulk of the non-trivial numerical results.

Section II. begins by examining the physics of the Hubbard Hamiltonian in the limit of no disorder, and presents its strong, weak, and mean field treatments. The exact diagonalization method is also described. Section III. will summarize some of the central features of the Anderson localization transition, that is, the case with disorder and no interactions. A generalization, the Hatano-Nelson model, in which the left and right hopping amplitudes are unequal, and hence the Hamiltonian is not Hermitian provides an interesting way to look at the localization transition. Section IV. outlines the determinant Quantum Monte Carlo (DQMC) method. The emphasis will be on presenting the ‘pseudocode’ for DQMC, relegating a more complete derivation to Appendix C. Two further appendices give additional background: Appendix A briefly reviews the formalism of second quantization, for those students for whom it is not so familiar. Quantum Monte Carlo involves an understanding of classical monte carlo, a topic which is summarized in Appendix B.

After having considered the effects of randomness and interactions separately, and introduced DQMC, Section V. puts things together. Results of simulations of the “Anderson-Hubbard Hamiltonian”, including evidence that, in two dimensions, interactions can drive a state that is localized by randomness into a metallic phase form the first topic. A Zeeman field, which spin polarizes the electrons and thereby reduces their effective interaction, can return the system to insulating behavior. Evidence is presented that particle-hole symmetry, and whether the disorder directly competes with the formation of magnetic moments, plays a crucial role in these transitions. Appendix D contains a review of aspects of this particle-hole mapping. This section concludes with a discussion of the band insulator to metal

transition in which it is shown that an insulating phase caused by a periodic potential which doubles the unit cell can, like a disorder-induced Anderson insulator, also be made metallic by interactions.

Since this is a paper prepared for a summer school, these notes are interspersed with exercises. Some are rather simple- a few lines of analytic derivation might serve to complete them. Others go down the road to being small research topics, and involve writing a nontrivial program. The lecture notes contain substantially more material than can be covered in a week, especially when the Exercises are attempted. They will provide additional avenues for exploration after this summer school is completed, or topics for the more advanced student who wishes to proceed a bit further or more rapidly.

This introduction closes with a very brief review of the history of some of these problems. For details concerning the two dimensional MIT and the Anderson-Hubbard Hamiltonian, the student is encouraged to look at the various reviews of the field [2, 3]. An exceptionally nice introduction to the correlated electron problem and to the Hubbard model, is contained in the book by Fazekas[4]. Further summaries of DQMC may be found in a variety of articles and summer school notes, including [5, 6, 7, 8].

B. Brief Overview of Physics

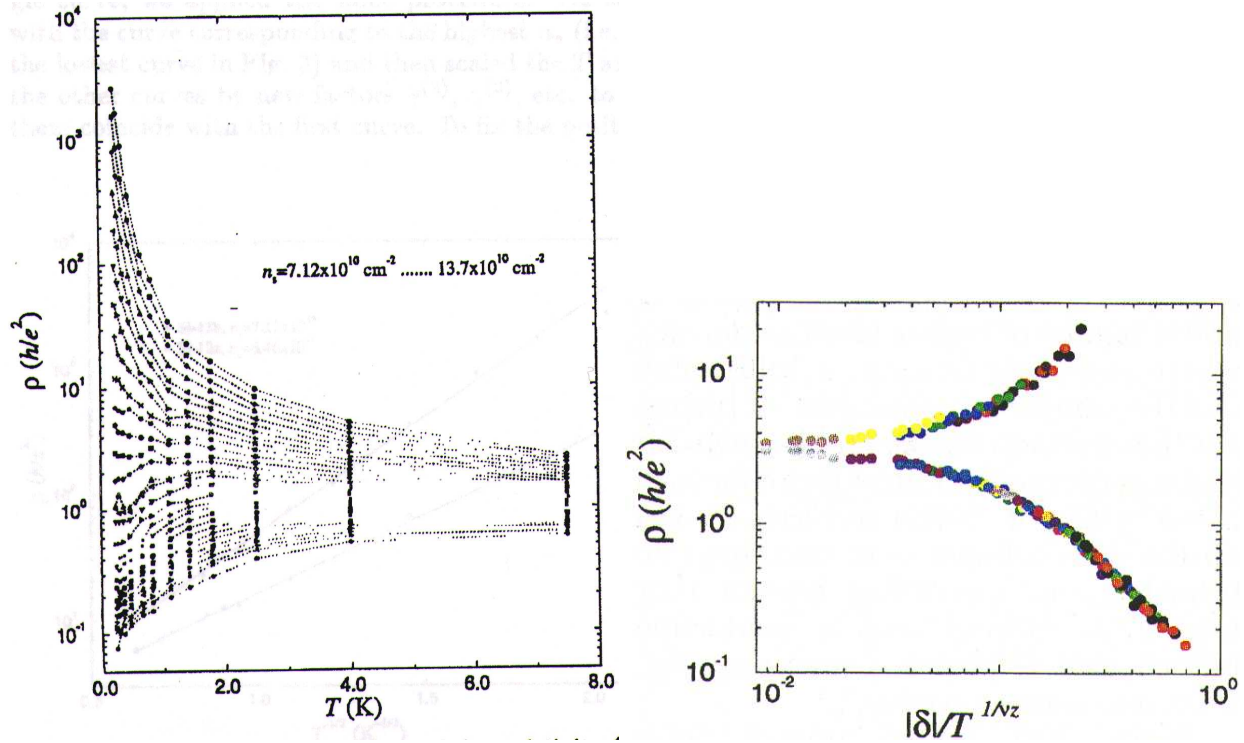
When electrons are confined to two dimensions in a disordered environment, common understanding until relatively recently was that the electronic states would always be localized and the system would therefore be an insulator. This idea is based on the scaling theory of localization [9] for non-interacting electrons and corroborated by subsequent studies using renormalization group (RG) methods [10, 11]. The scaling theory highlights the importance of the number of spatial dimensions and demonstrates that while in three dimensions for non-interacting electrons there exists a transition from a metal to an Anderson insulator upon increasing the amount of disorder, a similar metal-insulator transition (MIT) is not possible in two dimensions.

The inclusion of interactions into the theory has been problematic, certainly when both disorder and interactions are strong and perturbative approaches break down. Following the scaling theory the effect of weak interactions in the presence of weak disorder was studied by diagrammatic techniques and found to increase the tendency to localize [12]. Subsequent perturbative RG calculations, including both interactions and disorder, found indications of metallic behavior, but also, for the case without a magnetic field or magnetic impurities, found runaway flows to strong coupling outside the controlled perturbative regime, and hence were not conclusive [13, 14, 15]. The results of such approaches therefore did not change the widely held opinion that, in the absence of a magnetic field coupling to orbital motion, or magnetic impurities, the MIT does not occur in two dimensions.

In the middle of the 1990's, the situation changed dramatically with transport experiments on effectively 2D electron systems in silicon MOSFETs which provided surprising evidence that a MIT can occur in 2D [16, 17, 18]. In these experiments the temperature dependence of the resistivity ρ changes from that typical of an insulator (increase of ρ upon lowering T) at lower density to that typical of a conductor (decrease of ρ upon lowering T) as the density is increased above a critical value. (See Fig. 1, left panel.) The fact that the data can be scaled onto two curves (one for the metal, one for the insulator) is seen as evidence for a quantum phase transition with carrier density n as the tuning parameter. (See Fig. 1, right panel.) The possibility of such a transition has stimulated a large number of further experimental [19, 20, 21, 22] and also theoretical investigations [23, 24, 25, 26], including proposals that a superconducting state is involved [27, 28]. Explanations in terms of trapping of electrons at impurities, i.e. not requiring a quantum phase transition have also been put forward [29, 30].

A common thread in many of the different explanations of the 2D MIT is the importance of electron-electron interactions. Indeed, one of the most central questions motivated by the experiments is whether correlations can enhance the conductivity of a 2D disordered electron system, and possibly lead to a conducting phase [31, 32]. In order to address this issue theoretically, one approach is to identify an appropriate model and, then, work out its properties. This will be the strategy here.

To this end, these lectures will begin by providing some background on the "Anderson-Hubbard" Hamiltonian, which is one of the most simple models that incorporates both disorder and interactions. Several methods are discussed which help develop an initial insight into the physics of this Hamiltonian, but the focus will be on Determinant Quantum Monte Carlo (DQMC). The notes conclude with a detailed description of the MIT studied with this model and method. DQMC has previously been applied extensively to the Hubbard model without disorder. [1, 6, 33, 34, 35, 36] While the strengths of DQMC in addressing this problem are considerable: disorder and interaction can be varied in a controlled (ie exact) way and strong interaction is treatable, it is important also to acknowledge its serious limitations:



Source: S.V. Kravchenko et al [17]

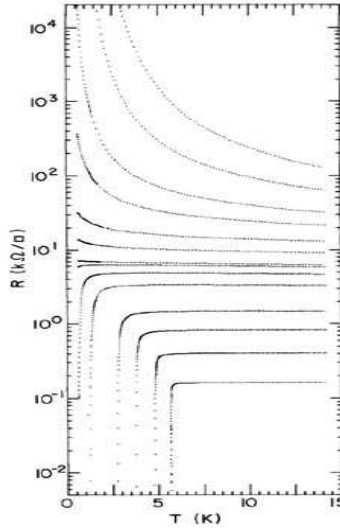
FIGURE 1. Left: Resistivity ρ versus temperature T for samples with a varying density of electrons n . As the density increases, the system undergoes a transition from insulating to metallic. Right: Similar data for a transition tuned by disorder strength δ . Horizontal axis is an appropriately scaled form. A large family of curves collapses to just two trajectories, one for metallic disorder strengths, and one for insulating ones, suggesting a quantum phase transition.

the size of the lattice is finite (a few hundred sites) and low temperatures are often not accessible due to the sign problem.

There are many analogies between the MIT and the superconducting-insulator transition (SIT). As for the MIT, one of the most interesting issues again focuses on the behavior in two dimensions. A transition from superconductor to insulator is observed as the degree of disorder or the magnetic field is changed, but the fundamental question is not whether a superconducting phase can exist (it surely can!), but rather why the value of resistance at the transition appears to take on a universal value. Interestingly, the connection between the MIT and SIT can be brought out in the context of the Hubbard Hamiltonian through a particle-hole transformation which changes the sign of the interaction between the electrons from repulsive to attractive, since the latter case allows for superconducting phases. The interested reader can examine reviews such as [37, 38, 39, 40, 41, 42] or, for applications of DQMC, to [43, 44].

C. Guide to Exercises

These notes attempt to provide interesting problems for students of different levels of familiarity with numerical work and with the Hubbard model. The most advanced/ambitious students might wish to construct a determinant Quantum Monte Carlo code. Though not phrased in the form of exercises, Section IV. writes down all the required equations and shows some simple results. Appendix C provides a derivation. It is, however, unlikely such a task could be fully accomplished in the evening sessions of this summer school. A less time consuming objective for a student who wants a 'research' code is to try a mean field or exact diagonalization program. These are discussed in Section II., and also in the material presented by other lecturers. The exercises provide many options to those wishing to develop further their knowledge of the material, without writing a major code. Here is a rough guide to where the different problems can be found.



Source: Haviland et al, [38]

FIGURE 2. A superconductor to insulator transition is well established in two dimensional thin films. Here results for the resistance $R(T)$ of Pb films of varying thickness are shown. The transition can also be controlled with degree of disorder, and magnetic field.

Section II: Exercises extending aspects of the weak ($U = 0$) and strong ($t = 0$) coupling limits of the Hubbard Hamiltonian, for example, determining the tight binding dispersion relations and density of states of the periodic Anderson model, the three band Emery model, or the Hubbard model on triangular and honeycomb lattices.

Section III: Exercises involving the Hatano-Nelson model.

Appendix A: Exercises involving the manipulation of creation and destruction operators and the Hubbard Hamiltonian.

Appendix B: Exercises involving the formal foundations of *classical* monte carlo (detailed balance, the Metropolis algorithm, the relation of monte carlo to molecular dynamics and the Langevin equation, etc).

Appendix D: Exercises involving particle-hole symmetry and the relation between the attractive and repulsive Hubbard Hamiltonians.

Tutorials: The tutorials contain tasks involving using the DQMC code provided in the summer school.

II. THE TRANSLATIONALLY INVARIANT HUBBARD MODEL

The Hubbard Hamiltonian, in the absence of disorder, is,

$$H = -t \sum_{\langle \mathbf{j}, \mathbf{l} \rangle \sigma} c_{\mathbf{j}\sigma}^\dagger c_{\mathbf{l}\sigma} + U \sum_{\mathbf{j}} n_{\mathbf{j}\uparrow} n_{\mathbf{j}\downarrow} - \mu \sum_{\mathbf{j}} (n_{\mathbf{j}\uparrow} + n_{\mathbf{j}\downarrow}). \quad (1)$$

Here $c_{\mathbf{j}\sigma}^\dagger$ ($c_{\mathbf{j}\sigma}$) are creation(destruction) operators for electrons on site \mathbf{j} with spin σ . (Their properties are reviewed in Appendix A.) The first term of H is the kinetic energy since it describes the destruction of an electron of spin σ on site \mathbf{l} and its creation on site \mathbf{j} (or *vice-versa*). The symbol $\langle \mathbf{j}, \mathbf{l} \rangle$ indicates that hopping is allowed only between specified pairs of sites (usually the near neighbors). These notes mostly concern square lattices in two dimensions. The second term is the interaction energy: a doubly occupied site ($n_{\mathbf{j}\uparrow} = n_{\mathbf{j}\downarrow} = 1$) adds an energy U to the state. The final term is a chemical potential which controls the filling. The situation where the filling is one electron per site is referred to as ‘half-filling,’ since the lattice contains half as many electrons as the maximum number (two per site). The value $\mu = U/2$ results in half-filling for any choice of hopping t or temperature T , if the lattice is bipartite and the hopping only connects sites on the two independent sublattices. Studies of the Hubbard model often focus on the half-filled case because it exhibits many interesting phenomena (Mott insulating behavior, antiferromagnetic order, etc.)

The Hubbard Hamiltonian offers a way to get qualitative insight into how the interactions between electrons can give rise to insulating, magnetic, and even novel superconducting effects in a solid. It was written down in the early

1960's and initially applied to understanding the behavior of the transition metal monoxides like FeO, NiO, CoO. These compounds are antiferromagnetic insulators, but are predicted to be metallic by "electronic structure" methods which treat strong interactions less carefully.

Over the intervening years, the Hubbard model has been applied to the understanding of many systems, from 'heavy fermion' systems in the 1980's, to high temperature superconductors in the 1990's. In the last several years the 'boson-Hubbard' and fermion Hubbard models have been invoked to study the physics of ultra-cold atoms. Indeed, it is an amazing feature of the Hamiltonian that, despite its simplicity, it exhibits behavior relevant to many of the most subtle and beautiful properties of solid state (and now atomic) systems.

The Hubbard model has been studied by the full range of analytic techniques developed by condensed matter theorists, from simple mean field approaches to field theoretic methods employing Feynman diagrams, expansions in the degeneracy of the number of 'flavors' (spin, orbital angular momentum), the Bethe Ansatz, etc. It has also been extensively attacked with numerical methods like diagonalization and variational and path-integral Quantum Monte Carlo (QMC). In these lectures, the main tool will be determinant QMC, but the non-interacting and zero hopping limits, and static mean field theory, will be described to develop some simple pictures of the physics.

A. Noninteracting Limit ($U = 0$)

In Appendix A, two, equivalent, ways to solve the Hubbard Hamiltonian at $U = 0$ are presented. The first is based on explicitly constructing the matrix for \hat{H} in the single particle sector. The second considers a change to momentum creation and destruction operators,

$$c_{\mathbf{k}\sigma}^\dagger = \frac{1}{\sqrt{N}} \sum_{\mathbf{l}} e^{i\mathbf{k}\cdot\mathbf{l}} c_{\mathbf{l}\sigma}^\dagger. \quad (2)$$

Appendix A provides many details concerning this change of basis such as the preservation of the anticommutation relations etc. The key result is that the kinetic energy term in the Hamiltonian can be rewritten as

$$H = \sum_{\mathbf{k}\sigma} (\epsilon_{\mathbf{k}} - \mu) c_{\mathbf{k}\sigma}^\dagger c_{\mathbf{k}\sigma} \quad (3)$$

where $\epsilon_{\mathbf{k}}$ depends on the specific lattice geometry, as do the discrete allowed values of the momentum \mathbf{k} . For a one dimensional lattice of length N with near neighbor hopping, $\epsilon_k = -2t \cos k$ and $k = k_n = 2\pi n/N$ with $n = 1, 2, 3, \dots, N$. This choice of momenta reflects the use of periodic boundary conditions, which minimize finite size effects, an important consideration in numerical work which tends to be on lattices of limited size. The use of momentum space in Eq. 3 provides a much more simple representation than the original real-space expression of Eq. 1 because it is diagonal. That is, the Hamiltonian only counts the number of electrons in each momentum state without converting electrons from one momentum to another. A useful analogy is of course with normal modes in classical physics which can be excited without setting other modes into motion. Just as the normal mode construction in classical physics is possible only for quadratic potential energies, the diagonalization of a tight binding Hamiltonian can be done only when it is quadratic in the fermion creation and destruction operators.

Because the case of the two dimensional square lattice is of interest physically for the cuprate superconductors, and because it forms the bulk of the applications discussed in Section V., it is useful to review a few of its properties. The dispersion relation is $\epsilon_{\mathbf{k}} = -2t (\cos k_x + \cos k_y)$. This dispersion relation has a number of interesting and important features. First, its Fermi surface, ie the contours of constant energy, is 'nested' at half-filling. That is, a particular wave-vector, $\mathbf{k} = (\pi, \pi)$ connects extended lengths of the Fermi surface. See Fig. 3. A number of response functions, for example the non-interacting magnetic susceptibility $\chi^0(\mathbf{q})$, involve energy denominators of the form $\epsilon_{\mathbf{k}+\mathbf{q}} - \epsilon_{\mathbf{k}}$ and hence become large at (π, π) when nesting occurs.

A second interesting feature of the square lattice dispersion is that its density of states,

$$N(E) = \frac{1}{N} \sum_{\mathbf{k}} \delta(E - \epsilon_{\mathbf{k}}). \quad (4)$$

is singular at half-filling, $E = 0$. Possible implications of both nesting and van-Hove singularities have been discussed in the context of theories of high temperature superconductivity.

The average energy of the $U = 0$ Hubbard model is,

$$\langle E \rangle(T) = \frac{1}{N} \sum_{\mathbf{k}} \epsilon_{\mathbf{k}} (1 + e^{+\beta(\epsilon_{\mathbf{k}} - \mu)})^{-1}. \quad (5)$$

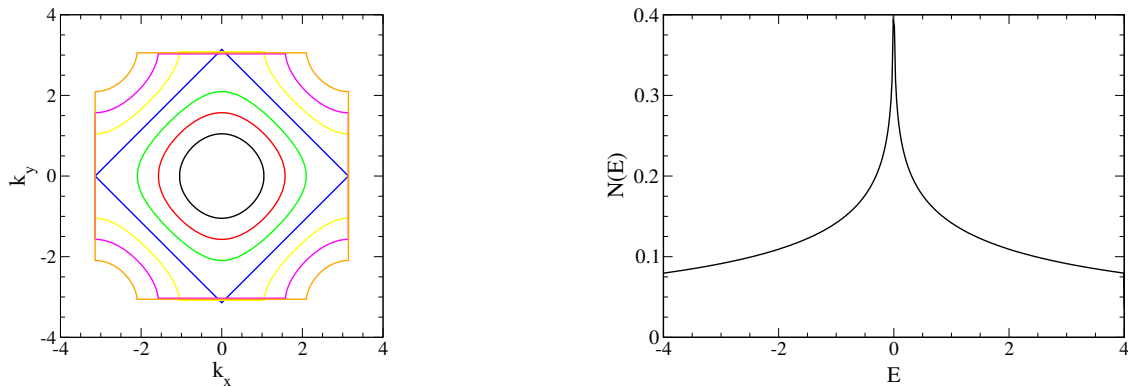


FIGURE 3. Left: Surfaces of constant energy E for the square lattice dispersion relation. Note that for $E = 0$ the topology is a rotated square and that $\epsilon_{\mathbf{k}+(\pi,\pi)} = \epsilon_{\mathbf{k}}$ for points \mathbf{k} on the surface. Right: The density of states. Note the divergence ('van Hove singularity') at $E = 0$.

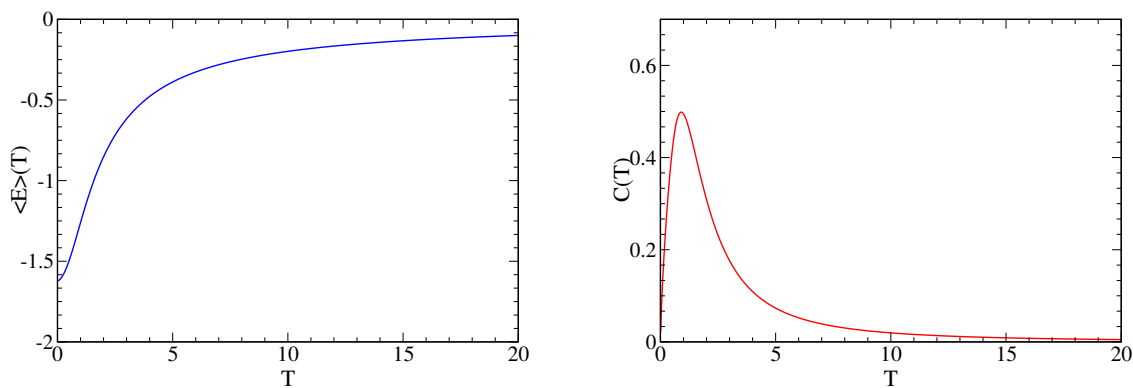


FIGURE 4. Left: Energy $\langle E \rangle(T)$ of the square lattice Hubbard Hamiltonian with $t = 1$, $U = 0$, and density $\rho = 1$ (half-filling). Right: Specific heat $C(T)$.

Fig. 4 shows the energy and specific heat, $\langle E \rangle(T)$ and $C(T) = d\langle E \rangle/dT$, as functions of temperature. As expected, $C(T)$ has a peak at a temperature T set by the hopping t . The following exercises explore several refinements of the $U = 0$ Hubbard Hamiltonian.

Exercise 1: Consider the one-dimensional Hubbard Hamiltonian with a staggered site energy $V = A \sum_l (-1)^l n_l$. Solve the $U = 0$ limit by going to momentum space. Show that you get two energy bands separated by a gap.

Exercise 2: Compute (numerically) the density of states $N(E)$ of the Hubbard model on a two dimensional honeycomb lattice. You will need to determine the dispersion relation and how the periodic boundary conditions restrict the allowed \mathbf{k} values. You should find that $N(E)$ vanishes linearly at $E = 0$. The system is said to be a *semi-metal* there. Appendix A contains exercises which explore the dispersion relation and density of states for a number of other tight binding Hamiltonians.

Exercise 3: Compute (numerically) the density of states $N(E)$ of the Hubbard model on a two dimensional triangular lattice. Again, you will need to determine the dispersion relation and how the periodic boundary conditions restrict the allowed \mathbf{k} values. Unlike the preceding cases, you will find that $N(E) \neq N(-E)$. This is a consequence of the fact that the model is not ‘‘particle-hole’’ symmetric on a triangular lattice. This will be discussed further in Sections V.C. and

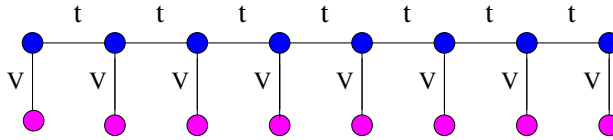


FIGURE 5. Lattice connections of a one-dimensional periodic Anderson model. Sites of the top ('conduction') chain are connected to one another by hopping parameter t . Sites of the lower ('localized') chain are not connected to each other, but hybridize with a hopping parameter V with the sites in the top chain.

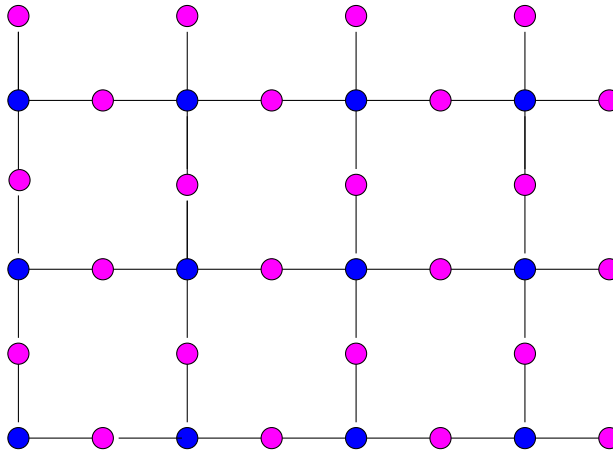


FIGURE 6. Lattice connections of a three band Emery model of the CuO_2 sheets of the cuprate superconductors. The Cu atoms lie in a square array with intervening O atoms. Pairs of Cu and O atoms are connected by hopping t . Sometimes an additional hopping t' between oxygen atoms is also included. The O sites are also usually given a site energy ϵ_{pd} relative to the Cu sites.

Appendix D below.

Exercise 4: Almost as widely studied as the Hubbard Hamiltonian is the 'Periodic Anderson Model' (PAM). It consists first of a set of 'conduction' sites (orbitals) whose near neighbors are connected with hopping ' t '. These might be in a one-d chain, or a two-d square lattice arrangement for example. A second set of 'localized' sites (orbitals) are disconnected from each other but hybridize with their conduction partners with amplitude ' V ', as illustrated in Fig. 5. Compute $E(k)$ and $N(E)$ for this model, in $d = 1$. Show there is a band gap when $V \neq 0$. If one adds a Hubbard U on the localized orbitals one gets the Periodic Anderson model.

Exercise 5: A three-band Hubbard model introduced by Emery and widely studied for high temperature superconductivity has the geometry shown in Fig. 6. One set of atoms forms a square array while a second set, with higher on-site energy, sits at the midpoints of the bonds between them. Compute $E(k)$ and $N(E)$ for this model.

B. Strong Coupling Limit ($t=0$)

Having looked at some of features of the noninteracting Hubbard Hamiltonian in various geometries, a first insight into the role of interactions is obtained by considering a single site. That is, by setting $t = 0$ in the Hamiltonian. This situation is easily solved. There are four possibilities corresponding to the site being empty, having a single electron (either spin up or spin down) or being doubly occupied. Each of the states $|0\rangle, |\uparrow\rangle, |\downarrow\rangle, |\uparrow\downarrow\rangle$ is an eigenstate of H with eigenvalues $0, -\mu, -\mu, U - 2\mu$ respectively. The partition function is

$$Z = \sum_{\alpha} \langle \alpha | e^{-\beta H} | \alpha \rangle = 1 + 2e^{\beta\mu} + e^{2\beta\mu - \beta U}, \quad (6)$$

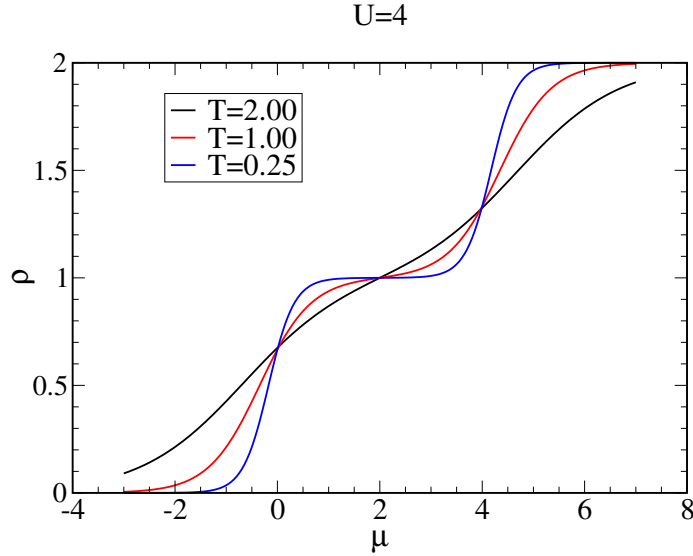


FIGURE 7. Density ρ as a function of chemical potential for the single site ($t = 0$) Hubbard model at $U = 4$ for three different temperatures. At low T a ‘Mott plateau’ develops.

and the energy is,

$$E = \langle H + \mu n \rangle = Z^{-1} \sum_{\alpha} \langle \alpha | H e^{-\beta H} | \alpha \rangle = U e^{2\beta\mu - \beta U} (1 + 2e^{\beta\mu} + e^{2\beta\mu - \beta U})^{-1} \quad (7)$$

The occupation is given by,

$$\rho = \langle n \rangle = 2(e^{\beta\mu} + e^{2\beta\mu - \beta U}) (1 + 2e^{\beta\mu} + e^{2\beta\mu - \beta U})^{-1} \quad (8)$$

Fig. 7 is a plot of ρ vs. μ for $U = 4$ and $T = 2, 1$ and $T = 0.25$ and exhibits one of the fundamental features of the Hubbard model, namely the ‘‘Mott insulating gap’’. How is this understood? At $T = 0$ the chemical potential $\mu = \partial E / \partial \rho$ measures how much the energy changes when the density changes, ie. the cost to add a particle. In a noninteracting system described by a set of energy levels, with levels filled up to some ‘Fermi energy’ E_F , the cost to add a particle is the next energy level just above the last occupied level, that is, $\mu = E_F$. The jump in μ at $\rho = 1$ arises from the interactions: Consider a nearly empty lattice and ask the energy cost to add an electron. This cost need not involve U because empty sites are abundant. When one gets to half-filling, however, suddenly the cost to add an electron jumps by U since inevitably an added electron must sit on top of an electron which is already there. This sudden jump in the cost to add a particle is referred to as the ‘‘Mott gap.’’ Besides the plateau in $\rho(\mu)$, Mott and band gaps are characterized by a density of states (spectral function) which vanishes at the Fermi surface. Examples of this are given in Section V.

Similar jumps in μ also occur in the context of band theory, where a gap between two bands likewise causes μ to change discontinuously. In both cases, the jump in μ indicates the existence of a gapped, insulating phase. However, band and Mott insulators are very different in other ways. ‘Anderson insulators’, arising from disorder, differ from both by having a finite $N(E_F)$, as discussed in the next section.

Half-filling $\rho = 1$ occurs when $\mu = U/2$. Because half-filling is so often studied, it is convenient to write the Hubbard Hamiltonian as,

$$H = -t \sum_{\langle j,l \rangle \sigma} c_{j\sigma}^{\dagger} c_{l\sigma} + U \sum_{\mathbf{j}} (n_{\mathbf{j}\uparrow} - \frac{1}{2})(n_{\mathbf{j}\downarrow} - \frac{1}{2}) - \mu \sum_{\mathbf{j}} (n_{\mathbf{j}\uparrow} + n_{\mathbf{j}\downarrow}) \quad (9)$$

This just corresponds to a shift in the chemical potential μ by $U/2$. With this convention, half-filling always occurs at $\mu = 0$ for any value of t, T, U on a bipartite lattice. To emphasize, the properties of this ‘new’ model are identical to

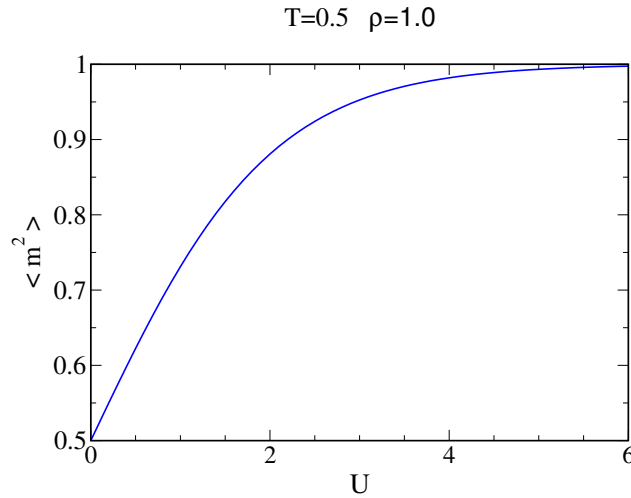


FIGURE 8. Local moment $\langle m_j^2 \rangle$ as a function of U for the single site ($t = 0$) Hubbard model at half-filling $\rho = 1$ and temperature $T = 0.5$. As U increases, a perfect moment develops.

the old one, if one compares them at the same density. The chemical potentials used to get those densities are simply offset.

Exercise 6: Write expressions for Z , E and ρ at $t = 0$ with this new convention for the interaction term in the Hubbard model. You should notice that they are a bit more symmetric looking at $\mu = 0$.

A fundamental physical quantity in the Hubbard model is the ‘local moment’,

$$\langle m_j^2 \rangle = \langle (n_{j\uparrow} - n_{j\downarrow})^2 \rangle. \quad (10)$$

The local moment is zero if the site is either empty, $|0\rangle$, or has two oppositely pointed spins, $|\uparrow\downarrow\rangle$, but takes the value one if the site has a single electron, $|\uparrow\rangle$ or $|\downarrow\rangle$. Fig. 8 is a plot of the local moment as a function of U at half-filling for fixed $T = 0.5$. As U increases, the local moment rises from its uncorrelated value $\langle m_j^2 \rangle = 0.5$ which reflects a uniform mixture of empty, singly occupied, and doubly occupied sites, to the value $\langle m_j^2 \rangle = 1.0$ which reflects the presence only of singly occupied sites. This is a first indication of the tendency towards magnetism in the Hubbard model. An obvious question is whether, when these moments form on individual sites, there is a mechanism for developing correlations between them. This will be one of the central issues addressed in these notes. In Fig. 9 we show the energy $\langle E \rangle$ and the specific heat $C = d\langle E \rangle / dT$ for the half-filled $t = 0$ Hubbard Hamiltonian, as a function of T for $U = 8$. $C(T)$ has a peak at $T \sim U/3$ associated with the suppression of double occupation.

Exercise 7: Show the local moment is related to the ‘double occupancy’ $d_j = \langle n_{j\uparrow} n_{j\downarrow} \rangle$ by

$$\langle m_j^2 \rangle = \langle n_{j\uparrow} + n_{j\downarrow} \rangle - 2d_j. \quad (11)$$

At half-filling, the relation between the moment and the double occupancy becomes $\langle m_j^2 \rangle = 1 - 2d_j$. Interpret the evolution of the local moment between the two limits $\langle m_j^2 \rangle = \frac{1}{2}$ and $\langle m_j^2 \rangle = 1$ in terms of the behavior of the double occupancy d_j .

Having understood the limit of strictly zero hopping, $t = 0$, it is natural to consider perturbation theory in t . Indeed, this is a very fruitful approach and connects the half-filled Hubbard Hamiltonian with the spin- $\frac{1}{2}$ Heisenberg model. A discussion of this is deferred until Section IIB. There, a solution of the two site Hubbard Hamiltonian by exact diagonalization is presented which can be examined in the limit of small, but nonzero, t/U .

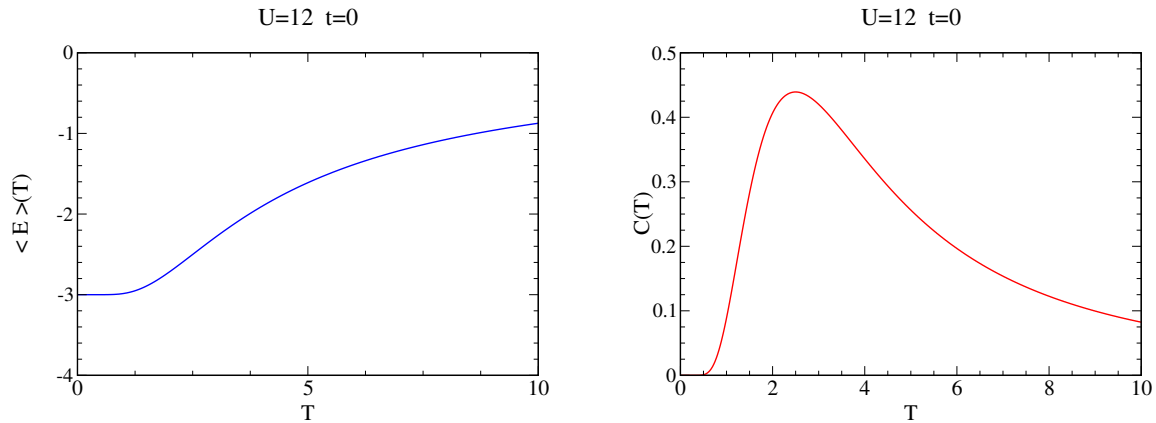


FIGURE 9. Energy (left) and specific heat (right) as functions of temperature T for the single site Hubbard model with $U = 12$.

C. Green's Functions for the Hubbard Hamiltonian

As mentioned, the Hubbard Hamiltonian has been extensively studied via diagrammatic Green's function methods. These lectures do not discuss that approach, but it may be useful to students who do know that technology to make contact with the material discussed so far by computing the Green's function in the weak and strong coupling limits. The one particle Greens function,

$$\begin{aligned} G_{\mathbf{jn}}(\tau) &= \langle c_{\mathbf{j}}(\tau) c_{\mathbf{n}}^{\dagger}(0) \rangle \\ c_{\mathbf{l}}(\tau) &= e^{H\tau} c_{\mathbf{l}}(0) e^{-H\tau}, \end{aligned} \quad (12)$$

is a fundamental quantity in understanding the many body physics of interacting electron systems. Its momentum space and frequency transform, the spectral function $A(\mathbf{k}, \omega)$, yields the angle-resolved photoemission spectrum. From $G_{\mathbf{jn}}(\tau)$, the two particle Greens functions which yield the charge and spin susceptibilities can also be obtained. In the limit of no interactions, $G_{\mathbf{jn}}(\tau)$ can be computed analytically.

Exercise 8: Show that at $U = 0$,

$$c_{\mathbf{k}}(\tau) = e^{H\tau} c_{\mathbf{k}}(0) e^{-H\tau} = e^{-\epsilon_{\mathbf{k}}\tau} c_{\mathbf{k}}(0) \quad (13)$$

You should do this two ways: First show that both expressions give the same result on the two states $|0\rangle$ and $|1\rangle$. Next, prove the result using $\partial \hat{O}(\tau) \partial \tau = [\hat{H}, \hat{O}(\tau)]$ which immediately follows from the definition $\hat{O}(\tau) = e^{\hat{H}\tau} \hat{O}(0) e^{-\hat{H}\tau}$.

Exercise 9: Show that at $U = 0$,

$$G_{\mathbf{jn}}(\tau) = \frac{1}{N} \sum_{\mathbf{k}} e^{i\mathbf{k} \cdot (\mathbf{n} - \mathbf{j})} (1 - f_{\mathbf{k}}) e^{-\epsilon_{\mathbf{k}}\tau}. \quad (14)$$

G is a function of the difference $\mathbf{n} - \mathbf{j}$, as you would expect for a translationally invariant Hamiltonian.

Exercise 10: Write a program to evaluate $G_{\mathbf{jn}}(\tau)$ numerically at $U = 0$ for a $d = 1$ chain and a $d = 2$ square lattice. This is a useful calculation in checking a DQMC code.

Actually, the definition of G is a bit more subtle. In many-body theory one considers the so-called 'time ordered' Green's function, $G_{\mathbf{k}}(\tau) = -\langle \mathcal{T} c_{\mathbf{j}}(\tau) c_{\mathbf{n}}(0) \rangle$ where the time ordering operator \mathcal{T} ,

$$\begin{aligned} \mathcal{T} c_{\mathbf{j}}(\tau) c_{\mathbf{n}}(0) &= c_{\mathbf{j}}(\tau) c_{\mathbf{n}}(0) & \tau > 0 \\ \mathcal{T} c_{\mathbf{j}}(\tau) c_{\mathbf{n}}(0) &= -c_{\mathbf{n}}(0) c_{\mathbf{j}}(\tau) & \tau < 0 \end{aligned} \quad (15)$$

This definition of G and associated formalism opens the door into the huge world of diagrammatic perturbation theory and its application to the Hubbard model. The next few Exercises take you down the road just a little way.

Exercise 11: Prove that the time-ordered Greens function obeys $G(\tau + \beta) = -G(\tau)$ for $-\beta < \tau < 0$.

Exercise 12: Using the preceding exercise, argue that the Fourier transform of G given by,

$$G(\tau) = \sum_n G(i\omega_n) e^{-i\omega_n \tau} \quad (16)$$

involves the ‘Matsubara frequencies’ $\omega_n = \pi(2n + 1)/\beta$.

Exercise 13: Prove the inversion relation

$$G(i\omega_n) = \int_0^\beta \frac{d\tau}{\beta} G(\tau) e^{i\omega_n \tau} \quad (17)$$

Exercise 14: Show that the Greens function in momentum space is given by,

$$\begin{aligned} G_{\mathbf{k}}(\tau) &= -e^{-\varepsilon_{\mathbf{k}}\tau} (1 - f_{\mathbf{k}}) & 0 < \tau < \beta \\ G_{\mathbf{k}}(\tau) &= e^{-\varepsilon_{\mathbf{k}}\tau} f_{\mathbf{k}} & -\beta < \tau < 0 \end{aligned} \quad (18)$$

and hence that,

$$G_{\mathbf{k}}(i\omega_n) = \frac{1}{i\omega_n - \varepsilon_{\mathbf{k}}}. \quad (19)$$

Exercise 15: Provide an alternate demonstration of this result by considering $\partial/\partial\tau$ of the definition of the time ordered Greens function written in the form

$$G_{\mathbf{k}}(\tau) = \langle c_{\mathbf{k}}(\tau) c_{\mathbf{k}}(0) \rangle \theta(\tau) - \langle c_{\mathbf{k}}(0) c_{\mathbf{k}}(\tau) \rangle \theta(-\tau). \quad (20)$$

Be careful to take the appropriate derivatives of the step functions! Then Fourier transform both sides and solve for $G_{\mathbf{k}}(i\omega_n)$.

The approach used in the last exercise is the basis of the ‘equation of motion’ method for computing G . One starts with the definition of G , takes a time derivative, evaluates the resulting commutators of H with $c_{\mathbf{k}}$ and then Fourier transforms. If the Hamiltonian is quadratic in the fermion operators, then the set of equations closes, even if the different fermion operators mix. Otherwise, one can introduce an approximate truncation to terminate the hierarchy.

Exercise 16: The ambitious student should use the above procedure to evaluate $G_{\mathbf{k}}(i\omega_n)$ and $G_d(i\omega_n)$ for

$$H = \sum_{\mathbf{k}} \varepsilon_{\mathbf{k}} c_{\mathbf{k}}^\dagger c_{\mathbf{k}} + V \sum_{\mathbf{k}} (c_{\mathbf{k}}^\dagger d + d^\dagger c_{\mathbf{k}}) + \varepsilon_d d^\dagger d \quad (21)$$

which describes the mixing of a *single* impurity orbital (labeled by ‘d’) with a band of conduction electrons (labeled by ‘k’). This is a model akin to the PAM mentioned earlier and is referred to as the Anderson impurity model (AIM). You will need to write the two definitions of $G_{\mathbf{k}}(\tau)$ and $G_d(\tau)$, take their τ derivatives, and Fourier transform. You’ll end up with two equations in two unknowns (the two Greens functions). Solving, your result for G_d should be

$$G_d(i\omega_n) = \frac{1}{i\omega_n - \varepsilon_d - V^2 \sum_{\mathbf{k}} \frac{1}{i\omega_n - \varepsilon_{\mathbf{k}}}} \quad (22)$$

Exercise 17: The Greens function for $U = 0$ offers the jumping-off place for perturbative studies of the Hubbard, and related, Hamiltonians. If you have some familiarity with those approaches, you can attempt to rederive the Greens function for the AIM by evaluating the diagrammatic form of the self-energy, pictured in Fig. 10, by inserting the forms of the $U = 0$ Greens function and performing the necessary summations. Plugging into the Dyson Equation

$$\begin{aligned} G(k, i\omega_n) &= G_0(k, i\omega_n) + G_0(k, i\omega_n) \Sigma(k, i\omega_n) G(k, i\omega_n) \\ G^{-1}(k, i\omega_n) &= G_0^{-1}(k, i\omega_n) + \Sigma(k, i\omega_n) \end{aligned} \quad (23)$$

$$\begin{aligned}
 \text{---} &= \text{---} + \text{---} \text{---} \text{---} \\
 G_d(i\omega_n) &= G_d^0(i\omega_n) + G_d^0(i\omega_n) \Sigma(i\omega_n) G_d(i\omega_n) \\
 \Sigma(i\omega_n) &= \frac{x \text{---} x}{V G^0(k, i\omega_n) V}
 \end{aligned}$$

FIGURE 10. Dyson equation and self-energy for the localized (d) electron for the Anderson impurity model.

should reproduce the equation of motion result for the Greens function. In this case, the perturbative Feynman diagram method, like the equation of motion method, provides an exact expression (ie correct to all orders in V). This provides a simple illustration of the method, but it should be kept in mind that this simple result is highly atypical.

It is also instructive to look at the Green's function for a single site, that is, the $t = 0$ Hubbard model. Previously the Hilbert space for this problem was written down and the partition function and various equal time quantities were obtained. Now consider the calculation of

$$G_{\uparrow}(\tau) = \langle c_{\uparrow}(\tau) c_{\uparrow}^{\dagger}(0) \rangle. \quad (24)$$

Only the states $|00\rangle$ and $|01\rangle$ contribute to the expectation value since the creation operator for up electrons needs to see an empty up state. The action of the sequence of operators on the states is, $|00\rangle$:

$$\begin{aligned}
 c_{\uparrow}(\tau) c_{\uparrow}^{\dagger}(0) |00\rangle &= e^{H\tau} c_{\uparrow}(0) e^{-H\tau} c_{\uparrow}^{\dagger}(0) |00\rangle = e^{H\tau} c_{\uparrow}(0) e^{-H\tau} |10\rangle \\
 &= e^{H\tau} c_{\uparrow}(0) e^{+U\tau/4} |10\rangle = e^{H\tau} e^{+U\tau/4} |00\rangle = e^{+U\tau/2} |00\rangle
 \end{aligned} \quad (25)$$

and similarly for $|01\rangle$.

Exercise 18: Complete the calculation begun above to show that,

$$G_{\uparrow}(\tau) = \frac{e^{+\beta U/4} e^{-\tau U/2} + e^{-\beta U/4} e^{+\tau U/2}}{2e^{\beta U/4} + 2e^{-\beta U/4}}. \quad (26)$$

Exercise 19: The Green's function is related to the spectral density $A(\omega)$ by the relation,

$$G(\tau) = \int_{-\infty}^{+\infty} A(\omega) \frac{e^{-\omega\tau}}{e^{-\beta\omega} + 1} d\omega. \quad (27)$$

Show that if you plug in

$$A(\omega) = \frac{1}{2} (\delta(\omega - U/2) + \delta(\omega + U/2)) \quad (28)$$

and do the integral you get the correct $G(\tau)$. The spectral function of the single site Hubbard model consists of two delta function peaks separated by U (the Mott gap).

As discussed earlier (Fig. 7 and below Eq. 8), the Mott transition is associated with the development of a plateau in ρ vs μ at $\rho = 1$. The connection to insulating behavior is simple: In a dilute lattice electrons can move without double occupation. However, for an electron to move in a half-filled lattice in which each site is singly occupied, double occupation must occur. This costs an energy U . It is plausible to imagine that if U is very large, the electrons will not want to move at all, and one will have an "Mott" insulator. The structure of $A(\omega)$, evaluated in the $t = 0$ limit above, which consists of two delta functions separated by U , provides another illustration of the opening of a gap and Mott insulating phenomenon. Though the Mott gap is similar to the way that the cost to add an electron jumps if there is a gap separating single particle energy bands, it is worth noting that this analogy goes only so far, and the Mott gap differs in very fundamental ways from band gaps.

Exercise 20: It is also interesting to compute G and A when there is a local site energy or chemical potential present. Work with the Hamiltonian $H = U(n_{\uparrow} - \frac{1}{2})(n_{\downarrow} - \frac{1}{2}) - \mu(n_{\uparrow} + n_{\downarrow})$. Show that,

$$\begin{aligned} A(\omega) &= a_+ \delta(\omega - U/2 + \mu) + a_- \delta(\omega + U/2 + \mu). \\ a_+ &= (e^{\beta U/2} e^{\beta \mu} + e^{2\beta \mu}) / (1 + 2e^{\beta U/2} e^{\beta \mu} + e^{2\beta \mu}) \\ a_- &= (1 + e^{\beta U/2} e^{\beta \mu}) / (1 + 2e^{\beta U/2} e^{\beta \mu} + e^{2\beta \mu}) \end{aligned}$$

by evaluating $G(\tau)$ explicitly from its definition. μ now enters both the partition function Z and the imaginary time propagation. The coefficients a_+ and a_- are obtained by equating this expression for $G(\tau)$ with what you get from plugging $A(\omega)$ into the formula relating G and A . Notice that at $\mu = 0$, $a_+ = a_- = \frac{1}{2}$, and that, regardless of what μ , β and U are, $a_+ + a_- = 1$. Interestingly, the spectral function is not just shifted by μ as one might have expected. The peak heights are also changed.

We have discussed the Hubbard model at $U = 0$ and at $t = 0$. In the noninteracting case, going to momentum creation and destruction operators diagonalized H . The single site limit was more easy in the sense that the interaction term is already diagonal in the original site operators. It is sometimes useful to consider the representation of the interaction term in momentum space, as done in the following exercise.

Exercise 21: Consider the form of the interaction term in momentum space. Substitute the equation which relates real and momentum space operators for each of the four real space creation operators in the interaction term of the Hubbard model. As with the hopping term, the sum over sites leads to momentum conservation and reduces the four momentum sums to three. Show that the result is,

$$\frac{U}{N} \sum_{\mathbf{k}_1, \mathbf{k}_2, \mathbf{k}_3} c_{\mathbf{k}_1 + \mathbf{k}_2 - \mathbf{k}_3 \uparrow}^\dagger c_{\mathbf{k}_3 \downarrow}^\dagger c_{\mathbf{k}_2 \uparrow} c_{\mathbf{k}_1 \downarrow}. \quad (29)$$

The physical content of this form is that an up and down electron of momentum \mathbf{k}_2 and \mathbf{k}_1 scatter and emerge with momenta \mathbf{k}_3 and $\mathbf{k}_1 + \mathbf{k}_2 - \mathbf{k}_3$, the same total momentum as initially. One can rewrite the sum over the three momentum variables in the more appealing form,

$$\frac{U}{N} \sum_{\mathbf{k}_1, \mathbf{k}_2, \mathbf{q}} c_{\mathbf{k}_2 + \mathbf{q} \uparrow}^\dagger c_{\mathbf{k}_1 - \mathbf{q} \downarrow}^\dagger c_{\mathbf{k}_2 \uparrow} c_{\mathbf{k}_1 \downarrow}. \quad (30)$$

Here \mathbf{q} is seen to be the momentum exchanged in the collision of the two electrons of initial momenta \mathbf{k}_1 and \mathbf{k}_2 .

D. Exact Diagonalization

After considering the limits $t = 0$ and $U = 0$, it is natural to examine the full problem on a small cluster of sites. However, before discussing diagonalization of the Hubbard model, it is useful to examine the Heisenberg model, since it describes the physics of the Hubbard model when U is large. Consider a set of quantum mechanical spins, with spin-1/2, localized on a set of sites i , and interacting on neighboring sites $\langle ij \rangle$ through inter-atomic exchange,

$$H = J \sum_{\langle ij \rangle} \vec{S}_i \cdot \vec{S}_j. \quad (31)$$

For two sites,

$$H = J \vec{S}_1 \cdot \vec{S}_2 = J [S_{1,x} S_{2,x} + S_{1,y} S_{2,y} + S_{1,z} S_{2,z}] = J \left[\frac{1}{2} (S_{1,+} S_{2,-} + S_{1,-} S_{2,+}) + S_{1,z} S_{2,z} \right] \quad (32)$$

There are four states in the Hilbert space, since each z component can take on one of two values. Denote these by $|S_{1,z} S_{2,z}\rangle = |++\rangle, |--\rangle, |+-\rangle, |-+\rangle$.

Compute the eigenvalues of the two site Heisenberg model by writing,

$$H = J \vec{S}_1 \cdot \vec{S}_2 = \frac{1}{2} J [(S_1 + S_2)^2 - S_1^2 - S_2^2]. \quad (33)$$

Replace S_1^2 and S_2^2 with $j(j+1) = \frac{1}{2}(\frac{1}{2}+1) = \frac{3}{4}$, since these operators give the same value on all states in the Hilbert space. $S_1 + S_2$ can take the two possible values $S_1 + S_2 = 0, 1$ when two spin-1/2 angular momenta are added. The choice $S_1 + S_2 = 1$ is three-fold degenerate, corresponding to $S_{1z} + S_{2z} = -1, 0, 1$. Finally, the eigenvalues of H are $\frac{1}{2}J[1(1+1) - \frac{3}{4} - \frac{3}{4}] = +\frac{1}{4}J$ (three-fold degenerate) and $\frac{1}{2}J[0(0+1) - \frac{3}{4} - \frac{3}{4}] = -\frac{3}{4}J$ (nondegenerate).

The ‘brute force’ method of constructing the matrix of H and diagonalizing of course yields the same result.

$$\begin{aligned}
H|++\rangle &= +\frac{1}{4}J|++\rangle \\
H|--\rangle &= +\frac{1}{4}J|--\rangle \\
H|+-\rangle &= -\frac{1}{4}J|+-\rangle + \frac{1}{2}J|-+\rangle \\
H|-+\rangle &= -\frac{1}{4}J|-+\rangle + \frac{1}{2}J|+-\rangle.
\end{aligned} \tag{34}$$

Thus the matrix for H (with the basis vectors in the order listed above) is

$$H = \frac{1}{4}J \begin{pmatrix} 1 & 0 & 0 & 0 \\ 0 & 1 & 0 & 0 \\ 0 & 0 & -1 & 2 \\ 0 & 0 & 2 & -1 \end{pmatrix}. \tag{35}$$

Two of the basis vectors, $|++\rangle$ and $|--\rangle$ are already eigenstates of H with eigenvalue $\frac{1}{4}J$. These are the states with $S_1 + S_2 = 1$ and $S_1^z + S_2^z = 1, -1$. form the symmetric and antisymmetric linear combinations of the other two to get the remaining eigenvectors: $\frac{1}{\sqrt{2}}(|+-\rangle + |-+\rangle)$ and $\frac{1}{\sqrt{2}}(|+-\rangle - |-+\rangle)$. These have eigenvalues $\frac{1}{4}J$ and $-\frac{3}{4}J$ respectively. Confirming the earlier analysis with the method using the square of the total spin, there are three eigenvectors of eigenvalue $\frac{1}{4}J$, and a single eigenvector of eigenvalue $-\frac{3}{4}J$. The ‘singlet’ is the ground state for $J > 0$ (antiferromagnetic coupling).

It is amusing that the four site Heisenberg model is also amenable to an analysis through examining the squares of the angular momentum.

$$H = J[\vec{S}_1 \cdot \vec{S}_2 + \vec{S}_2 \cdot \vec{S}_3 + \vec{S}_3 \cdot \vec{S}_4 + \vec{S}_4 \cdot \vec{S}_1] = \frac{1}{2}J[(\vec{S}_1 + \vec{S}_2 + \vec{S}_3 + \vec{S}_4)^2 - (\vec{S}_1 + \vec{S}_3)^2 - (\vec{S}_2 + \vec{S}_4)^2] \tag{36}$$

The possible values of $S_1 + S_3$ are 0, 1 and likewise for $S_2 + S_4$. When $S_1 + S_3 = 0$ and $S_2 + S_4 = 0$ are combined, a single total spin $S_1 + S_3 + S_2 + S_4 = 0$ state results. Putting together $S_1 + S_3 = 1$ and $S_2 + S_4 = 0$ yields three $S_1 + S_3 + S_2 + S_4 = 1$ states, as does combining $S_1 + S_3 = 0$ and $S_2 + S_4 = 1$. Adding $S_1 + S_3 = 1$ and $S_2 + S_4 = 1$ yields one $S_1 + S_3 + S_2 + S_4 = 0$ state, three $S_1 + S_3 + S_2 + S_4 = 1$ states, and five $S_1 + S_3 + S_2 + S_4 = 2$ states.

In the sector formed by putting together $S_1 + S_3 = 0$ and $S_2 + S_4 = 0$, the eigenvalue is $\frac{1}{2}J[0(0+1) - 0(0+1) - 0(0+1)] = 0$. In the sector formed by putting together $S_1 + S_3 = 1$ and $S_2 + S_4 = 0$, the (three) eigenvalues are $\frac{1}{2}J[1(1+1) - 1(1+1) - 0(0+1)] = 0$. The same holds for the sector formed by putting together $S_1 + S_3 = 0$ and $S_2 + S_4 = 1$. In the sector formed by putting together $S_1 + S_3 = 1$ and $S_2 + S_4 = 1$, the eigenvalues are $\frac{1}{2}J[2(2+1) - 1(1+1) - 1(1+1)] = J$ for the five total spin 2 states, $\frac{1}{2}J[1(1+1) - 1(1+1) - 1(1+1)] = -J$ for the three total spin 1 states, and $\frac{1}{2}J[0(0+1) - 1(1+1) - 1(1+1)] = -2J$ for the spin 0 state.

Exercise 22: Solve the four spin “ $J_1 - J_2$ ” Heisenberg in which the bonds along the sides of the square are J_1 and additional bonds of strength J_2 are introduced along the diagonal.

Exercise 23: Show there is a level crossing as the relative size of J_1 and J_2 changes. What is the physics in the limits of J_1 dominant and J_2 dominant? You might speculate that in the thermodynamic limit this small size level crossing might evolve into a phase transition.

With this localized spin model background in hand, the two site Hubbard model, whose Hilbert space has dimension sixteen, can be diagonalized and its strong coupling limit understood. Consider the largest subspace, the sector with one spin up and one spin down electron. Denote by $|\uparrow\downarrow 0\rangle, |0\uparrow\downarrow\rangle, |\uparrow\downarrow\rangle$, and $|\uparrow\downarrow\rangle$, the state with a spin up electron and a spin down electron on site 1, and site 2 empty; the state with a spin up electron and a spin down electron

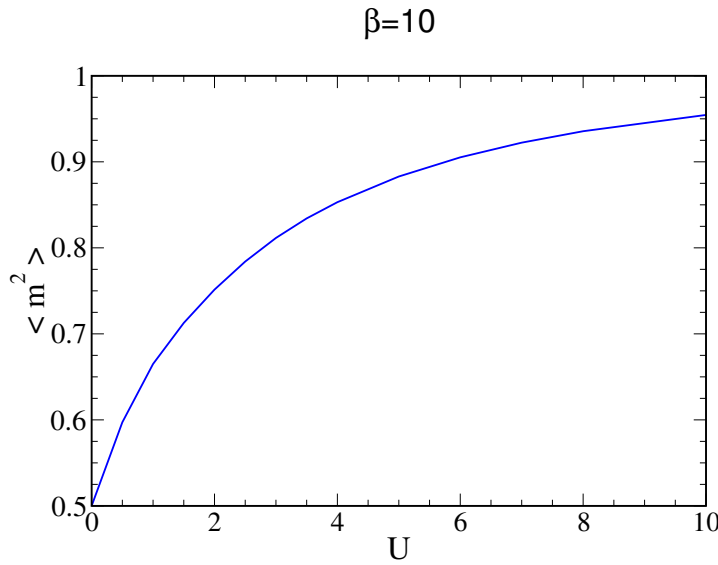


FIGURE 11. Local moment of the 2x2 Hubbard model as a function of U . Here $t = 1$, $\rho = 1$. The temperature $T = 0.1$ is low enough so that the suppression of the moment at small U is due to quantum, rather than thermal, fluctuations.

on site 2, and site 1 empty; the state with a spin up on site 1 and a spin down electron on site 2; and the state with a spin up on site 2 and a spin down electron on site 1, respectively.

It is easy to see that the associated matrix for the Hamiltonian is

$$H = \begin{pmatrix} U & 0 & -t & -t \\ 0 & U & -t & -t \\ -t & -t & 0 & 0 \\ -t & -t & 0 & 0 \end{pmatrix} \quad (37)$$

It is immediately obvious that two of the eigenvalues of H are 0 and U . Two others are $\frac{1}{2}(U \pm \sqrt{U^2 + 16t^2})$. If the last two eigenvalues are expanded in t/U , the result is $-4t^2/U$ and $U + 4t^2/U$, and the energy scale $J = 4t^2/U$ arises. The significance of J will be discussed further below.

The Heisenberg model emerges as a limit of the Hubbard model when t/U is small. To see this, note that the sector of the two site Hubbard model with one up and one down spin, considered above, can be expanded to include all sectors with two electrons, by adding the states $|\uparrow \uparrow\rangle$, and $|\downarrow \downarrow\rangle$. These states are eigenstates of H with eigenvalue 0. All together, the two electron space of the two site Hubbard model has four ‘small’ eigenvalues 0,0,0, and $\frac{1}{2}(U - \sqrt{U^2 + 16t^2}) \approx -4t^2/U$ and two ‘large’ ones U and $\frac{1}{2}(U + \sqrt{U^2 + 16t^2})$. The large eigenvalues are associated with eigenvectors whose components have significant mixtures of the states with doubly occupied sites. The existence of the two groups of states whose eigenvalues are separated by U is a reflection of the ‘upper and lower Hubbard bands’. The ‘Mott-Hubbard’ gap in the spectrum gives rise to a metal-insulator transition. The two site Heisenberg model had three eigenvalues $J/4$ and one $-3J/4$. Apart from a trivial shift in energies, this is the same spectrum as that of the small eigenvalue sector of the Hubbard model, with the identification $J = 4t^2/U$.

Fig. 8 showed how the moment $\langle m^2 \rangle$ of the single site Hubbard model ($t = 0$) develops as the interaction U is increased at constant temperature T and $\rho = 1$. When U is small, thermal fluctuations reduce the moment to its uncorrelated value $\langle m^2 \rangle = 0.5$. Quantum fluctuations similarly reduce the moment, as is apparent in Fig. 11.

Exercise 24: Write a program to diagonalize the four site Hubbard model. Compute E and $\langle m^2 \rangle$.

The four site Hubbard model matrices are small enough that they can be constructed by hand. However, for larger lattices, one clearly wants to write a program which will generate the matrix elements automatically. Indeed, the routines entering such a code are needed also to evaluate expectation values of physically interesting quantities. This will be covered in lectures of other speakers. Here it is noted that there are two crucial elements to such a program:

A first routine which computes the Hilbert state number given the occupations of the individual sites and a second routine which does the converse, namely computes the individual site occupation, for a given state number. With these available, the Hamiltonian can be constructed by looping over all states i , computing the occupation numbers using the second routine, then applying the kinetic energy to change the occupations and using the first routine to figure out the associated state number j . H_{ij} is then set to $-t$ (or $+t$) depending on the number of anticommutations involved, see Appendix A. The diagonal entry H_{ii} is a trivial function of the occupations. Here is some pseudocode that builds the required arrays for a four site system.

```
state=0
loop:  n1=0,1
loop:  n2=0,1
loop:  n3=0,1
loop:  n4=0,1
      if (n1+n2+n3+n4=npart)
          occ1(state)=n1
          occ2(state)=n2
          occ3(state)=n3
          occ4(state)=n4
          state=state+1
          binary=n1+2*n2+4*n3+8*n4
          getstate(binary)=state
      endif
```

This code loops over the occupations of the different sites. (Here for simplicity four sites are chosen.) A check is performed to see if the total occupation equals the desired one: $npart$. If it does, arrays $occ1, occ2, \dots$ are used to store the site occupations, and the counter recording the number of states is incremented. These arrays allow us to look up the occupation on any site given the state. At the same time, the array $getstate$ contains the state corresponding to a given set of site occupations. To access it, one first constructs the single number ‘binary’ from the occupations. This part is a little sloppy, because the array $getstate$ is considerably larger (dimension 2^4 , or more generally 2^N where N is the number of sites) than necessary. (If $npart=2$ the Hilbert space is only dimension 6, not 16.)

A few final comments: First, the action of the kinetic energy term in the Hubbard model is very similar to that of the exchange term $S_{+i}S_{-j} + S_{+j}S_{-i}$ of the Heisenberg model. So the same ideas/codes that work for the Heisenberg case for labeling the states and constructing the Hamiltonian can be carried over to the Hubbard case (and vice-versa). One very important difference, though, is the existence of minus signs which arise from the anticommutation of the fermion operators on different sites. In one dimension, these minus signs can be eliminated for near-neighbor hopping with a choice of appropriate boundary conditions. Indeed, this is one way of understanding the existence of exact maps between fermions and quantum spins, like the Jordan-Wigner transformation, in 1-d. In 2-d, it is no longer possible to eliminate the minus signs.

Indeed, in one dimension, for the half-filled Hubbard model, it is sometimes useful to alternate periodic (pbc) and antiperiodic boundary conditions (apbc) for lattices of length $4n$ and $4n+2$. (Even chain lengths are usually chosen, otherwise the antiferromagnetic order would be frustrated.) The reason is that at half-filling, lattices of length $4n$ have an even number of electrons of each spin species. Thus when an electron hops across the ends of the chain, ie between sites 1 and n , it passes an *odd* number of the remaining electrons of the same spin. This introduces a minus sign in the end-to-end hopping t . For lattice lengths $4n+2$, clearly this minus sign does not occur. Employing apbc for length $4n$ eliminates the minus sign. With the pbc/apbc alternation, measured quantities monotonically approach the large spatial size limit rather than oscillating above and below the asymptotic value. A more general trick to reducing finite size effects is boundary condition averaging [46, 47].

The obvious drawback of the exact diagonalization approach is the system size it is able to handle. Even using symmetries of the Hamiltonian, the matrix to be diagonalized grows exponentially with the number of sites. Typically, diagonalization methods are limited to a few tens of lattice sites, where the exact number is determined by the values of the degrees of freedom at each site (and the effort the programmer is willing to make!). To explore the systematic effects of the restriction to finite size it is useful to be able to compare results on lattices of different extent. One trick to facilitate this is to consider non-standard tilings. For example, rather than considering only $2 \times 2, 3 \times 3, 4 \times 4, \dots$ lattices, one can tile the 2-d square lattice with other configurations such as groups of eight sites,

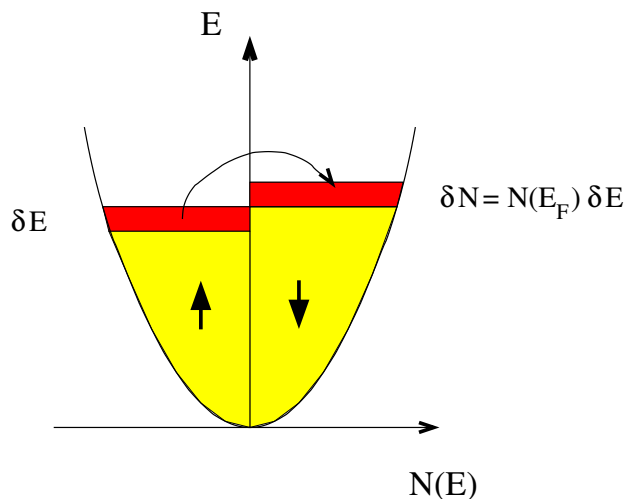


FIGURE 12. Qualitative picture of Stoner construction. δN down spin electrons are converted to up spin electrons, at a cost in kinetic energy $\delta K = +\delta n \delta E$. If this is less than the potential energy lowering, a ferromagnetic state is favored.

$$\begin{array}{cccc}
 & A & B & \\
 C & D & E & F \\
 & G & H &
 \end{array} \quad (38)$$

as follows:

$$\begin{array}{cccccc}
 & & A & B & & \\
 & & C & D & E & F \\
 A & B & G & H & A & B \\
 C & D & E & F & C & D & E & F \\
 G & H & A & B & G & H \\
 & & C & D & E & F \\
 & & G & H & &
 \end{array} \quad (39)$$

This construction corresponds to dividing the 2-d lattice into $\sqrt{8}$ by $\sqrt{8}$ squares whose axes are rotated with respect to the grid lines defining the array of sites. Notice that the natural connections which implement periodic boundary conditions can be seen from the picture. For example, site B has neighbors C (above), A (left), G (right) and E (below).

A further reason for looking at these oddly shaped lattices in two dimensions has to do with special symmetries of the 4×4 lattice which is frequently studied in 2-d exact diagonalization. It is easy to verify that the 4×4 lattice has the same connectivity as the $2 \times 2 \times 2 \times 2$ lattice in four dimensions. That the 4×4 lattice has unusual properties can be illustrated by the observation that correlation functions between observables separated by $\hat{x} + \hat{y}$ are identical to those separated by $2\hat{x}$ or $2\hat{y}$!

E. Mean Field Theory

So far, the solutions to the Hubbard model in the simple limits of no hopping ($t = 0$), no interactions ($U = 0$), and very small system sizes (two sites) have been described. The next goal is to study ferromagnetism using mean field theory. Before doing this, it is useful to describe Stoner's argument for magnetism, which will later be demonstrated to give quantitatively equivalent results to the (more general) mean field approach.

Stoner developed a very simple picture of ferromagnetism based on the competition between the kinetic energy cost of making the up and down spin electron numbers different and the associated potential energy gain. The basic idea is the following: Because of the Pauli principle, the way to occupy a given set of energy levels with the lowest energy is to start filling from the bottom and put two electrons, one of each spin, in each level. Otherwise, if you make the

numbers of up and down electrons unequal, and don't fill each level with two electrons, you have to occupy higher energies. However, if you make the number of up and down electrons unequal, you can reduce the potential energy. In the limit of complete spin polarization where there are no electrons of one spin species, the potential energy is zero in the Hubbard model.

Perhaps this competition can lead to non-trivial effects. Consider a system with density of states $N(E)$ and both up and down spin electrons filling the energy levels up to the same 'Fermi level' E_F . The density of up and down electrons is equal. Call it n . Let's compute the change in energy which results from a reduction in the density of down spin electrons by δn and at the same time an increase in the number of up spin electrons by δn . The potential energy changes by,

$$\delta P = U(n + \delta n)(n - \delta n) - Un^2 = -U(\delta n)^2.$$

If an additional δn electrons are shifted into the up group, then energy levels above the original E_F are occupied. See Fig. 12. The definition of the density of states as the number of levels at an energy E , that is $N(E) = dN/dE$, implies $\delta n = N(E_F)\delta E$. This describes the range of energies above E_F filled in terms of δn . Likewise, levels below E_F that used to be occupied by down spin electrons are emptied. The net result of this process is to shift δn electrons up in energy by an amount δE . The change in the kinetic energy is then,

$$\delta K = +\delta n\delta E = +\frac{1}{N(E_F)}(\delta n)^2.$$

Putting these two expressions together,

$$\delta E = \delta P + \delta K = (-U + \frac{1}{N(E_F)})(\delta n)^2 = (-UN(E_F) + 1)\frac{(\delta n)^2}{N(E_F)}.$$

If $UN(E_F) > 1$ the total energy change $\delta E < 0$, so it is favorable to have the up and down electron densities different and hence to have ferromagnetism. This is called the Stoner criterion. It tells us that magnetism is associated with large electron interactions and density of states. As described later, this simple calculation yields results in precise agreement with mean field theory.

What is mean field theory? As commented in an earlier section, a Hamiltonian which is quadratic in the fermion creation and destruction operators, $H = \sum_{i,j} c_i^\dagger h_{i,j} c_j$, can be solved by diagonalizing the matrix h . Mean field theory is a method which produces such a quadratic Hamiltonian from a model like the Hubbard model which has quartic terms $Uc_{i\uparrow}^\dagger c_{i\uparrow} c_{i\downarrow}^\dagger c_{i\downarrow}$ involving four fermion creation and destruction operators. The approach begins by expressing the number operators as an average value plus a deviation from the average:

$$\begin{aligned} n_{i\uparrow} &= \langle n_{i\uparrow} \rangle + (n_{i\uparrow} - \langle n_{i\uparrow} \rangle) \\ n_{i\downarrow} &= \langle n_{i\downarrow} \rangle + (n_{i\downarrow} - \langle n_{i\downarrow} \rangle). \end{aligned} \quad (40)$$

Substituting these expressions into the Hubbard interaction term, and dropping the 'small' term which is the product of the two deviations from the average yields,

$$\begin{aligned} n_{i\uparrow} n_{i\downarrow} &= [\langle n_{i\uparrow} \rangle + (n_{i\uparrow} - \langle n_{i\uparrow} \rangle)][\langle n_{i\downarrow} \rangle + (n_{i\downarrow} - \langle n_{i\downarrow} \rangle)] \\ &\approx \langle n_{i\uparrow} \rangle \langle n_{i\downarrow} \rangle + \langle n_{i\downarrow} \rangle (n_{i\uparrow} - \langle n_{i\uparrow} \rangle) + \langle n_{i\uparrow} \rangle (n_{i\downarrow} - \langle n_{i\downarrow} \rangle) \\ &= n_{i\uparrow} \langle n_{i\downarrow} \rangle + n_{i\downarrow} \langle n_{i\uparrow} \rangle - \langle n_{i\uparrow} \rangle \langle n_{i\downarrow} \rangle. \end{aligned} \quad (41)$$

The interpretation of this expression is simple. The up spin electrons interact with the average density of down spin electrons, and similarly the down spin electrons interact with the average density of up spin electrons. These two terms overcount the original single interaction term, so the product of the average densities is subtracted off.

Within this mean field replacement, the Hubbard Hamiltonian is now quadratic, and takes the form (in one dimension)

$$H = -t \sum_{l\sigma} (c_{l\sigma}^\dagger c_{l+1\sigma} + c_{l+1\sigma}^\dagger c_{l\sigma}) + n_{i\uparrow} \langle n_{i\downarrow} \rangle + n_{i\downarrow} \langle n_{i\uparrow} \rangle - \langle n_{i\uparrow} \rangle \langle n_{i\downarrow} \rangle. \quad (42)$$

Since H is quadratic, its solution is a matter of diagonalizing an appropriate matrix. Specifically, for the case of ferromagnetism, one imagines that the average occupation is independent of spatial site i but allowed to be different

for the two spin species. That is, $\langle n_{i\uparrow} \rangle = n + m$ and $\langle n_{i\downarrow} \rangle = n - m$. The goal is to calculate the energy E for fixed n as a function of m and see whether the minimum is at $m = 0$ (paramagnetic state, no ferromagnetism) or $m \neq 0$ (ferromagnetism). Because the expectation values $\langle n_{i\uparrow} \rangle$ and $\langle n_{i\downarrow} \rangle$ have such a simple, site independent form, the energy levels can easily be written down. In $d = 1$ they are,

$$\begin{aligned}\epsilon_{k\uparrow} &= U(n - m) - 2t \cos k \\ \epsilon_{k\downarrow} &= U(n + m) - 2t \cos k.\end{aligned}\tag{43}$$

To determine the ground state phase diagram,

- (1) Fix the lattice size, N , and choose a ratio U/t and particle number N_{tot} .
- (2) Loop over $N_{\uparrow} = 0, 1, 2, \dots, N_{\text{tot}}$, setting $N_{\downarrow} = N_{\text{tot}} - N_{\uparrow}$. Define the densities, $n_{\uparrow} = N_{\uparrow}/N$ and $n_{\downarrow} = N_{\downarrow}/N$.
- (3) Fill up the lowest N_{\uparrow} and N_{\downarrow} energy levels, $\epsilon_{k\uparrow} = -2t \cos k + U \langle n_{\downarrow} \rangle$ and $\epsilon_{k\downarrow} = -2t \cos k + U \langle n_{\uparrow} \rangle$. The momentum values are $k = 2\pi/N \{-N/2 + 1, -N/2 + 2, \dots, N/2\}$.
- (4) Normalize the energy accumulator to the number of sites and include the term $-U \langle n_{\uparrow} \rangle \langle n_{\downarrow} \rangle$. This gives the energy for the given N_{\uparrow} and $N_{\downarrow} = N_{\text{tot}} - N_{\uparrow}$. Make a list of them and see which is lowest.
- (5) Repeat the calculation for different U and N_{tot} to get the phase diagram.

Simple (Fortran) code

```
implicit none
integer i, N, Nup, Ndn, Ntot
real*8 t, U, tpin, k, ekup, ekdn, denup, dendn
real*8 efup, efdn, eftot

write (6, *) 'N, Ntot, t, U'
read (5, *) N, Ntot, t, U
tpin=8.d0*datan(1.d0)/dfloat(N)
do 1000 Nup=0, Ntot, 2

Ndn=Ntot-Nup
denup=dfloat(Nup)/dfloat(N)
dendn=dfloat(Ndn)/dfloat(N)

efup=0.d0
efdn=0.d0
do 200 i=-N/2+1, N/2
k=tpin*dfloat(i)
if (i.ge.-Nup/2+1.and.i.le.Nup/2) then
ekup=-2.d0*t*dcos(k)+U*dendn
efup=efup+ekup
endif
if (i.ge.-Ndn/2+1.and.i.le.Ndn/2) then
ekdn=-2.d0*t*dcos(k)+U*denup
efdn=efdn+ekdn
endif
200 continue
eftot=(efup+efdn)/dfloat(N)-U*denup*dendn

write (36, 990) Nup, Ndn, eftot
990 format(2i6, f16.6)

1000 continue
end
```

Fig. 13(left) shows $E(M)$ for one quarter filling, $\rho = \rho_{\uparrow} + \rho_{\downarrow} = 1/2$. The magnetization $M = (\rho_{\uparrow} - \rho_{\downarrow})/(\rho_{\uparrow} + \rho_{\downarrow})$. At $U/t = 2$ the optimal energy is paramagnetic: the energy E is minimized at $M = 0$. For $U/t = 6$ the minima are fully spin polarized, $M = \pm 1$. Fig. 13(right) focuses on the transition region. When $U/t = 4.2$ the energies for large M have started to turn down and are lower than intermediate M , though $E(M = 0)$ is still lowest. $U/t = 4.4$ has just

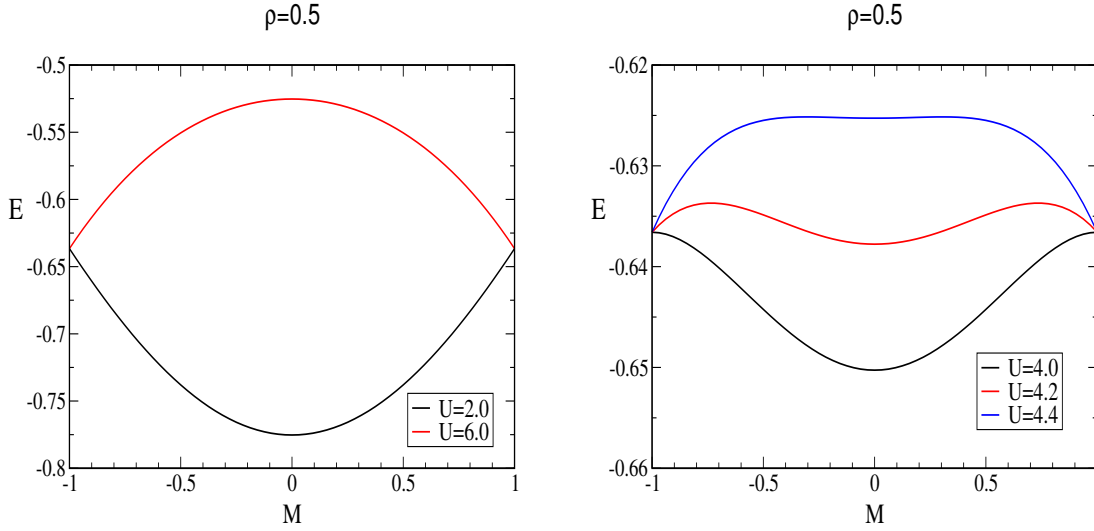


FIGURE 13. Left: Energy versus magnetization of the $d = 1$ Hubbard model at quarter filling, $\rho = 1/2$ (128 electrons on an $N = 256$ site lattice). A paramagnetic state, $M = 0$, is favored at $U = 2.0t$, and a ferromagnetic one, with full spin polarization $M = 1$, at $U = 6.0t$. Right: Same as left panel, except in the transition region $U \approx 4.0t$. The Stoner criterion gives $U_{\text{crit}} = \sqrt{2\pi}t \approx 4.44t$.

gone ferromagnetic. Notice that the transition is *first order*. That is, as U/t increases the minimum jumps from $M = 0$ to $M = \pm 1$. Another possibility would have been a second order transition in which the minimum at $M = 0$ gradually shifts to larger M and partially polarized solutions are best for a range of U/t . An examination of other MFT solutions (like antiferromagnetic ones) is required to determine if this first order transition is ‘real’ or simply occurs because of the restriction to ferromagnetic solutions.

These MFT results are consistent with the Stoner Criterion for Ferromagnetism $UN(E_F) > 1$. For the $d=1$ Hubbard model where $\varepsilon_k = -2t\cos(k)$,

$$N(E) = 2 \sum_k \delta(E - \varepsilon_k) = 2 \int \frac{dk}{2\pi} \delta(E - \varepsilon_k) = \frac{1}{\pi\sqrt{4t^2 - E^2}}. \quad (44)$$

The density ρ and the Fermi energy E_F are related by:

$$\rho = 2 \int_{-2t}^{E_F} dE N(E) = \frac{2}{\pi} \cos^{-1}\left(-\frac{E}{2t}\right). \quad (45)$$

This relation obeys the expected limits: $\rho = 0$ when $E_F = -2t$, $\rho = 1$ when $E_F = 0$, and $\rho = 2$ when $E_F = +2t$.

Putting these equations together, the density of states at E_F for a given filling is:

$$N(\rho) = \frac{1}{2\pi t} \frac{1}{\sin(\pi\rho/2)}. \quad (46)$$

For half-filling, $N(\rho = 1) = 1/2\pi t$ and hence $U_{\text{crit}} = 2\pi t$. For quarter-filling, $N(\rho = 1/2) = 1/\sqrt{2}\pi t$ and hence $U_{\text{crit}} = \sqrt{2}\pi t = 4.44t$. This is in good agreement with Fig. 13(right) where U_{crit} appears to be around $4.4t$. The slight difference between mean field theory and Stoner (Fig. 13 suggests U_{crit} a bit less than $4.4t$ while Stoner gives U_{crit} a bit more than $4.4t$) is a finite size effect. $N = 256$ was used in Fig. 13.

Exercise 25: Write a code to do mean field theory for the $d = 1$ Hubbard model and compute the critical U above which the ferromagnetic state is lower in energy than the paramagnetic one for $N_{\text{tot}} = 3N/4$. Verify that the critical U agrees with the Stoner criterion.

It is also interesting to work through the antiferromagnetic MFT solution in detail. The reason is the formal connection to many other problems in solid state physics. The most obvious is the opening of a gap in an energy band by a periodic potential $V(G)$ with wavevector G (e.g. see Ashcroft and Mermin). As discussed below, in the antiferromagnetic MFT solution, the up spin electrons move in a periodic potential resulting from the oscillating down

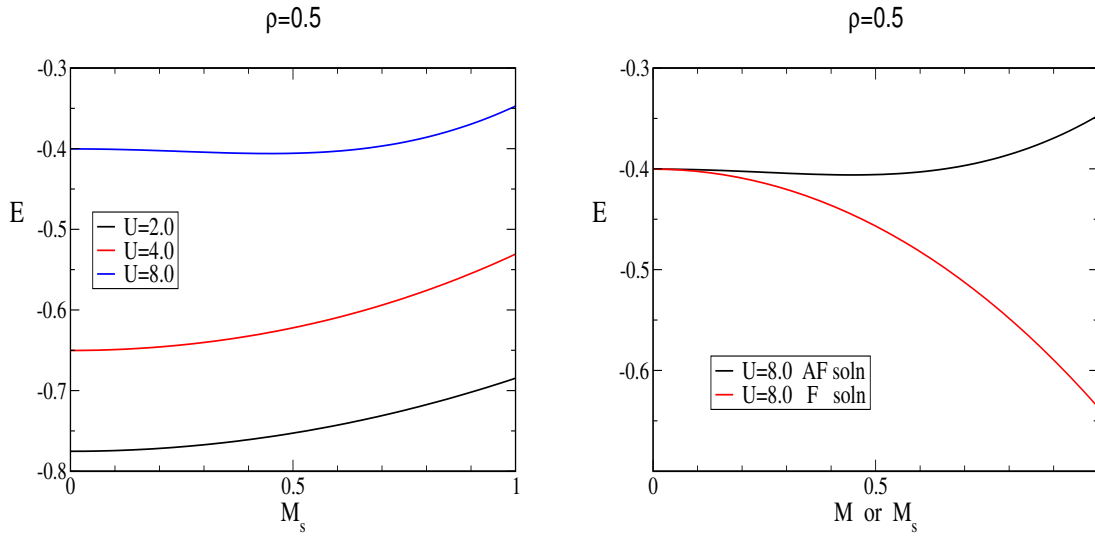


FIGURE 14. Left: Energy versus staggered magnetization of $d = 1$ Hubbard model at quarter filling, $\rho = \frac{1}{2}$ (128 electrons on an $N = 256$ site lattice). A paramagnetic state, $M_s = 0$, is favored at $U = 2.0t$ and $U = 4.0t$. Nonzero staggered magnetization with partial staggered spin polarization, $M_s = 21/48$, has lower energy than $M_s = 0$ at $U = 8.0t$. Right: However, the ferromagnetic solution has yet lower energy for this filling and interaction strength.

spin density (and vice-versa). A gap is opened at $k = \pm\pi/2$. There is also a connection to simple phonon problems where one makes the masses or spring constants vary. Again, the single phonon dispersion curve for uniform masses and springs breaks into two branches, optic and acoustic.

An antiferromagnetic configuration allows a simple *spatial* dependence in which the densities alternate by m_s , the ‘staggered magnetization’: $n_{l\uparrow} = n + (-1)^l m_s$, and $n_{l\downarrow} = n - (-1)^l m_s$. The even sites have a surplus of up spin electron density: $n_{\text{even}\uparrow} = n + m_s$, and $n_{\text{even}\downarrow} = n - m_s$. The odd sites have a surplus of down spin electron density: $n_{\text{odd}\uparrow} = n - m_s$, and $n_{\text{odd}\downarrow} = n + m_s$. Note that the total number of up and down electrons in the whole system is the same, nN , and that each site has the same total density $2n$.

The form of the Hamiltonian in mean field theory is, $H = \sum_{j,l} c_{j\sigma}^\dagger h_\sigma(j,l) c_{l\sigma}$, where $h_\sigma(j,l)$ has $-t$ just above and below the main diagonal, with $h_\uparrow(l,l) = U(n - (-1)^l m_s)$, or $h_\downarrow(l,l) = U(n + (-1)^l m_s)$ along the diagonal. When h is nonzero, the eigenvectors of momentum k and $k + \pi$ are mixed and the eigenvalues are, $E(k) = \pm\sqrt{(-2t\cos k)^2 + (Um_s)^2} + Un$. Here k is now defined in a ‘reduced zone’, $k = 2\pi/N\{-N/4 + 1, -N/4 + 2, \dots, +N/4\}$. The process for computing the energy of an antiferromagnetic configuration is basically the same as for ferromagnetism: the lowest energy levels are simply filled up. The difference is that here $N_\uparrow = N_\downarrow$ and one loops over different m_s .

Simple (Fortran) code

```

implicit none
integer i,N,Ntot,istag
real*8 t,U,tpin,k,ek,mstag
real*8 rho,Umstag,Urho
real*8 eaf,eaftot,lambdaminus

write (6,*) 'N,Ntot,t,U'
read (5,*) N,Ntot,t,U
write (36,*) Ntot/2+1

tpin=8.d0*datan(1.d0)/dfloat(N)
rho=dfloat(Ntot)/dfloat(N)
Urho=U*rho/2.d0

do 1000 istag=0,Ntot,2

```

```

mstag=dfloat(istag)/dfloat(N)
Umstag=U*mstag/2.d0

eaftot=0.d0
do 200 i=-Ntot/4+1,Ntot/4
  k=tpin*dfloat(i)
  ek = -2.d0*t*dcos(k)
  lambdaminus=-dsqrt(ek*ek+Umstag*Umstag)
  lambdaminus=lambdaminus+Urho
  eaftot=eaftot+lambdaminus
200  continue
  eaftot=2.d0*eaftot/dfloat(N)-U*(rho*rho-mstag*mstag)/4.d0

write(36,990) istag,eaftot
990  format(i6,f16.6)

1000 continue

end

```

Fig. 14(left) shows that antiferromagnetic solutions are not favored at quarter filling and weak coupling $U = 2t, 4t$: The energy is minimized for $M_s = 0$. For $U = 8t$, E has its minimum at nonzero M_s . However, as seen in Fig. 14(right) the ferromagnetic energy is lower still.

Fig. 15(left) shows the energy as a function of (ferromagnetic) magnetization m and (antiferromagnetic) staggered magnetization m_s for half-filling $\rho = 1$. While the ferromagnetic energy is minimized at $m = 0$, a lower value is obtained by a non-zero m_s . In Fig. 15(right) the staggered magnetization m_s which minimizes the energy is shown as a function of density ρ for different couplings. Let's consider the case of one quarter filling, that is, a density $n = n_\uparrow + n_\downarrow = 1/2$ electrons per site. For $U = 2$, $m_s = 0$ has lowest energy. From the preceding analysis it is seen that $m = 0$ is the lowest of the ferromagnetic energies. Thus the Hubbard model at $U/t = 2$ and $\rho = 1/2$ is paramagnetic. It is a simple matter to construct the MFT phase diagram by considering all choices of filling and coupling strength. (Fig. 15(right) has results for a range of U values.) The complete diagram is shown in Fazekas [4] and also by Hirsch [36].

MFT codes can also be written in the grand canonical ensemble where one provides a chemical potential μ and then computes N_\downarrow and N_\uparrow by filling those levels which are below μ . An advantage of this method is that one easily work at finite temperature. by accumulating $\epsilon_\sigma(k)$ times the Fermi function $1/[1 + e^{\beta(\epsilon_\sigma(k) - \mu)}]$ for the energy and the Fermi function alone for the density. Grand canonical approaches are also convenient since they generalize better to considering complex, density patterns ('striped phases' etc). There is no longer an analytic form for the energy levels but it is a simple (and fast) matrix diagonalization problem to get them. The site and spin dependent densities can be computed self-consistently from the eigenvalues and eigenvectors, and iterated to convergence. (However, be careful that it is fairly common for this iteration to get stuck in metastable patterns.)

Exercise 26: Write a finite temperature MFT code for the $d = 1$ Hubbard model in the grand canonical ensemble. Show that at half-filling the Neel temperature for antiferromagnetism increases linearly with U at strong coupling. The correct result, as seen in the discussion of the Heisenberg model, is that $T_{\text{Neel}} \propto t^2/U$.

In concluding the discussion of mean field theory, it should be emphasized that the approach, while very useful in yielding insight into the possible phases of the system, is a completely uncontrolled approximation. MFT overestimates the tendency for ordered phases, and can (and does) predict magnetic order where none occurs. Even if a particular phase transition is correctly predicted, the details of the transition (critical temperature, critical exponents, etc) are usually incorrect. These failures can be illustrated by noting that MFT gets the functional form of the Neel temperature wrong at strong coupling in the half-filled Hubbard model, giving $T_N \propto U$ rather than the correct $T_N \propto t^2/U$ seen from the mapping to the Heisenberg model. MFT does not distinguish the moment formation and moment ordering temperatures. MFT is also provides a fundamentally misleading picture of the physics, since it implies the existence of sharp (non-decaying) single particle energy levels which are just shifted from their $U = 0$ values. Instead, interactions also introduce a finite lifetime, a phenomena which MFT misses. Phrased more formally, MFT, like $U = 0$ produces a spectral function consisting of delta-function peaks. One of the great achievements of 'Dynamical Mean Field Theory' is that it includes the finite lifetime broadening of energy levels.

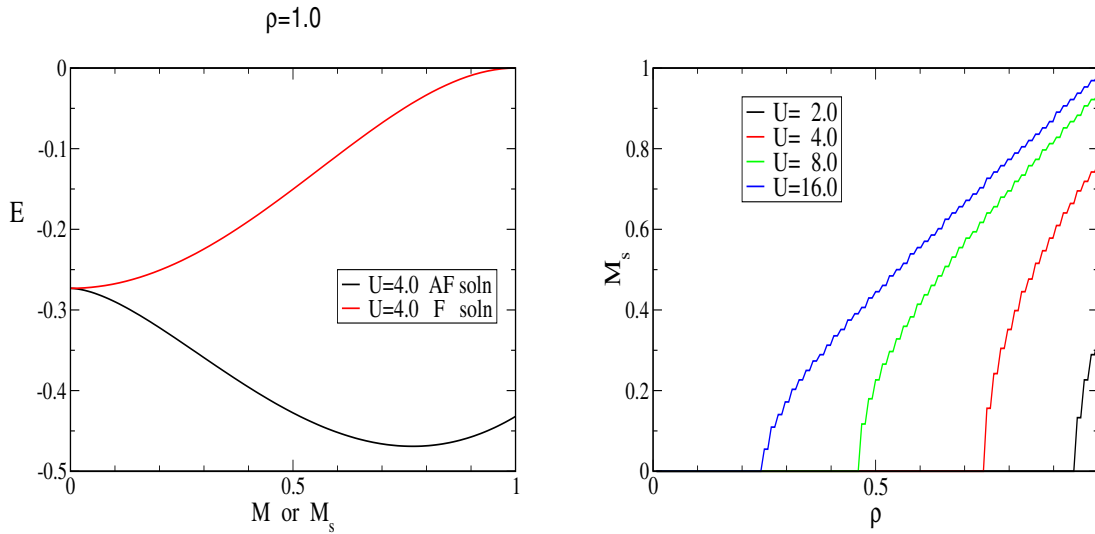


FIGURE 15. Left: Energy versus magnetization and staggered magnetization of $d = 1$ Hubbard model with $U = 4.0t$ and at half filling, $\rho = 1$ (256 electrons on an $N = 256$ site lattice). Nonzero staggered magnetization with partial staggered spin polarization, $M_s = 21/48$, has lower energy than $M_s = 0$. Unlike the quarter filled case of the right panel of Fig. 14 this antiferromagnetic solution is lower in energy than ferromagnetic ones. Right: Staggered magnetization which minimizes the energy, when restricted to the antiferromagnetic sector, as a function of filling, for different interaction strengths. In all cases, it is essential to check to see whether ferromagnetic solutions might be yet lower. Steps in the curves are a result of the finite lattice size.

III. DISORDER IN THE ABSENCE OF INTERACTIONS

A. The Anderson Transition

The development of insulating behavior of noninteracting electrons in a random potential is called ‘Anderson localization.’ To make contact with the material in these lectures, the Anderson transition can be examined as a particular instance of the Hubbard Hamiltonian at $U = 0$ with a spatially varying (random) chemical potential $-\mu \sum_{j\sigma} n_{j\sigma} \rightarrow -\sum_{j\sigma} \mu_j n_{j\sigma}$. Numerically, the Anderson transition then can be analyzed by diagonalizing matrices of dimension the number of spatial sites N (where of course the interest is in the thermodynamic limit, N large) which have the random chemical potential μ_j down the diagonal, and the hopping t in positions of the matrix corresponding to pairs of sites between which electrons can hop in the geometry in question.

The general picture is this: When randomness is turned on, the eigenstates with energies near the extremes of the density of states become localized, with those near the center remaining extended. As the randomness increases, the ‘mobility edges’ which demark the energies dividing localized from extended states move towards the center of the density of states. Given a fixed number of particles, when the mobility edge sweeps upward through E_F for increasing randomness, there is a metal to insulator transition. Alternately, the transition can be driven by varying particle number at fixed randomness, moving the Fermi level through the mobility edge. Ultimately, given sufficiently large randomness, it may be that all states are localized.

As for phase transitions in general, dimensionality plays a key role in whether the insulator-metal transition occurs. In one dimension, it is fairly easy to see that all states are localized by an arbitrarily small amount of randomness. Only the situation where there is zero disorder is metallic. The celebrated ‘gang-of-four’ paper [9] showed the much less trivial result that the same applies in two dimensions. As discussed previously, this was part of the basis for the conjecture that, perhaps, even when interactions are included, there is no metallic phase in two dimensions. Only in three dimensions does the above picture of the coexistence of localized and delocalized states, separated by a mobility edge, really apply.

Approaches to the inclusion of correlations in the Anderson localization problem form a vast field. However, within the context of ideas developed in these notes, one can easily imagine a MFT treatment of the problem. Disorder can be very simply included in a grand canonical MFT code for the Hubbard model through an additional random chemical potential term along the diagonal. A simple physical picture that the insulator to metal transition originates in a screening (reduction) of the disorder. This occurs because the sites with low energy ϵ_i have the highest local density $\langle n_i \rangle$ and the sites with greatest ϵ_i have the lowest local density. ϵ_i becomes screened to $\tilde{\epsilon}_i + U \langle n_i \rangle$, which has a smaller variance and thus represents a smoother energy landscape, in which the electrons might be more delocalized.

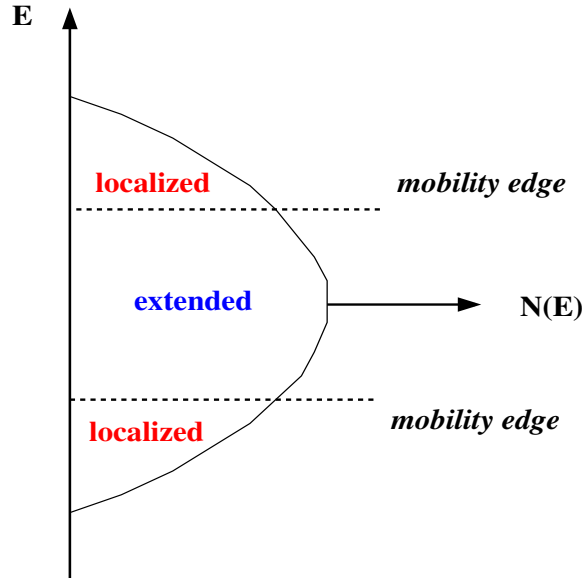


FIGURE 16. Disorder localizes states at the edges of the density of states. The mobility edge separates localized and extended states, and moves towards the band center as randomness increases.

Of course, in $d = 2$, since *any amount* of disorder localizes all the states, this metallic behavior cannot occur, and so the above picture is fatally flawed.

Exercise 27: Use a grand canonical MFT code to explore the localization-delocalization transition. Specifically, look at how the localization length and participation ratio (see below) of the eigenstates evolve as U is increased.

B. A Digression into Non-Hermiticity: The Hatano-Nelson Model

A non-Hermitian generalization of the Anderson Hamiltonian is the Hatano-Nelson model, which has been used to describe a number of phenomena, including the motion of flux lines in disordered type-II superconductors [48] and nuclear decay, dissipative systems, and quantum chromodynamics [49, 50, 51, 52, 53, 54, 55, 56, 57]. It is interesting here because it provides useful insight into the localization transition [48, 58], especially since, unlike the Anderson Hamiltonian, it allows for the existence of both localized and extended states in low dimension.

In one dimension, the Hatano-Nelson Hamiltonian is,

$$H = -\frac{t}{2} \sum_{l=1}^N (e^h c_{l+1}^\dagger c_l + e^{-h} c_l^\dagger c_{l+1}) + \sum_l \mu_l c_l^\dagger c_l. \quad (47)$$

The parameter h controls the asymmetry between the hopping amplitudes in the $+x$ and $-x$ directions. μ_l are a collection of random site energies which is chosen to have a uniform distribution on $[-\Delta/2, +\Delta/2]$. N is the number of lattice sites. The periodic boundary conditions which connect the two ends of the lattice have a fundamental influence on localization, as discussed further below. The choice of hopping parameter $t = 1$ sets the scale of energy,

When $\Delta = 0$, the eigenvalues of the Hatano-Nelson Hamiltonian are easily obtained,

$$\lambda(k) = \frac{1}{2} (e^h e^{ik} + e^{-h} e^{-ik}). \quad (48)$$

Here $0 < k < 2\pi$. The eigenvalues lie on an ellipse in the complex plane, centered at the origin, with a semimajor axis of length $2 \cosh h$ aligned with the real axis, and a semiminor axis of length $2 \sinh h$ aligned with the imaginary axis. When disorder is turned on, $\Delta \neq 0$, lines of real eigenvalues extend outward from this ellipse. Fig. 17 shows the eigenspectrum for $h = 0.2$ and $\Delta = 2$.

A crucial observation to make is the relationship between the location of the eigenvalue: on the ellipse (complex) or the wings (real), and the nature of the associated eigenvector. Consider the eigenvalue problem in component form,

$$-\frac{t}{2} e^h \psi_{l+1} + \mu_l \psi_l - \frac{t}{2} e^{-h} \psi_{l-1} = \lambda \psi_l.$$

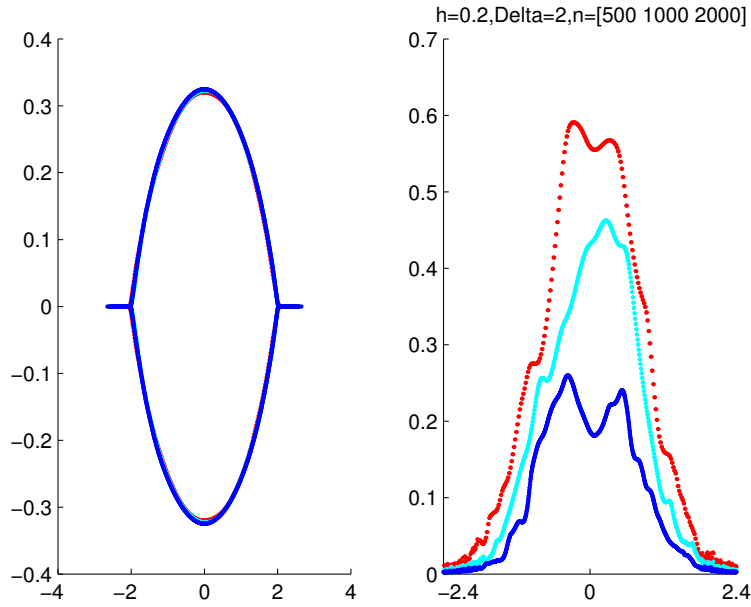


FIGURE 17. Left: Eigenspectrum of the Hatano-Nelson Hamiltonian with $h = 0.2$ and $\Delta = 2$. The eigenvalues are located on an ellipse centered at the origin, with two 'wings' extending out along the real axis. Right: Corresponding (normalized) participation ratios: \mathcal{P}_n/N . Numerical results were obtained for $N = 500, 1000, 2000$ sites, averaging over ten disorder realizations.

Performing the 'gauge transformation' $\psi_l = e^{-hl} \tilde{\psi}_l$ yields

$$-\frac{t}{2} \tilde{\psi}_{l+1} + \mu_l \tilde{\psi}_l - \frac{t}{2} \tilde{\psi}_{l-1} = \lambda \tilde{\psi}_l. \quad (49)$$

h has vanished from the equation and the eigenproblem of the (Hermitian) Anderson problem is recovered! Since the eigenstates are localized in $d = 1$ for the Anderson Hamiltonian, this analysis has seemingly proved the same to be true for the Hatano-Nelson model!

The flaw in this argument concerns the boundary conditions. The gauge transformation does not work if the ends of the $d = 1$ lattice are connected. This observation holds the key to connecting the topology of the eigenvalue phase diagram (complex ring with real wings) to whether the associated eigenvectors are extended or localized. Consider a localized eigenvector (and periodic boundary conditions). As described above, a gauge transformation which moves all the h factors away from the region of the lattice where the eigenvector is non-zero can be performed. For a localized eigenvector, the boundary conditions are irrelevant because by the time the edge of the lattice is reached, the eigenvector components are exponentially small. It is then plausible that the eigenvector will be described by the same properties as the Anderson Hamiltonian. Hence its eigenvalue will be real. The conclusion is that the eigenvectors whose eigenvalues lie on the real wings are localized.

Meanwhile, for delocalized eigenvectors, this reduction to the Anderson model fails, suggesting that the complex eigenvalues on the ring encircling the origin are delocalized. Fig. 17(right) shows the participation ratio,

$$\mathcal{P}_n = \left(\sum_{l=1}^N |\psi_l^n|^4 \right)^{-1} \quad (50)$$

a measure of the number of components which are 'large' for the eigenvector ψ^n with components ψ_l^n . Parameters are the same as Fig. 17(left). This plot is consistent with the above picture. The number of sites participating in eigenvectors with real eigenvalues does not grow with lattice size, and hence are localized. For complex eigenvalues the participation ratio grows roughly linearly with N . Of course, a more careful analysis of the finite size scaling is called for to make this completely compelling.

Perhaps not surprisingly for a problem concerning localization and transport, boundaries are crucial to the physics. The eigenvalues of the non-Hermitian matrix of the Hatano-Nelson Hamiltonian are *real* and identical to those of the Anderson Hamiltonian, when open boundary conditions are used, but differ dramatically otherwise. (Interestingly,

even in the case when periodic boundary conditions are included, the gauge transformation allows all the factors of h to be accumulated in a single link.)

Quite a bit is known analytically about the Hatano-Nelson model. For example, if the disordered site energies are taken from the Cauchy distribution,

$$p(\mu_l) = \frac{1}{\pi} \frac{\gamma}{\gamma^2 + \mu_l^2}, \quad (51)$$

then the height of the ellipse (parallel to the imaginary axis), gets reduced by γ while the base of the ellipse (parallel to the real axis) remains fixed! Since the ellipse height in the imaginary direction is $\sinh h$ (with $t = 1$), the ellipse gets completely squashed down when γ exceeds a critical value $\gamma_c = \sinh h$. The eigenspectrum is completely real (all eigenvalues localized) for $\gamma > \gamma_c$. The $d = 1$ Hatano-Nelson model thereby mimics what happens in the Anderson Hamiltonian only in higher dimension.

IV. PRESCRIPTION FOR DETERMINANT QUANTUM MONTE CARLO

A. Basic Formalism

These notes now turn to the Determinant Quantum Monte Carlo (DQMC) method. Section V shows that considerable insight can be obtained concerning the interplay of disorder and interactions with this approach. A possible goal for students going through these notes is to write, or at least begin to write, a DQMC code. In fact, this is a rather ambitious target. To make it a bit more feasible, this discussion begins with the prescription for writing a DQMC program, literally by writing down some ‘pseudo-code’ for it in the same way as for diagonalization. This makes the discussion succinct and understandable in the ‘what to do’ sense. Of course, it is unsatisfactory since nothing is proven. Appendix C presents the background derivations.

By now the discussion of MFT has emphasized that the non-interacting electron problem, that is, one whose Hamiltonian is quadratic in the fermion creation and destruction operators, can be rather easily solved by diagonalizing an appropriate matrix. DQMC works by reducing the interacting problem into a non-interacting one! In order to do this, a classical Hubbard-Stratonovich field is introduced to decouple the interaction. The Monte Carlo then sums over different field configurations. Appendix C provides the details. For now, these notes simply describe how to construct the matrix used in the simulation.

Consider the part of \hat{H} which includes the terms which are quadratic in the fermion creation and destruction operators, eg the hopping and site energies (chemical potential),

$$\hat{K} = \sum_{\sigma} \begin{pmatrix} c_{1\sigma}^{\dagger} & c_{2\sigma}^{\dagger} & \dots \end{pmatrix} \begin{pmatrix} k_{11} & k_{12} & \dots \\ k_{21} & k_{22} & \dots \\ \vdots & \vdots & \ddots \end{pmatrix} \begin{pmatrix} c_{1\sigma} \\ c_{2\sigma} \\ \vdots \end{pmatrix} \quad (52)$$

k is defined to be the $N \times N$ matrix with elements $\Delta\tau k_{ij}$.

As an example, for a one dimensional Hubbard model with $N = 6$ sites, nearest neighbor hopping, no disorder, and periodic boundary conditions,

$$k = \Delta\tau \begin{pmatrix} -\mu & -t & 0 & 0 & 0 & -t \\ -t & -\mu & -t & 0 & 0 & 0 \\ 0 & -t & -\mu & -t & 0 & 0 \\ 0 & 0 & -t & -\mu & -t & 0 \\ 0 & 0 & 0 & -t & -\mu & -t \\ -t & 0 & 0 & 0 & -t & -\mu \end{pmatrix} \quad (53)$$

The matrix k will be one of the ingredients in constructing the probability used in the DQMC simulation.

For reasons made clear in Appendix C, in DQMC it is necessary to divide the inverse temperature β into L ‘imaginary time intervals’, $\beta = L\Delta\tau$. The length of each interval $\Delta\tau$ should be chosen such that $tU(\Delta\tau)^2 < 1/10$. The interaction term U is then included via the ‘Hubbard-Stratonovich field’ $s(i, l)$ which has a spatial index $i = 1, 2, \dots, N$ and an ‘imaginary time index’ $l = 1, 2, \dots, L$ and takes on values $s(i, l) = \pm 1$. (This discrete version of the Hubbard-Stratonovich transformation introduced by Hirsch [36] is more efficient than a continuous one.) Again, the reader is referred to Appendix C for the details. The bottom line is that the simulation begins by filling the array $s(i, l)$ randomly

with values ± 1 . One then defines a set of L diagonal matrices, each of dimension N ,

$$v_{\uparrow}(l) = \lambda \begin{pmatrix} s(1,l) & 0 & 0 & 0 & \cdots \\ 0 & s(2,l) & 0 & 0 & \cdots \\ 0 & 0 & s(3,l) & 0 & \cdots \\ 0 & 0 & 0 & s(4,l) & \cdots \\ \vdots & \vdots & \vdots & \vdots & \ddots \end{pmatrix} \quad (54)$$

Here the parameter λ is given by $\cosh \lambda = e^{U\Delta\tau/2}$. The matrices for the down spin electrons differ only by a sign: $v_{\downarrow}(l) = -v_{\uparrow}(l)$.

The next step is to compute the up and down ‘Green’s functions’,

$$G_{\sigma} = [I + e^k e^{v_{\sigma}(1)} e^k e^{v_{\sigma}(2)} e^k e^{v_{\sigma}(3)} \dots e^k e^{v_{\sigma}(L)}]^{-1} \quad (55)$$

Here I is the N dimensional identity matrix.

In order to sample the Hubbard-Stratonovich field configurations, suggest a change in $s(i, l) \rightarrow -s(i, l)$ on the first spatial site $i = 1$ of imaginary time slice $l = L$. Compute the quantities,

$$\begin{aligned} d_{\uparrow} &= 1 + (1 - [G_{\uparrow}]_{ii}) (e^{-2\lambda s(i,l)} - 1) \\ d_{\downarrow} &= 1 + (1 - [G_{\downarrow}]_{ii}) (e^{+2\lambda s(i,l)} - 1) \\ d &= d_{\uparrow} d_{\downarrow}. \end{aligned} \quad (56)$$

Next throw a uniformly distributed random number, $0 < r < 1$. If $r < d$, accept the update of the Hubbard Stratonovich field by setting $s(i, l) = -s(i, l)$.

If the move was accepted, the Green’s functions, which depend on s (see Eqs. 54-55) will now be different. One could recompute G_{σ} from Eq. 55, using the new s . This will take a time which goes as N^3 , since it involves a matrix inversion. There’s a faster (order N^2) trick to get the new G_{σ} , which takes advantage of the fact that only one element in one of the $v_{\sigma}(l)$ has changed. Compute the vectors,

$$\begin{aligned} a_{k\uparrow} &= -(e^{-2\lambda s(i,l)} - 1) [G_{\uparrow}]_{ik} + \delta_{ki} (e^{-2\lambda s(i,l)} - 1) \\ a_{k\downarrow} &= -(e^{+2\lambda s(i,l)} - 1) [G_{\downarrow}]_{ik} + \delta_{ki} (e^{+2\lambda s(i,l)} - 1) \\ b_{j\uparrow} &= [G_{\uparrow}]_{ji} / (1 + c_{i\uparrow}) \\ b_{j\downarrow} &= [G_{\downarrow}]_{ji} / (1 + c_{i\downarrow}) \end{aligned} \quad (57)$$

Here δ_{ij} is the usual Kronecker δ . Remember that i, l is the fixed site (time slice) whose Hubbard-Stratonovich field is being updated. The free indices j, k run from 1 to N . Then the new G_{σ} are given by

$$[G_{\sigma}]_{jk} = [G_{\sigma}]_{jk} - b_{j\sigma} a_{k\sigma}. \quad (58)$$

The interaction energy matrix (Eq. 54) is updated if the move is accepted. After the new G_{σ} are computed, go to Hubbard-Stratonovich field on the second spatial site $i = 2$ on imaginary time slice $l = L$ and suggest a change to it, and follow the procedure of Eq. 56 again to see if the move is accepted and Eqs. 57-58 to update G if it is. Continue this until all spatial sites of time slice $l = L$ are updated.

After all spatial sites i of imaginary time slice $l = L$ have been updated, change the Green’s functions via,

$$G_{\sigma} = [e^k e^{v_{\sigma}(l)}] G_{\sigma} [e^k e^{v_{\sigma}(l)}]^{-1} \quad (59)$$

This ‘wrapping’ replaces the exponential of $v_{\sigma}(L)$ by that of $v_{\sigma}(L-1)$ at the end of the string of matrices in Eq. 55. The Hubbard-Stratonovich variables on imaginary time slice $l = L-1$ can now be updated following the procedures of Eqs. 56-58. When all spatial sites of imaginary time slice are finished, wrap the Greens functions using Eq. 59 again. Continue the process of Eqs. 56-59 until all imaginary time slices are updated.

After completing an entire set of updates to all the space-time points of the lattice, make measurements. For example, the density of electrons of spin σ on site i is given by,

$$\langle n_{i\sigma} \rangle = 1 - [G_{\sigma}]_{ii}. \quad (60)$$

The double occupancy rate on site i is

$$\langle n_{i\uparrow} n_{i\downarrow} \rangle = (1 - [G_{\uparrow}]_{ii}) (1 - [G_{\downarrow}]_{ii}) \quad (61)$$

The local moment on site i is,

$$\langle (n_{i\uparrow} - n_{i\downarrow})^2 \rangle = \langle n_{i\uparrow} + n_{i\downarrow} \rangle - 2\langle n_{i\uparrow}n_{i\downarrow} \rangle. \quad (62)$$

The spin correlation function between moments on sites i and j , for $i \neq j$, is given by,

$$\begin{aligned} S_{+i} &= c_{i\uparrow}^\dagger c_{i\downarrow} \\ S_{-j} &= c_{j\downarrow}^\dagger c_{j\uparrow} \\ \langle S_{+i} S_{-j} \rangle &= -[G_\uparrow]_{ji} [G_\downarrow]_{ij} \end{aligned} \quad (63)$$

You can also measure pairing correlations, charge density wave correlations, etc.

A full simulation consists of performing the above updates of all the Hubbard-Stratonovich variables of the space-time lattice for several hundred ‘equilibration’ sweeps *without* making any measurements. This is followed by a few thousand ‘measurement’ sweeps in which you perform the update operations and also the measurements.

Note that there are a number of alternate Quantum Monte Carlo approaches to the Hubbard Hamiltonian closely related to that discussed here. These include a ground state projection method [34, 35], and approximate techniques which deal with the sign problem [68]. Dynamical mean field theory [69, 70, 71], especially when it employs the Hirsch-Fye QMC method [72] as its impurity solver, is a method of particular appeal since it not only provides a solution to tight-binding models (with the limit where the momentum dependence of the self-energy is neglected) but also offers a powerful methodology with which to put together electronic structure and many body physics.

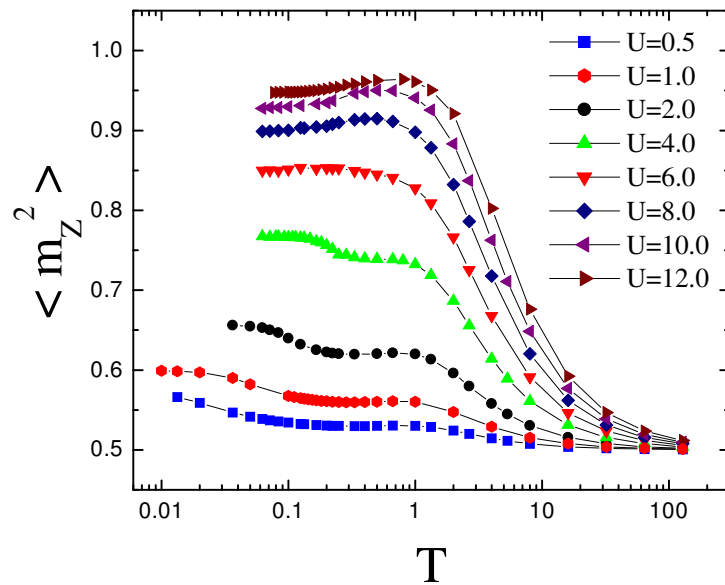


FIGURE 18. The local moment $\langle m_z^2 \rangle$ as a function of temperature for different interaction strengths U and lattice size 6×6 . The lattice is half-filled.

B. Results: Local Moment, Spin Correlation, and Specific Heat

The evolution of the local moment (Eq. 62) at half-filling as the temperature is decreased is shown in Fig. 18 on a 6×6 lattice for different interaction strengths U . The local moment begins to develop from its uncorrelated value $1/2$ at a temperature set by U , and then saturates at low T . The local moment does not reach 1 at $T = 0$ because significant quantum fluctuations allow doubly occupied and empty sites to occur even in the ground state. (Compare with Fig. 8.) However, as U/t increases, these fluctuations are suppressed and the moment becomes better and better formed. The local moment also makes a further small adjustment at low T , which is due to the onset of magnetic order.

The specific heat $C(T)$ (Fig. 19) is determined by the energy. It shows an interesting two peak structure. The high temperature peak is associated with the formation of local moments, and the low temperature peak with their ordering.

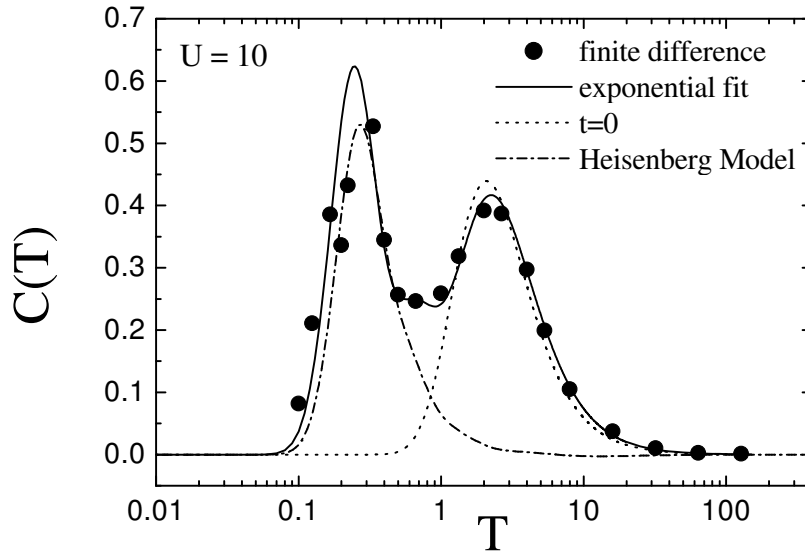


FIGURE 19. The specific heat of the Hubbard model for $U = 10t$. There is a high temperature peak which is fit well by considering a single site Hubbard model ($t = 0$) and a low temperature peak which agrees well with the Heisenberg model with $J = 4t^2/U = 0.4$.

The Hubbard model maps onto the Heisenberg model at large U . This connection is emphasized in Fig. 19 which shows that the low temperature peak in the specific heat of the Hubbard model can be mapped onto that of the Heisenberg model with $J = 4t^2/U$.

The near-neighbor spin correlation is shown in the top panel of Fig. 20. The bottom panel is the magnetic structure factor $S(\pi, \pi) = \frac{1}{N} \sum_{ij} \langle S_{z,i} S_{z,j} \rangle$ which sums the spin-spin correlations over the whole lattice. It is found that $S(\pi, \pi)$ grows linearly with N at low T , indicating that the correlations extend over the whole lattice. A finite size scaling analysis of these quantities can be used to demonstrate the existence of long range order in the ground state of the half-filled Hubbard model on a square lattice [36]. Finally, Fig. 21 shows the density of states at $\omega = 0$ for the half-filled Hubbard model at different values of U . The suppression of $N(\omega = 0)$ at low T and large U is a signature of the presence of an insulating gap caused by the on-site repulsion.

V. DQMC FOR THE ANDERSON-HUBBARD HAMILTONIAN

These notes have now provided an overview of simple analytic approaches to the Hubbard model- weak and strong coupling and mean field theory. The basics of the DQMC method have also been established. This section presents the results of such DQMC simulations, specifically of the Anderson-Hubbard Hamiltonian, that is, studies of the interplay of disordered one-body potential and two-body interactions. The effect of this interplay and of a Zeeman field on magnetism, thermodynamics, and metal-insulator transitions will be shown. The final topic concerns the effect of interactions on the band insulating phase which arises from a periodic potential, as opposed to a random one. Journal references are given at the beginning of each subsection.

A. Interaction driven Anderson Insulator to Metal Transition

Journal Reference: "Conducting phase in the two-dimensional disordered Hubbard model", P.J.H. Denteneer, R.T. Scalettar, and N. Trivedi, Phys. Rev. Lett. **83**, 4610 (1999).

As discussed in Section I, the central question motivated by experiments on silicon metal-oxide semiconductor field effect transistors is whether electron-electron interactions enhance the conductivity of a 2D disordered electron system, and possibly lead to a conducting phase and a metal-insulator transition. This question can be addressed by

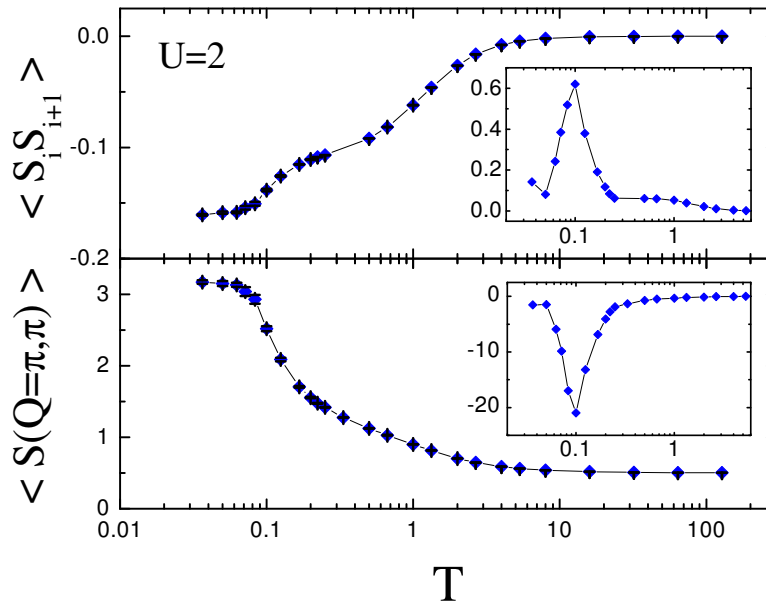


FIGURE 20. The near neighbor spin correlations and magnetic structure factor of the half-filled Hubbard model at $U = 2t$.

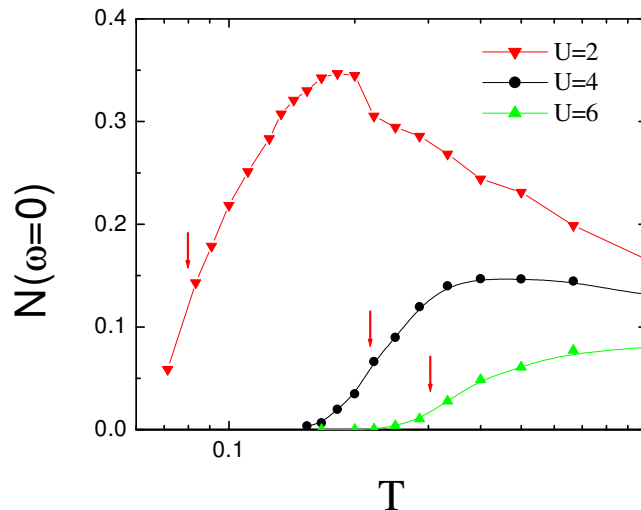


FIGURE 21. The density of states at $N(\omega = 0)$. As T is lowered, a Mott-Hubbard gap opens up. The half-filled Hubbard model is insulating.

studying the disordered Hubbard (or ‘Anderson-Hubbard’ model, which contains both relevant ingredients. Renormalization arguments suggest that the precise location of disorder is not important, since under changes of length scale randomness in one parameter introduces randomness into others. This is, in fact, not true if symmetries protect the spread of randomness. Initially the focus of the work here will be on bond randomness. It will be shown later that, indeed, different types of disorder can lead to different physics.

While the Hubbard model does not include the long range nature of the Coulomb repulsion, studying the simpler model of screened interactions is an important first step in answering the central qualitative question posed above.

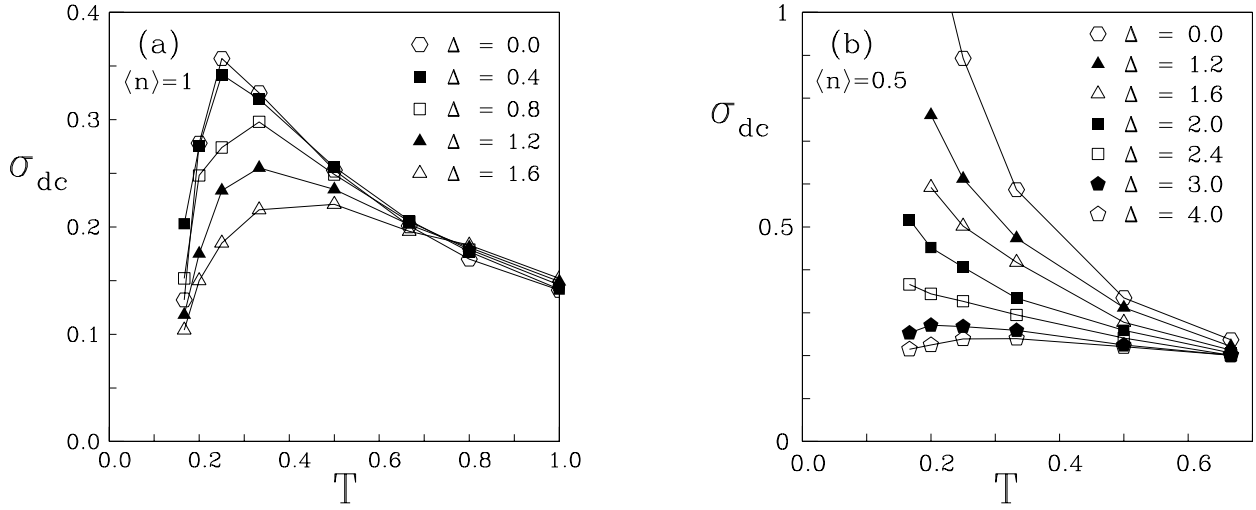


FIGURE 22. Conductivity σ_{dc} as a function of temperature T for various values of disorder strength Δ at $U = 4$ for (a) half-filling ($\langle n \rangle = 1$) and (b) $\langle n \rangle = 0.5$. Calculations are performed on an 8×8 square lattice; data points are averages over 4 realizations for a given disorder strength.

The Determinant Quantum Monte Carlo simulation techniques introduced in Section IV avoid the limitations of perturbative approaches (while of course being confronted with others). Recent studies using very different techniques have indicated that interactions may enhance conductivity: two interacting particles in a random potential experience a mutual delocalizing effect [31], and weak Coulomb interactions were found to increase the conductance of spinless electrons in (small) strongly disordered systems [32].

The quantity of immediate interest when studying a possible metal–insulator transition is the *conductivity* and especially its T -dependence. By the fluctuation–dissipation theorem σ_{dc} is related to the zero-frequency limit of the current-current correlation function. A complication of the QMC simulations is that the correlation functions are obtained as a function of *imaginary* time. To avoid a numerical analytic continuation procedure to obtain frequency-dependent quantities, which would require Monte Carlo data of high accuracy, one can employ an approximation that was used and tested in studies of the superconductor–insulator transition in the attractive Hubbard model [44]. This approximation is valid when the temperature is smaller than an appropriate energy scale in the problem. Additional checks and applicability to the present problem are discussed below. The approximation allows σ_{dc} to be computed directly from the wavevector \mathbf{q} - and imaginary time τ -dependent current-current correlation function $\Lambda_{xx}(\mathbf{q}, \tau)$:

$$\sigma_{dc} = \frac{\beta^2}{\pi} \Lambda_{xx}(\mathbf{q} = 0, \tau = \beta/2). \quad (64)$$

Here $\beta = 1/T$, $\Lambda_{xx}(\mathbf{q}, \tau) = \langle j_x(\mathbf{q}, \tau) j_x(-\mathbf{q}, 0) \rangle$, and $j_x(\mathbf{q}, \tau)$ the \mathbf{q} , τ -dependent current in the x -direction, is the Fourier transform of $j_x(\ell) = i \sum_{\sigma} t_{\ell+\hat{x}, \ell} (c_{\ell+\hat{x}, \sigma}^\dagger c_{\ell \sigma} - c_{\ell \sigma}^\dagger c_{\ell+\hat{x}, \sigma})$. (See also Ref. [73]).

As a test for the conductivity formula (Eq. 64) Fig. 22(a) presents results for $\sigma_{dc}(T)$ at half-filling for $U = 4$ and various disorder strengths Δ . The behavior of the conductivity shows that as the temperature is lowered below a characteristic gap energy, the high T “metallic” behavior crosses over to the expected low T Mott insulating behavior for all Δ , thereby providing a reassuring check of the formula and of the numerics. Fig. 22(b) shows $\sigma_{dc}(T)$ for a range of disorder strengths at density $\langle n \rangle = 0.5$ and $U = 4$. The figure displays a change from metallic behavior at low disorder to insulating behavior above a critical disorder strength, $\Delta_c \simeq 2.7$. If this persists to $T = 0$ and in the thermodynamic limit, it would describe a ground state metal–insulator transition driven by disorder.

In order to obtain a more precise understanding of the role of interactions on the conductivity, Fig. 23 compares the results of Fig. 22(b) with the disordered *non-interacting* σ_0 [74]. The comparison is made at strong enough disorder $\Delta = 2.0$ that the localization length is less than the lattice size and the non-interacting system is therefore insulating with $d\sigma_0/dT > 0$ at low T . Interactions are found to have a profound effect on the conductivity: in the high-temperature

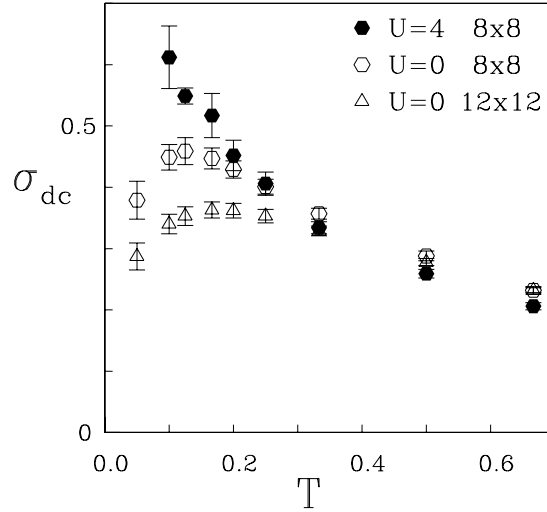


FIGURE 23. Conductivity σ_{dc} as a function of temperature T comparing $U = 4$ and $U = 0$ at $\langle n \rangle = 0.5$ and disorder strength $\Delta = 2.0$. Data points are averages over many realizations for this disorder strength (see text). Error bars are determined by the disorder averaging and not the Monte Carlo simulation.

“metallic” region, interactions slightly reduce σ compared to the non-interacting σ_0 behavior. On the other hand in the low-temperature “insulating” region of σ_0 the data shows that upon turning on the Hubbard interaction the behavior is completely changed with $d\sigma/dT < 0$, characteristic of metallic behavior. This is the regime of interest for the MIT.

To ascertain that the phase produced by repulsive interactions at low T is not an insulating phase with a localization length larger than the system size but a true metallic phase one can study the conductivity response for varying lattice sizes. There is a markedly different size dependence for the $U = 0$ insulator and the $U = 4$ metal, resulting in a confirmation of the picture given above. For $U = 0$, the conductivity on a larger (12×12) system is *lower* than that on a smaller (8×8) system (see Fig. 23), consistent with insulating behavior in the thermodynamic limit, whereas for $U = 4$ the conductivity on the larger (8×8) system is *higher* than that on the smaller (4×4) system (data not shown), indicative of metallic behavior. Thus the enhancement of the conductivity by repulsive interactions becomes more pronounced with increased lattice size [75].

Concerning finite-size effects for the non-interacting system, note that at lower values of Δ , where the localization length exceeds the lattice size, σ_0 shows “metallic” behavior which is diminished upon turning on the interactions [76]. Based on the analysis above, one would predict that at low enough T and large enough lattice size, the conductivity curves for the non-interacting σ_0 and interacting σ cross with $\sigma > \sigma_0$ at sufficiently low T .

To obtain information on the spin dynamics of the electrons and because it is a quantity often discussed in connection with the localization transition, one can also compute the spin susceptibility χ as a function of T (through $\chi(T) = \beta S_0(T)$ where S_0 is the magnetic structure factor at wavevector $\mathbf{q} = 0$). Fig. 24 shows two things: 1) $\chi(T)$ is enhanced by interactions with respect to the non-interacting case (at fixed disorder strength), and 2) starts to diverge when T is lowered, both on the metallic ($\Delta = 2$) and insulating ($\Delta = 4$) sides of the alleged transition. This is in agreement with experimental and theoretical work on phosphorus-doped silicon, where a (3D) MIT is known to occur and the behavior is explained by the existence of local moments[77], and also with diagrammatic work on 2D disordered, interacting systems[14].

To establish definitively the existence of a possible quantum phase transition in the disordered Hubbard model requires: (i) Extending the present data at $T = 0.1 = W/80$, where W is the non-interacting bandwidth, to lower T , which is however difficult because of the sign problem. (ii) A more detailed analysis of the scaling behavior in both linear dimension and some scaled temperature. (iii) A more accurate analytic continuation procedure to extract the conductivity. The condition for the validity of the approximate formula (Eq. 64) for $\sigma_{dc}(T)$, requires that T be less than an appropriate energy scale which is fulfilled within the two phases, but breaks down close to a quantum phase transition where the energy scale vanishes.

Given the well-known difficulty of DQMC simulations resolving the issue of d -wave superconductivity in the clean

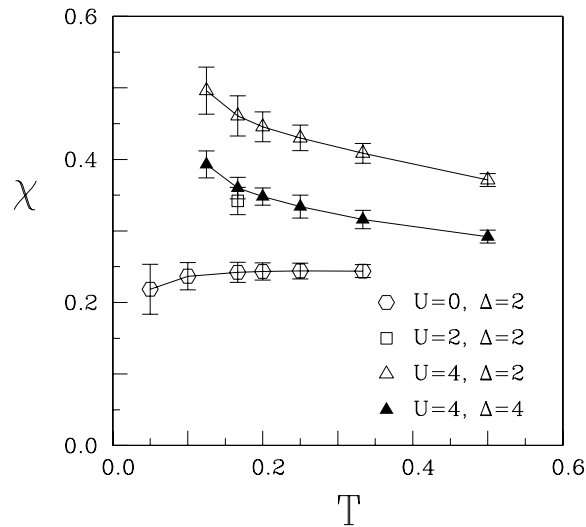


FIGURE 24. Spin susceptibility χ as a function of temperature T at $\langle n \rangle = 0.5$ comparing interaction strengths $U = 0, 2, 4$ and disorder strengths $\Delta = 2, 4$. Calculations are performed on 8×8 square lattices; error bars are from disorder averages over up to 8 realizations.

Hubbard model because of the sign problem mentioned in (i) above, it is worth discussing briefly why more definitive results are obtainable in this study of the MIT. The most important reason concerns the higher temperature scale of the phenomenon: interactions enhance the conductivity and lead to metallic behavior in a temperature range (about $1/10$ of the Fermi energy) here, similar to that of experiments. In the cuprates, although the transition temperatures are very high by the standards of other superconductors, they are of the order of $1/100$ of the Fermi energy, a factor of ten lower. Furthermore, the region of highest transition temperature is, very unfortunately, at a doping $\rho \approx 1 - \frac{1}{8}$ where the sign problem in the simulations is worst.

In summary, the temperature-dependent conductivity $\sigma(T)$ and spin susceptibility $\chi(T)$ of a model for two-dimensional electrons containing both disorder and interactions has been described. The Hubbard repulsion can enhance the conductivity and lead to a clear change in sign of $d\sigma/dT$. More significantly, a finite size scaling analysis demonstrates that repulsive interactions can drive the system from one phase to a different phase. $\sigma(T)$ has the opposite behavior as a function of system size in the two phases indicating that the transition is from a localized insulating to an extended metallic phase. The $\chi(T)$ data further suggests the formation of an unusual metal, a non-Fermi liquid with local moments. While the simplicity of the model studied prevents any quantitative connection to recent experiments on Si-MOSFETs, there is nevertheless an interesting qualitative similarity between Fig. 22(b) and the experiments. (See Fig. 1.) Varying the disorder strength Δ at fixed carrier density $\langle n \rangle$, as in the calculations, can be thought of as equivalent to varying carrier density at fixed disorder strength, as in experiments, since in a metal-insulator transition one expects no qualitative difference between tuning the mobility edge through the Fermi energy (by varying Δ) and *vice-versa* (by varying $\langle n \rangle$). This work then suggests that electron-electron interaction induced conductivity plays a key role in the 2D metal-insulator transition.

B. Effect of Zeeman Field

Journal Reference: "Interacting electrons in a two-dimensional disordered environment: Effect of a Zeeman magnetic field", P.J.H. Denteneer and R.T. Scalettar, Phys. Rev. Lett. **90**, 246401 (2003).

A hundred years after the Nobel prize was awarded in 1902 for the discovery of the Zeeman effect and the subsequent explanation by Lorentz, applying a magnetic field continues to be a powerful means to elucidate puzzling phenomena in nature. One of the most recent examples is to the topic of these notes: the interplay of interactions and disorder in electronic systems and the pioneering experiments on the metal-insulator transition (MIT) in effectively

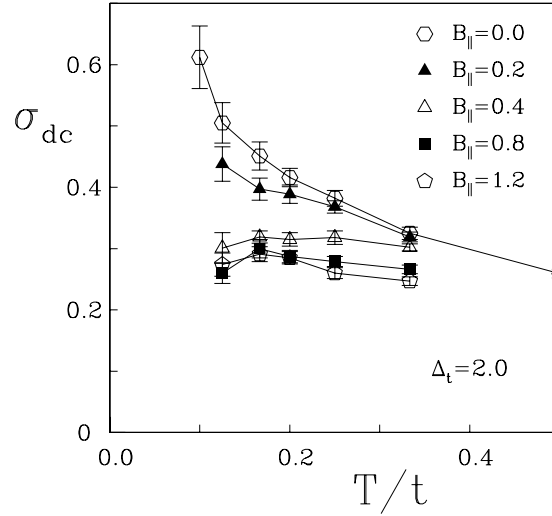


FIGURE 25. Conductivity σ_{dc} (in units of e^2/\hbar) as a function of temperature T for various strengths of Zeeman magnetic field B_{\parallel} . As B_{\parallel} increases, a transition from metallic to insulating behavior is seen in σ_{dc} . Calculations are performed on 8×8 lattices for $U/t = 4$ at density $\langle n \rangle = 0.5$ with disorder strength $\Delta_r = 2.0$ (see text); error bars result from averaging over typically 16 quenched disorder realizations. B_{\parallel} and Δ_r are given in units of t .

two-dimensional low-density silicon metal-oxide-semiconductor field-effect transistors (MOSFETs) discussed earlier [16, 17, 18].

Contrary to the well-known effect of a magnetic field in weak-localization theory to disturb interference phenomena and hence *undo* localization and insulating behavior, the negative magnetoresistance effect [2], in the Si MOSFETs and similar heterostructures, the magnetic field is found to suppress the metallic behavior and therefore *promote* insulating behavior [20, 78, 79]. The effect is present for all orientations of the magnetic field relative to the 2D plane of the electrons. In particular, a Zeeman magnetic field, applied parallel to the 2D plane of electrons and therefore coupling only to the spin, and not the orbital motion of the electrons, has been used extensively. This puts into focus the important role played by the spin degree of freedom of the electron, and its polarization [80, 81, 82, 83].

This section continues the DQMC study of the Anderson-Hubbard Hamiltonian, but now includes the effect of a Zeeman magnetic field, that is, an additional term in H of the form,

$$+B_{\parallel} \sum_{j\sigma} \sigma n_{j\sigma} \quad (65)$$

While the numerical evidence is mixed concerning the occurrence of a MIT due to interactions, [84, 85, 86, 87] there is a consensus in favor of a Zeeman magnetic field tuned transition [86, 87, 88, 89], as described in more detail below.

The main focus of this work continues to be on the conductivity, although now the B_{\parallel} -dependence is explored as well as the T -dependence. Another interesting quantity to study in conjunction with the magnetoconductivity is the degree of spin-polarization P of the electronic system:

$$P = \frac{n_{\downarrow} - n_{\uparrow}}{n_{\downarrow} + n_{\uparrow}}, \quad (66)$$

where $n_{\downarrow}, n_{\uparrow}$ are the average spin-densities of the corresponding number operators.

In order to study the effect of the Zeeman magnetic field B_{\parallel} on the metallic behavior, one can start from the case with density $\langle n \rangle = 0.5$ and disorder strength $\Delta_r = 2.0$ for which the model exhibits clear metallic behavior: σ_{dc} rising when lowering temperature T [90]. Fig. 25 shows that turning on B_{\parallel} reduces the conductivity and suppresses the metallic behavior; at field strength $B_{\parallel} = 0.4$, σ_{dc} appears T -independent (within the error bars), and at larger field

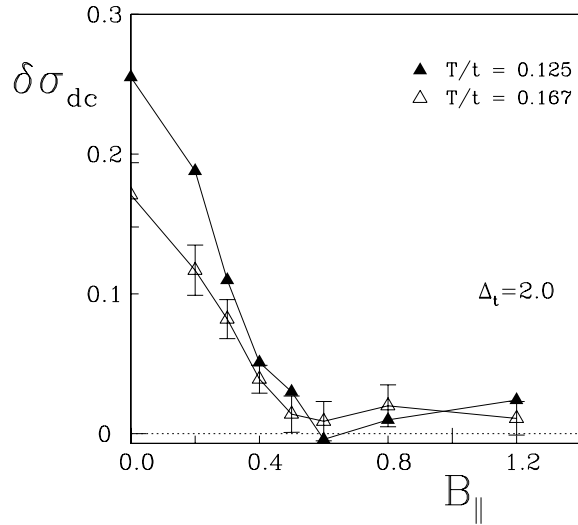


FIGURE 26. Conductivity difference $\delta\sigma_{dc} \equiv \sigma_{dc}(B_{||}, T) - \sigma_{dc}(B_{||} = 4, T)$, with conductivity at very high B -field subtracted, as a function of $B_{||}$ for low temperature T . A sharp onset of conductivity is seen at a Zeeman field at which the slope of $\sigma_{dc}(T)$ changes sign in Fig. 25. Computational details and units are as in Fig. 25; for clarity, only error bars on $T = t/6$ -data are shown; those on $T = t/8$ -data are typically slightly larger (cf. Fig. 25).

strengths shows a tendency to decrease upon lowering T . σ_{dc} does not go to zero, as for a real insulator, unless very low T and very large lattices (out of reach of the computational approach) are employed. Nevertheless, Fig. 25 shows the qualitative features of a magnetic-field-driven metal–insulator transition, similar to what is seen in experiment [20, 78, 79]. Previous numerical approaches using different techniques have also produced this effect [86, 87, 88].

The physical picture of this metal to insulator transition is the following: Since the effect of $B_{||}$ is to polarize the electronic system (with the sign choice in Eq. 60), n_{\downarrow} is promoted at the expense of n_{\uparrow} , a large enough $B_{||}$ will result in electrons with spin down only and, because of the nature of the Hubbard interaction, in a non-interacting system [91]. Therefore, in the limit of large 2D lattices and low temperature, the hopping disorder will force the conductivity to vanish. The nonzero value of σ_{dc} at very large $B_{||}$ is then a direct measure of the systematic errors due to finite size and non-zero T . In Fig. 27, this value is subtracted, and fields close to $B_{||} = 0.4$ are the primary focus. The resulting $\delta\sigma_{dc}$ vs. $B_{||}$ for the lowest temperatures is a rather abrupt onset of $\delta\sigma_{dc}$ below $B_{||} \approx 0.5$, which is about the field value where the curves of σ_{dc} vs. T change from insulating to metallic (Fig. 25). The data for a 2D system in Fig. 26 are consistent with a linear vanishing of $\delta\sigma_{dc}$ as the (quantum) critical point is approached. At present, the results, while presenting compelling evidence for the transition itself, are clearly not precise enough to obtain critical exponents. Interestingly, a transition from insulator to metal upon increasing magnetic field, i.e. the known negative magnetoresistance effect, occurs in an amorphous three-dimensional Gd-Si alloy (showing a MIT at zero field), also with a linear vanishing of the conductivity [92]. While it is possible that these observations are unrelated, it is also conceivable that this is an indication of a, yet hidden, connection between the two transitions.

Fig. 27 exhibits the *resistivity* ρ ($\equiv 1/\sigma_{dc}$) as a function of $B_{||}$ for low T . The crossing point (between $B_{||} = 0.3$ and 0.4) demarks a critical field strength B_c which separates fields for which the resistivity decreases when lowering temperature (low-field metallic behavior) from fields for which ρ increases upon lowering T (high-field insulating behavior). It is especially noteworthy that the critical field strength (which can be roughly estimated to lie between 0.3 and 0.5 from Figs. 26 and 27) is clearly lower than the field for which full spin-polarization sets in. Indeed, Fig. 28 shows how the spin polarization P , defined in (66), behaves as a function of $B_{||}$ at the lowest temperature used: there is no reflection of the critical field strength in the behavior of the polarization, and full spin-polarization only happens for $B_{||} > 1.2$. This feature of the data is in agreement with recent experiments performed on 2D electron- and hole-gases in GaAs and AlAs [82, 83]. Since complete spin-polarization is equivalent to a non-interacting system, the separation of the two field strengths and the incomplete polarization at the MIT present evidence that the Zeeman field tuned MIT

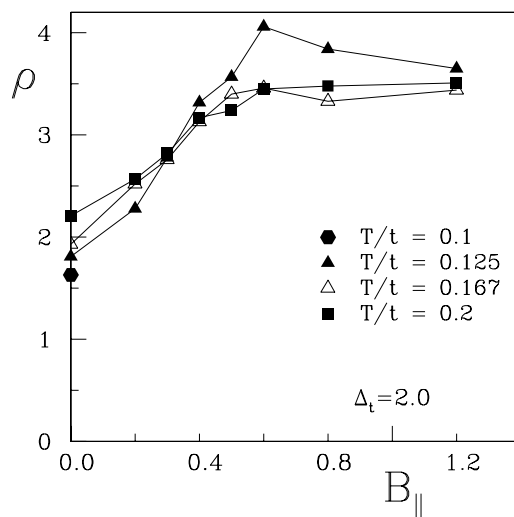


FIGURE 27. Resistivity ρ as a function of $B_{||}$ for various low T . The crossing point provides another estimate for the critical field strength. Computational details and units are as in Figs. 25 and 26; for clarity the error bars have been omitted, but can be estimated from Figs. 25 and 26.

must be seen as a property of a fully interacting many-body system, at least in the 2D disordered Hubbard model.

Another interesting feature of Fig. 27 is what appears to be the saturation of resistivity at a field not much higher than B_c . Experiments also show this behavior, but only for AIAs, where the saturation is shown to coincide with full spin polarization [82]. The on-site nature of the interactions in the Hubbard model make the saturation happen at much reduced field strength compared to that of complete polarization: at the rather low total density the minority spin species will effectively be decoupled from the majority spin species and both spin species form non-interacting subsystems at a field where the minority spin has not disappeared completely. Increasing magnetic field further at constant total density will then not change the conducting properties anymore.

The notion of a predictable and straightforward effect of $B_{||}$ is also concordant with the phenomenon that $\rho(B_{||})$ behaves qualitatively the same in the metallic and insulating phases [3], and therefore the same physical mechanism seems at play in both cases. The results here suggest the reduction of the effective interaction by spin polarization as a likely candidate for this mechanism.

In summary, applying a Zeeman magnetic field in the 2D disordered Hubbard model reduces the effect of the Hubbard interaction and is able to bring about a transition from a metallic phase to an insulator at a critical field strength. This critical field is considerably less than the field required for full spin polarization, emphasizing that, for the disordered Hubbard model, the metal-insulator transition occurs in a region where a considerable degree of electronic correlation remains. This is in good qualitative agreement with experimental observations when a magnetic field is applied parallel to a 2D electron or hole gas in GaAs- and AIAs-based heterostructures [82, 83]. For Si MOSFETs, the general phenomenon of suppression of the metallic behavior is in agreement, but the issue of the critical field being smaller than a saturating field is less clear [81]. Earlier in this section, the T -dependence of σ_{dc} was studied for various Δ_t without a B -field. It was shown that the Hubbard interaction enhances σ_{dc} and leads at low T to metallic behavior that can be made insulating by sufficiently strong disorder. The present results concerning the effect of a magnetic field are consistent with that conclusion and therefore strengthen it: the rather strong interactions that caused the conducting phase at disorder strength $\Delta_t = 2.0$ (below the critical disorder strength of approximately 2.4 above which the system is insulating) without B -field are reduced by a B -field which is able to drive the system back to its insulating phase. The latter is also its natural state in the absence of interactions. This consistency indicates that the disordered Hubbard model provides a coherent, qualitative picture of the phenomena in 2D electronic, disordered systems both in the presence and absence of a Zeeman magnetic field.

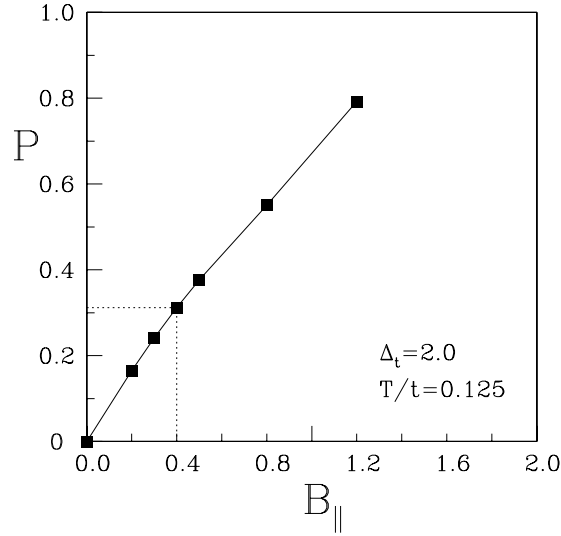


FIGURE 28. Degree of spin polarization P (defined in (66) in text) as a function of B_{\parallel} for fixed low $T = t/8$. The polarization shows little change through the metal-insulator transition and is only around 0.3 at the critical field strength $B_{\parallel} = 0.4$ (dotted lines).

C. The Role of Particle-Hole Symmetry

Journal Reference: “Particle–Hole Symmetry and the “Effect of Disorder on the Mott–Hubbard Insulator”, P.J.H. Denteneer, R.T. Scalettar, and N. Trivedi, Phys. Rev. Lett. **87**, 146401 (2001).

In recent years, it has become increasingly clear that for non-interacting electrons the presence or absence of certain symmetries is crucial in determining the effect of disorder on both transport and thermodynamic properties, as well as critical properties of the localization transition.[93] Recent examples where symmetry considerations are important are given in the context of quantum wires[94] and disordered superconductors,[95, 96] where chiral, time–reversal, and spin–rotation symmetries play an important role. In the preceding sections, bond-disordered Hamiltonians which retain the particle-hole symmetry of the clean Hubbard model were studied. This section examines the effect of different types of disorder, including those which break this symmetry, on both the dynamic and equilibrium thermodynamics in the vicinity of half-filling, electron density $\langle n \rangle = 1$. The results suggest that the presence or absence of *particle–hole symmetry* determines the effect of randomness on the conductivity and the Mott gap.

In order to make the distinction between the different types of disorder clear, it is useful to write down again the 2d Anderson-Hubbard Hamiltonian,

$$\begin{aligned}
 H = & - \sum_{\langle \mathbf{ij} \rangle, \sigma} t_{\mathbf{ij}} c_{\mathbf{i}\sigma}^{\dagger} c_{\mathbf{j}\sigma} - \sum_{\langle\langle \mathbf{ik} \rangle\rangle, \sigma} t'_{\mathbf{ik}} c_{\mathbf{i}\sigma}^{\dagger} c_{\mathbf{k}\sigma} \\
 & + U \sum_{\mathbf{j}} (n_{\mathbf{j}\uparrow} - \frac{1}{2})(n_{\mathbf{j}\downarrow} - \frac{1}{2}) - \sum_{\mathbf{j}, \sigma} \mu_{\mathbf{j}} n_{\mathbf{j}\sigma} .
 \end{aligned} \tag{67}$$

Here $t_{\mathbf{ij}}$ is a bond–dependent hopping matrix element on near-neighbor sites $\langle \mathbf{ij} \rangle$, $t'_{\mathbf{ik}}$ is a bond–dependent hopping matrix element on next-near-neighbor sites $\langle\langle \mathbf{ik} \rangle\rangle$, U is an on-site repulsion, and $\mu_{\mathbf{j}}$ is a site–dependent chemical potential. Choose $P(t_{\mathbf{ij}}) = 1/\Delta_t$ for $t_{\mathbf{ij}} \in [t - \Delta_t/2, t + \Delta_t/2]$, and zero otherwise, with $t = 1$ to set the scale of energy. Similarly, $P(t'_{\mathbf{ik}}) = 1/\Delta'_t$ for $t'_{\mathbf{ik}} \in [t' - \Delta'_t/2, t' + \Delta'_t/2]$, and $P(\mu_{\mathbf{j}}) = 1/\Delta_{\mu}$ for $\mu_{\mathbf{j}} \in [-\Delta_{\mu}/2, +\Delta_{\mu}/2]$, so that the various Δ measure the disorder strength. Now focus on half–filling where the effects of interactions are most prominent, as evidenced by the formation of antiferromagnetic correlations and a Mott-Hubbard charge gap at low temperatures. This Hamiltonian, Eq. 67, is particle–hole (ph) symmetric when $t'_{\mathbf{ik}} = \mu_{\mathbf{j}} = 0$. That is, under the transformation $c_{\mathbf{i}\sigma}^{\dagger} \rightarrow (-1)^{\mathbf{i}} c_{\mathbf{i}\sigma}$ the Hamiltonian is unchanged, and the system is precisely half–filled for all values of the parameters

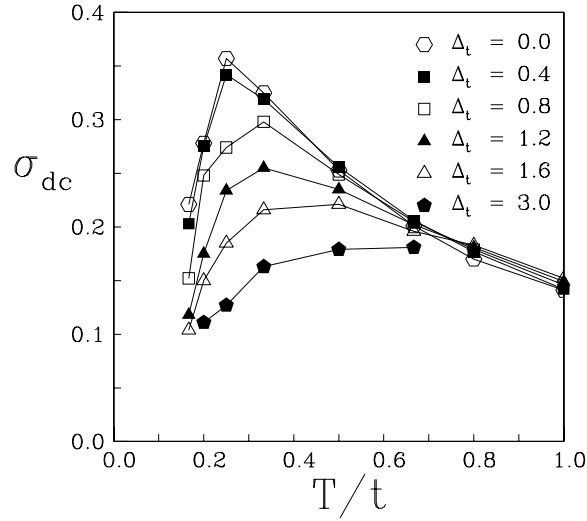


FIGURE 29. The effect of particle–hole–symmetry preserving (near-neighbor) bond disorder in the half-filled Hubbard Hamiltonian is to decrease the conductivity σ_{dc} . Data is for $U = 4t$ on a 8×8 square lattice; Δ_t measures the strength of the bond disorder.

in H and also for all T . (See Appendix D.) Therefore, while near-neighbor bond and local site disorder both introduce randomness into the system, they differ fundamentally in that site disorder breaks ph–symmetry.

In addition to the conductivity and spin polarization of the preceding sections, one can also extract the *temperature-dependent* density of states at the chemical potential $N(\varepsilon = 0)$ [97] from the one-electron Green function as a function of imaginary time,

$$N(0) \simeq -\beta G(\mathbf{r} = 0, \tau = \beta/2) / \pi . \quad (68)$$

This quantity allows a more clear characterization of the transport and thermodynamic properties of the system. For σ_{dc} and $N(0)$, “Trotter” errors associated with the discretization of imaginary time β are considerably less than the fluctuations associated with monte carlo and disorder averaging.

The transport properties are given in Fig. 29, which exhibits the effect of near-neighbor hopping (bond) disorder on the conductivity. For all disorder strengths Δ_t , at temperatures greater than a characteristic temperature T_* related to the Mott gap, the system shows metallic behavior with σ_{dc} increasing upon lowering T . The conductivity turns down sharply as the temperature drops below T_* and the system shows insulating behavior with σ_{dc} decreasing upon lowering T . In the case of zero randomness, the perfect nesting of the Fermi surface in 2d leads to antiferromagnetic long range order (AFLRO) in the ground state with an associated spin density wave gap for arbitrarily small U , evolving to a Mott gap at larger U . Hopping disorder reduces AFLRO via the formation of singlets on bonds with large hopping t_{ij} and hence large coupling $J = t_{ij}^2/U$ and ultimately destroys it beyond $\Delta_t \approx 1.6t$. [98] The fascinating result is that insulating behavior in the conductivity nevertheless persists to much larger Δ_t . Moreover the shift of the maximum in Fig. 29 implies that the mobility gap in fact increases with increasing Δ_t .

The situation is quite different in the case of site disorder, as shown in Fig. 30: at fixed temperature T , as site disorder Δ_μ is turned on, the conductivity increases, i.e. the Mott insulating state is weakened.[99] At weak disorder, the conductivity drops with decreasing T , reflecting again the presence of the Mott insulating phase. As the disorder strength becomes large enough to neglect U , one would expect a similar temperature dependence arising from Anderson insulating behavior. It is likely that in all cases the conductivity will ultimately turn over and go to zero at low T , but these simulations are limited to temperatures $T > W/48$ because of the fermion sign problem. Nevertheless, the data for site disorder offer a dramatic contrast to that of bond disorder (Fig. 29) where randomness decreases the conductivity.

What is the underlying reason for the distinct effects of bond and site disorder on the conductivity? There are several obvious differences in how they alter local and even longer range spin and charge correlations which could offer insight. Site disorder enhances the amount of double occupancy on the lattice, since the energy cost U of double

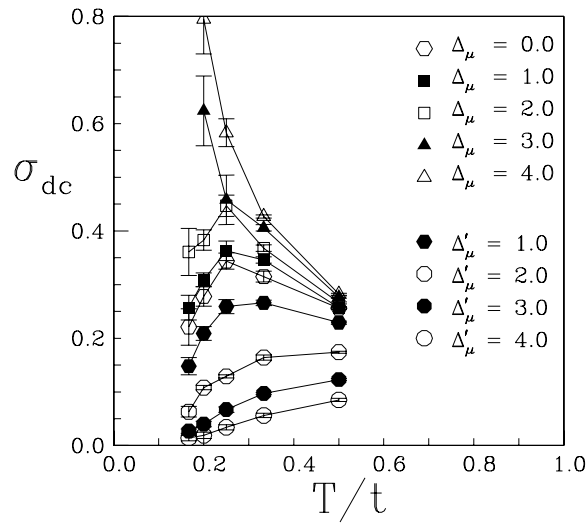


FIGURE 30. Canonical site disorder (with strength Δ_μ) enhances the conductivity. Particle-hole symmetric site disorder (with strength Δ'_μ), as with bond disorder (Fig. 29), suppresses the conductivity. Other parameters are as in Fig. 29.

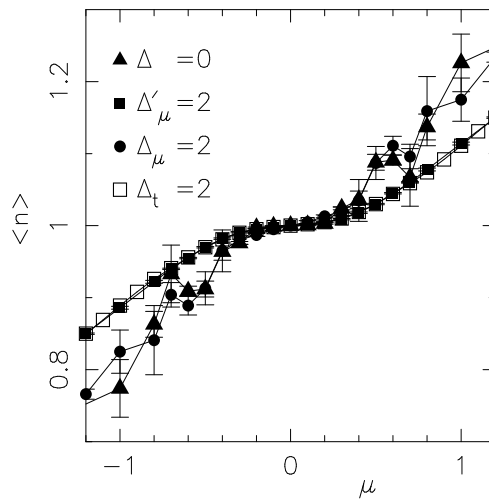


FIGURE 31. The Mott gap is made more robust by the addition of bond disorder or particle-hole symmetric site disorder (open and filled squares) of strength $\Delta = 2t = U/2$, as indicated by the response of the density to changes in the chemical potential. For canonical site disorder (filled circles) the Mott gap is practically unaffected by this strength of randomness. [19] Calculations are for $T = t/8 = W/64$ on a 8×8 lattice.

occupancy is compensated by differences in site energies. One explanation of why site disorder increases σ_{dc} is that the concomitant increase in empty sites leads to more mobility. This destruction of local moments ultimately also leads to the end of antiferromagnetic order. Surprisingly, the simulations suggest that bond disorder has a similar diminishing effect on local moments, so that the difference in the behavior of the conductivity arises from a different origin.

Particle-hole (ph) symmetry is the unifying criterion which underlies and determines the effect of disorder. As emphasized above, site and bond disorder have rather similar effects on the double occupancy. Moreover, the consequences of this effect for σ_{dc} are expected to become visible only above a threshold value of disorder strength, whereas

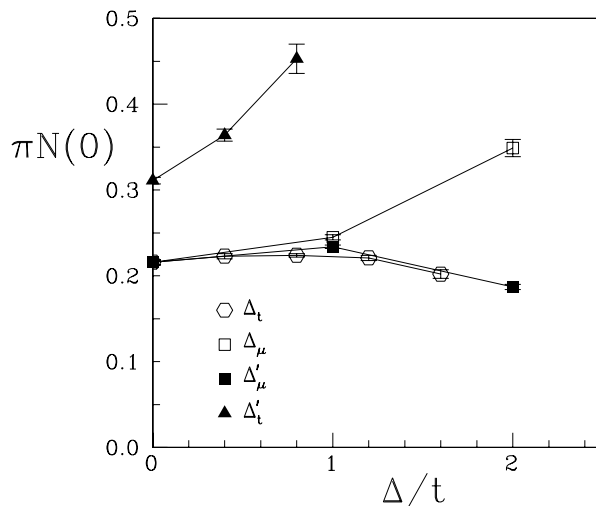


FIGURE 32. Behavior of the density of states $\pi N(0)$ at the Fermi level and at fixed low temperature as a function of disorder strength Δ/t for various types of disorder. All data are for $T = t/6$, except data for randomness in next-near-neighbor hopping (disorder strength Δ'_t) which are at temperature $T = t/5$ (the value $t' = 0$ is used). [19] Other parameters are as in Figs. 29 and 30.

σ_{dc} is affected already for weak disorder. Instead, the key distinction is in the presence or absence of ph-symmetry. In order to explore this conjecture more fully, one can study two other types of disorder: site disorder that preserves ph-symmetry and bond disorder that breaks ph-symmetry (by including next-near-neighbor hopping).

Particle-hole symmetric site disorder is introduced by adding random chemical potentials to the Hubbard model which couple with opposite sign to the density of up and down electrons, i.e. choose $\mu_j \equiv \mu_{j\sigma} = \sigma\mu_j$ in Eq. 67. This type of disorder represents a random (Zeeman) magnetic field. For $U = 0$ ph-symmetric site disorder has precisely the same effect as conventional site disorder, since moving in a given random chemical potential landscape or one obtained by reversing all the site energies is entirely equivalent. However the behavior of the conductivity at finite U is dramatically different. Fig. 30 shows that ph-symmetric site disorder (with strength Δ'_μ) has the *same* effect on σ_{dc} as bond disorder, i.e. conductivity decreases with increasing Δ'_μ .

To seek final confirmation of the conjecture, one can also explore the effect of next-near-neighbor (nnn) hopping and randomness therein. Such longer ranging hybridization breaks ph-symmetry on a square lattice, since it connects sites on the same sublattice. Disorder has the *same* effect as conventional site randomness, i.e. it increases the conductivity at finite T . Thus in all four types of disorder, the behavior of the conductivity falls into the appropriate class based on the preservation or destruction of ph-symmetry, strengthening the evidence that it is this symmetry which is playing the crucial role in determining the effect of randomness on the transport properties.

Now consider the thermodynamics. The most direct measure of the Mott gap is from the compressibility, or from the behavior of density $\langle n \rangle$ as a function of chemical potential μ , as shown in Fig. 31. The range of μ where $\langle n \rangle$ is constant (and the system is incompressible) determines the gap in the spectrum. Hopping and ph-symmetric site disorder stabilize the plateau of the density at half-filling. On the other hand, conventional site disorder (with $\Delta_\mu = U/2$) has a compressibility which is indistinguishable (within the available computational accuracy) from the clean system.

The density of states (DOS) at the Fermi level $N(0)$ gives valuable information on the effect of disorder on the Mott gap. In the pure system, QMC studies have shown that the DOS exhibits a clear Mott gap with $N(0) \rightarrow 0$ as T is lowered to zero. The nonzero values of $N(0)$ at nonzero T reflect the small residual slopes in the plateaus in the $\langle n \rangle$ vs. μ plot (cf. Fig. 31); at lower T , $N(0)$ approaches zero just as the plateaus become perfectly flat. The behavior of $N(0)$ at a fixed low T as a function of the strength of the various types of disorder is given in Fig. 32. $N(0)$ is rather insensitive to ph-symmetric disorder (Δ_t and Δ'_μ) and is even reduced by it: the Mott gap persists. On the other hand, ph-symmetry breaking disorder (Δ_μ and Δ'_t) clearly enhances $N(0)$, i.e. fills up the Mott gap.

These results provide a clear numerical demonstration of the key role of particle-hole symmetry. The effects can also be understood qualitatively as follows: In the clean case, at $\langle n \rangle = 1$ and strong coupling, the DOS consists of an

occupied lower Hubbard band (LHB) and an unoccupied upper Hubbard band (UHB), separated by a charge gap of the order of U . In the case of ph-symmetric disorder, the effect of disorder on LHB and UHB is identical. Therefore the Fermi energy remains in the middle of the gap: this enables the insulating behavior and Mott gap to stay intact. A stabilized charge gap for ph-symmetric *site* disorder is evident since double occupation is strongly suppressed. For nn-hopping disorder a simple argument is less obvious, but the data in Fig. 31 clearly show that these two cases fall into the same class. When ph-symmetry is broken, the LHB and the UHB will be affected differently; different numbers of states will appear at either side of the gap. As a consequence, the Fermi energy ends up in one of the tails of the DOS, resulting in an enhanced $N(0)$ (cf. Fig. 32) and increased conductivity (Fig. 30). The fact that the states introduced by disorder are localized [100] will keep the system in an insulating state (cf. Fig. 32).

A related example where symmetry plays a crucial role in the effects of disorder is the case of localization in the superconducting phase, where the quasiparticles are described by a Bogoliubov-de Gennes Hamiltonian.[96] In this case, one can classify the system according to the presence or absence of time reversal and spin rotation symmetries, and it is found in one dimension that in the absence of spin rotation symmetry, the conductance decays algebraically with system size, while in the symmetric case it decays exponentially. Therefore, in this situation as well, the extra spin rotation symmetry leads to a strengthening of insulating behavior.

The question of the behavior of the half-filled fermion Hubbard model as disorder is added is furthermore reminiscent of similar issues in the ph-symmetric boson Hubbard model.[37] At generic densities, it is believed that a new ‘Bose glass’ phase arises to intervene in the original ground state phase diagram between superfluid and Mott insulating phases, but the situation at the ph-symmetric tip of the Mott lobe is uniquely different. This work is a first step in the analysis of the nature of the behavior of the fermionic model.

D. Interaction driven Band Insulator to Metal Transition

Journal Reference: “Quantum Monte Carlo Study of an Interaction-Driven Band Insulator to Metal Transition”, N. Paris, K. Bouadim, F. Hebert, G.G. Batrouni, and R.T. Scalettar, Phys. Rev. Lett. **98**, 046403 (2007).

Thus far these notes have emphasized the role of interaction effects in disordered, tight-binding models such as the Hubbard Hamiltonian in driving a metallic transitions from an Anderson insulating states originating in the random potential. Actually, a somewhat more simple context in which to study the possibility of interaction driven insulator to metal transitions is to begin with a band insulating state, in which the insulating behavior is caused by a periodic external potential as opposed to a random one [59, 60, 61, 62, 67]. Recently, this issue has been addressed within dynamical mean field theory (DMFT) and a number of interesting conclusions emerged[101]. However, because DMFT treats only a single site (retaining, however, all the dynamical fluctuations of the self-energy ignored in conventional, static mean field theory) it is important to undertake complementary work which is able to retain intersite fluctuations.

This section investigates such band insulator-metal transitions with DQMC. The specific Hamiltonian we study is the “ionic Hubbard model”:

$$H = -t \sum_{\langle lj \rangle \sigma} (c_{j\sigma}^\dagger c_{l\sigma} + c_{l\sigma}^\dagger c_{j\sigma}) + U \sum_l n_{l\uparrow} n_{l\downarrow} + \sum_l (\Delta(-1)^l - \mu)(n_{l\uparrow} + n_{l\downarrow}) . \quad (69)$$

Instead of a random chemical potential, the term $\Delta(-1)^l$ provides a staggered site energy. In the noninteracting limit, $U = 0$, the effect of Δ is to produce a dispersion relation, $E(k) = \pm \sqrt{\varepsilon(k)^2 + \Delta^2}$ with $\varepsilon(k) = -2t[\cos k_x + \cos k_y]$, which is gapped at half-filling. (See Exercises.) A considerable amount is known concerning this model in one dimension[102], but the existence of an interaction driven metallic phase at half-filling is still unresolved even there. Metal-insulator transitions in a related system with *randomly* located site energies with a bimodal distribution have also been studied within DMFT [103, 104].

The temperature dependence of the conductivity σ_{dc} is shown for increasing values of the interaction strength for $\Delta = 0.5$ in Fig. 33. The insulating behavior at $U = 0$ signalled by $d\sigma_{dc}/dT > 0$ at low T is changed to metallic $d\sigma_{dc}/dT < 0$ at low T when $U = 1$. A further increase of the correlations to $U = 2$ weakens the metallic behavior, and which is finally destroys completely in a transition to a Mott insulator at $U = 4$. When the band gap is larger ($\Delta = 1$), the screening of the one-body potential is not sufficiently strong for $U = 1$ to cause metallic behavior, as is shown by the corresponding data set in Fig. 33. Here, and throughout this section unless otherwise mentioned, the lattice size used in the simulations is $N = 6 \times 6$ and the filling is $\rho = 1.0$ (half-filling).

In the single site ($t = 0$) limit, the ionic Hubbard model is a band insulator for $U < 2\Delta$ and a Mott insulator for $U > 2\Delta$. That is, at weak coupling and half-filling, the sites with lower energy $-\Delta$ are doubly occupied and those with higher energy $+\Delta$ are empty, with a gap to further addition of particle set by $2\Delta - U$. At strong coupling, both types of sites are singly occupied, with a gap to further addition of particles set by $U - 2\Delta$. correlations close the band gap At the single special value $U = 2\Delta$ correlations close the band gap [101, 67]. Fig. 34, which presents results for σ_{dc} for $\Delta = 0.5$, shows that when t is nonzero, this single metallic point is expanded to a finite range of U values.

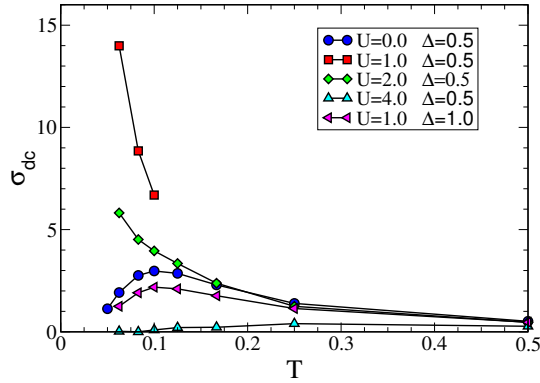


FIGURE 33. The transitions, at half-filling, from a band insulator to metal to Mott insulator with increasing U are shown for periodic potential strength $\Delta = 0.5$. At $U=0$ the conductivity σ_{dc} goes to zero as T is lowered. However, for at intermediate $U = 1, 2$ the system is metallic. Mott insulating behavior sets in for $U = 4$. The lattice size is 6×6 . When $\Delta = 1.0$, the band gap increases and $U = 1$ is no longer sufficiently large to screen the one body potential and drive the system metallic.

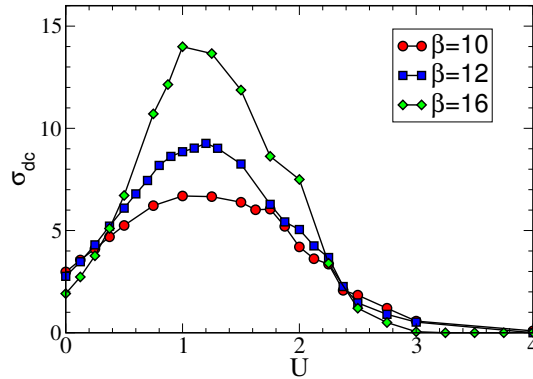


FIGURE 34. The conductivity σ_{dc} at half-filling for $\Delta = 0.5$ is shown as a function of U for three different low temperatures, $\beta = 10, 12, 16$. The band-insulator to metal transition is signaled by the crossing of the curves at $U_{c1} \approx 0.4t$. At $U_{c2} \approx 2.5t$ the three curves cross again, indicating the Mott insulator transition.

Interestingly, however, the largest conductivity remains at $U = 2\Delta = 1$ as one might expect from the $t = 0$ analysis. The band-insulator to metal transition occurs at $U_{c1} \approx 0.4t$, where the change in the order of the three curves indicates a transition from σ_{dc} decreasing as β increases to σ_{dc} increasing as β increases. The metal transition to Mott insulator transition is at $U_{c2} \approx 2.5t$, where σ_{dc} once again decreases as β increases.

The use of DQMC to study the ionic Hubbard model allows us to examine the behavior of intersite correlations, among them the spin-spin correlations and their Fourier transform $S(k)$. Fig. 35 shows results for the antiferromagnetic structure factor $S(\pi, \pi)$ as a function of U for $\beta = 10, 12, 16$. Comparing with Fig. 34 the band insulating and metallic phases are paramagnetic, but the transition to Mott insulating behavior is accompanied by the onset of antiferromagnetic order.

One way in which the inclusion of such intersite correlations changes the physics in a fundamental way is when the periodic potential is absent, that is, at $\Delta = 0$. In DMFT in the paramagnetic phase, the Hubbard model is a metal at weak coupling [69, 105]. However, it is known that the $d = 2$ square lattice Hubbard model being studied here is an antiferromagnetic insulator at *all* U , even weak coupling. Fig. 36 presents results for the conductivity which confirms this. At all U values shown, σ_{dc} ultimately decreases as T is lowered. Indeed, it is possible to verify that the value of T where σ_{dc} has its maximum correlates well with the temperature T_* at which antiferromagnetic correlations begin to

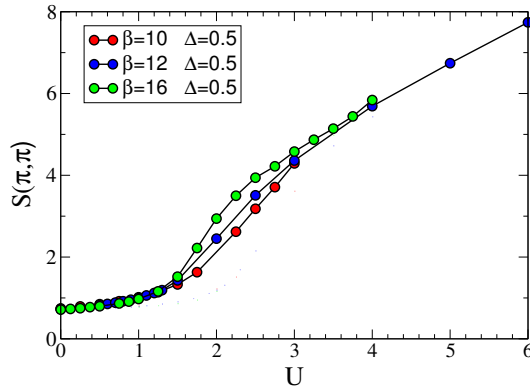


FIGURE 35. The antiferromagnetic structure factor is shown at half-filling as a function of U for two different values of the periodic potential $\Delta = 0.5$ and inverse temperature $\beta = 10, 12, 16$.

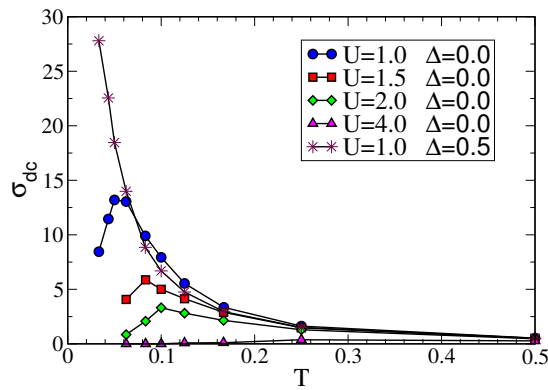


FIGURE 36. The conductivity σ_{dc} is shown as a function of temperature at half-filling. When the periodic potential, and hence the non-interacting band gap, is absent ($\Delta = 0.0$) the square lattice Hubbard model is insulating for *all* U , due to nesting of the Fermi surface. The data for $\delta = 0.5, U = 1$ from Figure 1 is redisplayed to emphasize the contrast between the metallic behavior there and the insulating behavior for all U when $\Delta = 0$.

rise rapidly. This temperature, like the Néel temperature in the $d = 3$ Hubbard model, is a non-monotonic function of U , falling to small values both at weak ($T_* \propto t \exp(a\sqrt{t}/U)$) and at strong ($T_* \propto t^2/U$) coupling. This is the first time the insulating nature of the square lattice Hubbard model at weak coupling has been shown from Quantum Monte Carlo studies of σ_{dc} . It is interesting to note that while all the $\Delta = 0$ curves share a common low temperature slope $d\sigma_{dc}/dT > 0$, a distinction between the antiferromagnetic and Mott origins of insulating behavior is clearly evident. At small U , σ_{dc} attains a much larger value before turning over as T is lowered than in the strong coupling Mott regime.

While DQMC allows us to look at intersite correlations and the associated phenomena like antiferromagnetism and insulating behavior deriving therefrom, the method employs lattices of finite size, unlike DMFT which directly probes the thermodynamic limit. Thus, it is important to verify that the observed metallic phase persists to larger lattices. Fig. 37 shows results for σ_{dc} as a function of temperature in the metallic phase for lattices up to 12×12 . The rise in σ_{dc} with decreasing T is seen to occur for all the lattices studied. It is not surprising that the lattice size has a rather substantial influence on the conductivity for these parameters, since it is known that such finite size effects are larger at weak coupling.

Fig. 38 shows the conductivity as a function of U for three different temperatures at $\Delta = 1.0$. There is now a much larger band-insulating phase at weak coupling, with a critical U for the metallic transition at $U_c \approx 1.5$. It is interesting that the conductivity again appears to peak at the value $U = 2\Delta$ where the $t = 0$ analysis suggests might be

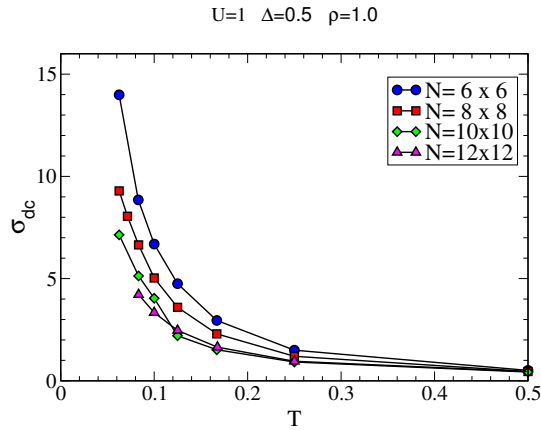


FIGURE 37. The conductivity at half-filling is shown for different lattice sizes for $U = 1$, close to the point where the system is most metallic for periodic potential $\Delta = 0.5$. (See Fig. 2.) Although σ_{dc} decreases with increasing lattice sizes, the signature of metallic behavior ($d\sigma_{dc}/dT < 0$) is unchanged.

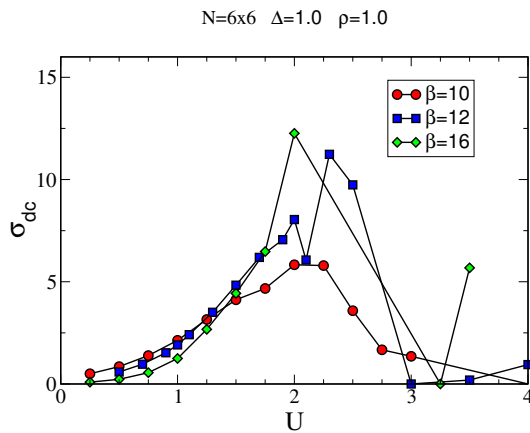


FIGURE 38. The conductivity at $\rho = 1.0$ is shown as a function of U for $\Delta = 1.0$ and $\beta = 10, 12, 16$. The system is a band insulator up to $U \approx 1.5$ whereupon metallic behavior onsets.

most amenable to the formation of a metal. Unfortunately, as U is increased into the metallic phase, the data become extremely noisy. This is a consequence of the sign problem. Fig. 39 shows the average sign as a function of U for $\Delta = 1$. It is not possible to do DQMC simulations at low T beyond $U = 2$ or so.

The evidence for metallic behavior at $\Delta = 1.0$ in Fig. 38 is a bit lost in the noise. Fig. 40 shows the conductivity, focussing on U values just inside the metallic region where the sign problem is not yet so bad. The steady increase of σ_{dc} as T decreases shows convincingly that the system is a metal at these U values.

In this section, we have presented determinant Quantum Monte Carlo studies of the two-dimensional Hubbard Hamiltonian which demonstrate that interactions can drive a band insulator metallic. This work complements DMFT by including intersite antiferromagnetic correlations which qualitatively alter the ground state phase diagram. Most of the results have focussed on $\Delta = 0.5$. It would be interesting to attempt to construct the full phase diagram in the $\Delta/t - U/t$ plane for the $d = 2$ ionic Hubbard model, and compare with that obtained in DMFT [101]. As these notes have emphasized, the behavior along the $\Delta = 0$ axis is significantly different. At intermediate values of Δ , DMFT indicates the interesting result the metallic phase closes, with a direct band insulator to Mott insulator transition occurring beyond $\Delta/W \approx 1/8$. Can this be studied within DQMC? Unfortunately, the sign problem, which becomes serious at intermediate $\Delta \approx t$, prevents us from exploring this full phase diagram at present.

However, one limit which is accessible, that is not have an insurmountable sign problem, is the case of large Δ , where we have very widely separated bands. Related studies of the boson-Hubbard model in a “superlattice” potential,

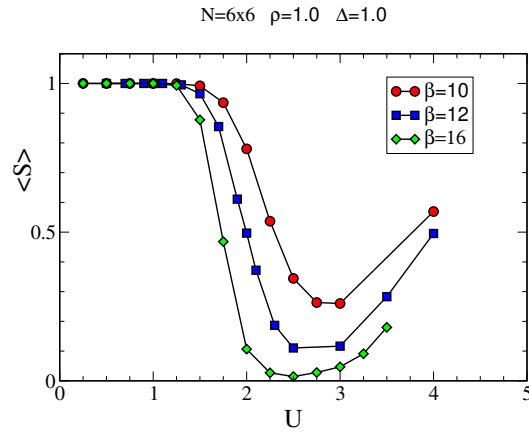


FIGURE 39. The average sign in the DQMC simulations as a function of U . $\langle S \rangle$ rapidly becomes small as the metallic region is entered. It rises again in the Mott insulator.

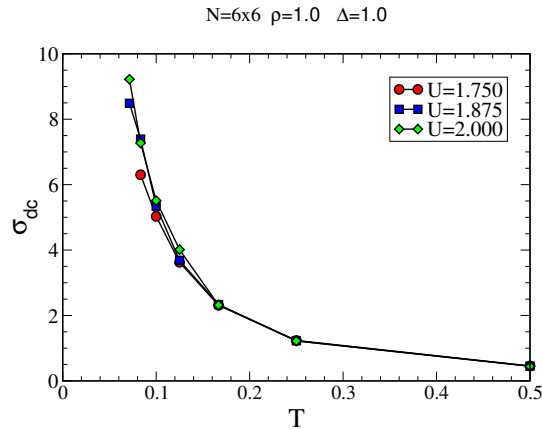


FIGURE 40. The conductivity as a function of T for $U = 1.750, 1.875,$ and 2.000 . The system is clearly metallic.

which exhibit a band-insulator to superfluid transition [59, 60, 61, 62, 67], show the appearance of insulating phases at half-integer fillings. These ‘charge-transfer’ insulators occur as a result of Mott splitting of the widely separated bands [103]. It would be interesting to explore this possibility in the fermion case.

VI. CONCLUSIONS

These notes have attempted to provide an introduction to the Anderson-Hubbard Hamiltonian and some of the physics arising from the combination of interactions and randomness. The behavior of the clean model in the limit of no interactions, no kinetic energy, small clusters, and mean field theory was established analytically, and then the determinant quantum monte carlo method was described and employed for the full problem on lattices of hundreds of sites.

One significant omission concerning the physics of the Hubbard model is the idea of a ‘Kondo resonance’. It turns out that as one progresses from weak to strong coupling, the spectral function of the Hubbard model does not smoothly evolve from a single blob to upper and lower Hubbard bands. Instead, in the course of changing the interaction strength a three peak structure is in evidence: nascent upper and lower Hubbard bands, but also a sharp peak at the Fermi energy. Actually, it was originally thought that such peaks only arise in variants of the Hubbard model which contain both localized and delocalized electrons. It is only relatively recently, with the introduction of dynamical mean field theory (DMFT), that it was realized this sharp peak occurs in the Hubbard model as well. This very important idea is

at the heart of much of the current research into the Hubbard model and its experimental realizations.

APPENDIX A: CREATION AND DESTRUCTION OPERATORS AND THE HUBBARD HAMILTONIAN

Creation and destruction operators,

$$\begin{aligned}\hat{a} &= \sqrt{\frac{m\omega}{2\hbar}}\hat{x} + i\sqrt{\frac{1}{2m\omega\hbar}}\hat{p} \\ \hat{a}^\dagger &= \sqrt{\frac{m\omega}{2\hbar}}\hat{x} - i\sqrt{\frac{1}{2m\omega\hbar}}\hat{p},\end{aligned}\tag{70}$$

are familiar from the treatment of the harmonic oscillator. They are the language in which tight-binding Hamiltonians like the Hubbard model are written, but differ in several respects. Perhaps most confusing is that the fermion operators in the Hubbard model are not introduced in terms of familiar position and momentum operators as are \hat{a}, \hat{a}^\dagger above. Rather they stand on their own.

Also, instead of just one creation and one destruction operator, in the Hubbard model there is a set of such operators, which are distinguished by attaching indices \mathbf{j} and σ . Thus one writes $\hat{c}_{\mathbf{j}\sigma}^\dagger$ and $\hat{c}_{\mathbf{j}\sigma}$. The index \mathbf{j} labels the spatial lattice site and the index σ labels the electron spin (up or down). As a consequence, the occupation number states are no longer characterized by a single number n , as for a single harmonic oscillator, but instead by a collection of occupation numbers $n_{\mathbf{j}\sigma}$. One writes such states as $|n_{1\uparrow} n_{2\uparrow} n_{3\uparrow} \dots n_{1\downarrow} n_{2\downarrow} n_{3\downarrow} \dots\rangle$

Finally, because these operators are meant to describe fermions, they obey *anticommutation* relations. (The anticommutator of two operators $\{\hat{A}, \hat{B}\}$ is defined to be $\hat{A}\hat{B} + \hat{B}\hat{A}$.)

$$\begin{aligned}\{\hat{c}_{\mathbf{j}\sigma}, \hat{c}_{\mathbf{l}\sigma'}^\dagger\} &= \delta_{\mathbf{j},\mathbf{l}}\delta_{\sigma,\sigma'} \\ \{\hat{c}_{\mathbf{j}\sigma}^\dagger, \hat{c}_{\mathbf{l}\sigma'}^\dagger\} &= 0 \\ \{\hat{c}_{\mathbf{j}\sigma}, \hat{c}_{\mathbf{l}\sigma'}\} &= 0.\end{aligned}\tag{71}$$

An immediate consequence of these anticommutation relations is the Pauli principle: the maximum occupation of a particular site with a given spin is 1.

Exercise A1: Show that the Pauli exclusion principle is a consequence of the anticommutation relation amongst the fermion creation operators by considering $\mathbf{j} = \mathbf{i}$ and showing that $\hat{c}_{\mathbf{j}\sigma}^\dagger|1\rangle = 0$. Here $|1\rangle$ is the state with one electron on site \mathbf{j} and with spin σ .

Note that while a fermion creation operator annihilates a state which already has a fermion in it, its action on the empty state is $\hat{c}^\dagger|0\rangle = |1\rangle$, which looks just like the bosonic operator \hat{a}^\dagger . Besides the Pauli principle, the anticommutation relations also ensure that the particles are fermions, that is, their wave function changes sign when two electrons with different labels \mathbf{j} are exchanged. To keep track of these signs, one needs to specify a convention for the relation between a state like $|10100\dots\rangle$ and the vacuum state $|\text{vac}\rangle = |00000\dots\rangle$. The two possibilities, $|10100\dots\rangle = c_1^\dagger c_3^\dagger|\text{vac}\rangle$ and $|10100\dots\rangle = c_3^\dagger c_1^\dagger|\text{vac}\rangle$ differ by a sign. Either definition is fine, but in all subsequent manipulations whatever convention was chosen must be followed consistently.

Exercise A2: Suppose the indices labeling the fermion operators runs over eight possible values. Figure out the occupation number state which results from the following applications of the indicated creation and destruction operators. Choose as your convention that a given occupation number state is formed by acting on the vacuum state with the lowest indices at the right of the string of creation operators. (This corresponds to the second of the two choices discussed above.)

$$\begin{aligned}\hat{c}_5^\dagger \hat{c}_4^\dagger \hat{c}_2^\dagger |\text{vac}\rangle &= ? \\ \hat{c}_2^\dagger \hat{c}_4^\dagger \hat{c}_5^\dagger |\text{vac}\rangle &= ? \\ \hat{c}_4^\dagger \hat{c}_5^\dagger |11000001\rangle &= ? \\ \hat{c}_4^\dagger \hat{c}_5^\dagger |11001001\rangle &= ? \\ \hat{c}_1^\dagger \hat{c}_2 |01001001\rangle &= ?\end{aligned}$$

$$\hat{c}_1^\dagger \hat{c}_4 |01001001\rangle = ?$$

$$\hat{c}_1^\dagger \hat{c}_5 |01001001\rangle = ?$$

Having introduced creation and annihilation operators, one can now write down the Hubbard Hamiltonian. Before doing so, think about how one might simply describe the motion and interactions of electrons in a solid. First, one needs to account for the fact that there is a regular array of nuclear positions in a solid, which for simplicity are considered to be fixed. (In other words, we will not worry about lattice vibrations.) This suggests one begin with a lattice of atoms (sites) on which the electrons move. A single atom is already a very complex structure, with many different energy levels. The most simple ‘atom’ would have a single energy level. Then, the Pauli principle would tell us that at most two electrons (one with spin up and one with spin down) can sit on this ‘atom’. In a solid where electrons can move around, the electrons interact via a screened Coulomb interaction. The biggest interaction will be for two electrons on the same atom. For simplicity, Hubbard stops just there, so that interactions are modeled by a term which is zero if the atom is empty of electrons or has only a single electron on it, but has the value U if the atom has two electrons. There is no interaction between electrons on different sites. The kinetic energy will consist of an expression which allows electrons to move from one site to its neighbors. The energy scale t which governs this ‘hopping’ will be determined by the overlap of two wavefunctions on the pair of atoms. Since wavefunctions die off exponentially, one can begin by allowing hopping only between the closest atoms in the lattice.

Now let’s formalize this construction. Define $c_{j\sigma}^\dagger$ to be the operator which creates an electron of spin σ on lattice site \mathbf{j} . (Drop all the ‘hats’ which up to now have been used to denote operators.) Similarly, $c_{j\sigma}$ is the destruction operator, and $n_{j\sigma} = c_{j\sigma}^\dagger c_{j\sigma}$ is the number operator.

The Hubbard Hamiltonian is then,

$$H = -t \sum_{\langle \mathbf{j}, \mathbf{l} \rangle \sigma} c_{j\sigma}^\dagger c_{l\sigma} + U \sum_{\mathbf{j}} n_{j\uparrow} n_{j\downarrow} - \mu \sum_{\mathbf{j}} (n_{j\uparrow} + n_{j\downarrow}). \quad (72)$$

The first term is the kinetic energy: It describes the destruction of an electron of spin σ on site \mathbf{l} and its creation on site \mathbf{j} (or *vice-versa*). The symbol $\langle \mathbf{j}, \mathbf{l} \rangle$ emphasizes that hopping is allowed only between two sites which are adjacent. The second term is the interaction energy. It goes through all the sites and adds an energy U if it finds that the site is doubly occupied. The final term is a chemical potential which controls the filling. The situation where the filling is one electron per site is referred to as ‘half-filling’ since the lattice contains half as many electrons as the maximum number (two per site). Studies of the Hubbard model often focus on the half-filled case because it exhibits a lot of interesting phenomena (Mott insulating behavior, antiferromagnetic order, etc.)

Exercise A3: Show that the Hubbard Hamiltonian commutes with the operators $N_\uparrow = \sum_{\mathbf{j}} n_{j\uparrow}$ and $N_\downarrow = \sum_{\mathbf{j}} n_{j\downarrow}$. It is useful to begin by considering the commutator of the kinetic energy on a single ‘link’ of the lattice connecting sites \mathbf{i} and \mathbf{j} with the total number of electrons on those two sites. That is, begin by computing,

$$[c_{i\sigma}^\dagger c_{j\sigma} + c_{j\sigma}^\dagger c_{i\sigma}, n_{i\sigma} + n_{j\sigma}] \quad (73)$$

After working through the algebra, can you think of an argument that this should be the case based on the structure of H , that is, based on how the creation and destruction operators appear together?

Since the Hubbard Hamiltonian commutes with the total spin up and spin down number operators, $N_\uparrow = \sum_{\mathbf{j}} n_{j\uparrow}$ and $N_\downarrow = \sum_{\mathbf{j}} n_{j\downarrow}$. In finding the eigenstates, one can consider different sectors of N_\uparrow and N_\downarrow separately. As might be expected, in the non-interacting limit, from a solution in the single particle sector, $N_\uparrow = 1$ and $N_\downarrow = 0$ a solution of the many electron problem can be built.

Exercise A4: Suppose you have a one dimensional lattice of eight sites. Write down all the occupation number states in the sector $N_\uparrow = 1, N_\downarrow = 0$. Figure out what H does to each state. Use ‘periodic boundary conditions’ so that site eight is considered a neighbor of site one. Write down the matrix for H using this basis. Show that $|11111111\rangle$ is an eigenvector of eigenvalue $-2t$. Show that $|1-11-11-11-1\rangle$ is an eigenvector of eigenvalue $+2t$.

An $N \times N$ tridiagonal matrix with “ a ” along the diagonal and “ b ” above and below the diagonal, with periodic boundary conditions has eigenvalues $\lambda_k = a + 2b \cos k$ where k takes on the discrete values $k_n = 2\pi n/N$ and $n = 1, 2, 3, \dots, N$.

Exercise A5: For general N , what is the eigenvector corresponding to $n = N$ so that the momentum $k = 2\pi = 0$? What is the eigenvector corresponding to $n = N/2$ which has momentum $k = 2\pi$?

Using this result for the eigenvalues of a tridiagonal matrix, one sees that the single particle, one-dimensional Hubbard Hamiltonian has energy levels $\epsilon_k = -2t \cos k$. One can view this as a simple ‘energy band’ of bandwidth

$W = 4t$. This establishes a rough connection between the hopping parameter t in the Hubbard Hamiltonian and physical energy scales like the bandwidth W of a real material.

The eigenvalues of the Hubbard Hamiltonian at $U = 0$ in higher particle sectors are obtained by occupying these single particle levels according to the restrictions of the Pauli principle. It is amusing explicitly to diagonalize H in the $N_{\uparrow} = 2, N_{\downarrow} = 0$ sector, computing the eigenvalues (perhaps numerically with a LAPACK routine- there are 28 states!), and verifying that they are indeed Pauli-restricted combinations of the eigenvalues obtained in the single particle case.

Let us now look at the non-interacting limit in a more formal way by transforming to momentum creation and destruction operators.

$$c_{\mathbf{k}\sigma}^{\dagger} = \frac{1}{\sqrt{N}} \sum_{\mathbf{l}} e^{i\mathbf{k}\cdot\mathbf{l}} c_{\mathbf{l}\sigma}^{\dagger}. \quad (74)$$

One can think about this process in analogy with the classical normal mode problem: Define new (momentum) creation operators as a linear combination of the old (position) ones. As shall be seen in Exercises which follow, in the Hubbard model at $U = 0$ the different momentum modes decouple from each other and behave independently, just as for classical normal modes. Notice that on a finite lattice the momentum \mathbf{k} cannot be any real number but has discretized values. For a one-dimensional lattice of N sites, the periodic boundary condition $c_{N+1}^{\dagger} = c_1^{\dagger}$ yields $k_n = 2\pi n/N$. This is of course the same condition as when one considers the eigenvalues of the tri-diagonal matrix above. For a two-dimensional square or three dimensional cubic lattice, each component separately has such a discretization.

Different Fourier functions are orthogonal. The analog for these discrete site and momentum variables is given in the following Exercise:

Exercise A6: Prove the following two ‘orthogonality’ relations:

$$\frac{1}{N} \sum_{\mathbf{l}} e^{i(k_n - k_m)\mathbf{l}} = \delta_{n,m} \quad (75)$$

$$\frac{1}{N} \sum_{k_n} e^{ik_n(l-j)} = \delta_{l,j} \quad (76)$$

Exercise A7: Use the orthogonality relations invert Eq. 2, that is, to prove,

$$c_{\mathbf{l}\sigma}^{\dagger} = \frac{1}{\sqrt{N}} \sum_{\mathbf{k}} e^{-i\mathbf{k}\cdot\mathbf{l}} c_{\mathbf{k}\sigma}^{\dagger}. \quad (77)$$

Here, of course, the sum over \mathbf{k} means you sum over the discrete allowed momenta \mathbf{k}_n .

With these relations in hand, one can show a lot of interesting things about the momentum space operators.

Exercise A8: Verify the anticommutation relations

$$\begin{aligned} \{c_{\mathbf{k}\sigma}, c_{\mathbf{p}\sigma'}^{\dagger}\} &= \delta_{\mathbf{k},\mathbf{p}} \delta_{\sigma,\sigma'} \\ \{c_{\mathbf{k}\sigma}^{\dagger}, c_{\mathbf{p}\sigma'}^{\dagger}\} &= 0 \\ \{c_{\mathbf{k}\sigma}, c_{\mathbf{p}\sigma'}\} &= 0. \end{aligned} \quad (78)$$

In other words, the anticommutation relations are “preserved” by this change in “basis” from site indices to momentum indices.

Now the $U = 0$ Hubbard model can be expressed in terms of these momentum space operators, leading in a more elegant way to the same dispersion relation (energy band) obtained by considering the matrix of H in the one particle sector.

Exercise A9: Show that for $U = 0$ the one dimensional Hubbard model is,

$$H = \sum_{\mathbf{k}\sigma} (\epsilon_{\mathbf{k}} - \mu) c_{\mathbf{k}\sigma}^{\dagger} c_{\mathbf{k}\sigma} \quad (79)$$

where $\epsilon_{\mathbf{k}} = -2t \cos k$. As part of this Exercise, you will show that the sum of all the number operators over different spatial sites and spin equals the sum of all the number operators over different momenta and spin.

It is important to realize that the result that an analysis of the one-particle sector gives us full information about the model for any particle number rests only on the fact that the interactions are turned off. It is not necessary that

the hopping t between different sites be the same for all pairs of sites, or that it be limited to near neighbors, or that the chemical potential be the same on all sites. All that matters is that H be a quadratic form in the fermion creation and destruction operators. To emphasize: To solve any Hamiltonian H which takes the form $H = \sum_{i,j} c_i^\dagger h_{ij} c_j$ with h a (symmetric) matrix of real numbers, simply diagonalize h and allow the resulting energy levels to be filled in a way which satisfies the exclusion principle. An important application of this theorem is given in the context of mean field theory, discussed in the second section of these notes.

Exercise A10: Show that for $U = 0$ the two dimensional Hubbard model on a square lattice is

$$H = \sum_{\mathbf{k}\sigma} (\epsilon_{\mathbf{k}} - \mu) c_{\mathbf{k}\sigma}^\dagger c_{\mathbf{k}\sigma} \quad (80)$$

where $\epsilon_{\mathbf{k}} = -2t(\cos k_x + \cos k_y)$.

In real space, all the different (site occupation) states in the $U = 0$ model are mixed with each other. In momentum space the different states are decoupled: A fermion operator of a give \mathbf{k} appears only together with operators of the same \mathbf{k} . This means that the different momentum modes can be treated independently, leading to the following result.

Exercise A11: Show that the partition function of the $U = 0$ Hubbard model is given by

$$Z = \prod_{\mathbf{k}} (1 + e^{-\beta(\epsilon_{\mathbf{k}} - \mu)}). \quad (81)$$

It is useful to remember that if a Hamiltonian is comprised of the sum of independent pieces then the partition function is the product of the associated partition functions.

Exercise A12: Compute the per site average occupation of the $U = 0$ Hubbard model and show it is given by,

$$\rho = \sum_{\mathbf{k}} (1 + e^{+\beta(\epsilon_{\mathbf{k}} - \mu)})^{-1}. \quad (82)$$

Note this takes the form of the sum of the occupations of different pieces, and that the Fermi function, $f_{\mathbf{k}} = 1/[1 + e^{\beta(\epsilon_{\mathbf{k}} - \mu)}]$, naturally arises. Show that when $\mu = 0$ the density $\rho = 1$ for any β if $\epsilon_{\mathbf{k}}$ is of the form derived for the $d = 1$ or $d = 2$ square lattice Hubbard model.

The allowed k values together with the dispersion relation determine the density of states $N(E)$ which counts the number of ways in which the system can have a given energy E . Formally, $N(E)$ is defined by

$$N(E) = \frac{1}{N} \sum_{\mathbf{k}} \delta(E - \epsilon_{\mathbf{k}}). \quad (83)$$

In the continuum limit (large number of sites) the sum over discrete momenta values is replaced by an integral according to the rule $\frac{1}{N} \sum_{\mathbf{k}} \rightarrow (2\pi)^{-d} \int d\mathbf{k}$, where d is the spatial dimension. As a simple example, consider one dimension with a relativistic dispersion relation $\epsilon_k = ck$ for $k > 0$. One can get the density of states as follows:

$$N(E) = (2\pi)^{-1} \int dk \delta(E - ck) = (2\pi)^{-1} \int dk \frac{1}{c} \delta(E/c - k) = (2c\pi)^{-1} (1 - \theta(k)). \quad (84)$$

Here the function $1 - \theta(k)$ emphasizes that $k > 0$ is required. Likewise, for a quadratic dispersion relation $\epsilon_k = ak^2$

$$N(E) = (2\pi)^{-1} \int dk \delta(E - ak^2) = (2\pi)^{-1} \int dk \frac{1}{2ak} \delta(\sqrt{E/a} - k) = (4a\pi)^{-1} \sqrt{a/E}. \quad (85)$$

Exercise A13: Compute (analytically) the density of states $N(E)$ of one dimensional Hubbard model. Explain why $N(E)$ diverges at $E = \pm 2t$ in terms of a picture of the dispersion relation $E(k) = -2t \cos k$. Compute $N(E)$ numerically and compare to your analytic calculation.

APPENDIX B: FORMAL FOUNDATION OF CLASSICAL MONTE CARLO

Why Monte Carlo Works: Detailed Balance, Transition Probabilities and All That

The Monte Carlo method is often referred to as a ‘computer experiment’. One might think of this as a way of conveying the fact that the output of simulations is not an equation, as in conventional theory. Instead, numbers appear

on the computer screen in somewhat the same way that numbers appear on a measuring device in the laboratory. Thus there is the implication that somehow simulations are a bit of a ‘black box’ and that the use of the computer is hiding the underlying physics. The purpose of this note is partly to emphasize some of the mathematical rigor behind Monte Carlo: It is not a happy accident that the computer is generating configurations with the desired probability distribution! Indeed, the fundamental equations underlying simulations are the same as analytic theories, and one can view simulations as a way of solving the mathematics (differential equations) when it becomes too complicated for analytic techniques.

With all that said, it is still useful to pursue the ‘Monte Carlo as experiment’ point of view. Consider the process of making a measurement in the laboratory. Nature prepares a ‘configuration’ i of the system, and the experimentalist takes that configuration and records a value for some quantity of interest. To get better statistics (or perhaps inevitably because of finite measuring time) nature actually produces many configurations, and the experimentalist averages over the values obtained. It is useful to emphasize that no matter how long the experimentalist measures, the configurations she sees are an *incredibly* small subset of those that the system is capable of exploring.

Nature uses some very complex rules for time evolving the system from configuration to configuration, for example the many particle Newton or Schroedinger equations. These rules govern the states that the experimentalist sees, and hence the data she takes.

Here’s one useful way to think about computer simulations: The goal of a computer simulation is to devise a method where the *computer* plays a similar role to that of *nature* for the experimentalist. That is, the computer generates configurations upon which one makes measurements. This leaves us with the problem of devising instructions for the computer that replicate nature’s way of generating configurations.

One approach to constructing a simulation would be actually coding up the microscopic equations governing the system’s time evolution. Simulations of classical systems going under the name ‘molecular dynamics’ are actually done precisely this way. One computes the force F_n on each particle n , uses the force to compute the acceleration $a_n = F_n/m$, and then moves the velocity and position forward a small time interval dt with, $v_n \rightarrow v_n + a_n dt$; $x_n \rightarrow x_n + v_n dt$. But in the spirit of statistical mechanics, one really doesn’t care about the microscopic time evolution and the paths $x_n(t)$ and $v_n(t)$ the particles take in phase space. All that is really needed is to replicate the *probability* $P(\{x_n, v_n\})$ that nature uses to generate her configurations. If one can do that, one will get the same answers as the experimentalist!

In doing classical statistical mechanics, the probability distribution that one would be attempting to emulate would be the Boltzmann distribution $P(\{x_n, v_n\}) = Z^{-1} e^{-\beta E(\{x_n, v_n\})}$. However, let’s discuss Monte Carlo within the context of a general probability distribution. This will emphasize that Monte Carlo is by no means limited to Boltzmann statistics. To make the notation less unwieldy, label the probabilities by a single index i which will be understood to represent particular values of all the degrees of freedom of the system being studied (for example i could mean a collection of positions and velocities $\{x_n, v_n\}$). In the remainder of this note the inverse temperature is denoted by $\beta = 1/T$, and Boltzmann’s constant is set to unity.

As will be seen, to do Monte Carlo, it is not necessary to know p_i , but only ratios of p_j/p_i for two configurations. This is certainly an important point for statistical mechanics since $p_j/p_i = e^{-\beta(E_j - E_i)}$ is known, but the individual p_i involve the unknown partition function Z .

The goal is to figure out a rule T_{ji} to evolve the configuration i into the configuration j which will generate configurations with a desired probability. More precisely, the process will not be deterministic, but will involve random changes, so T_{ji} will be the probability to generate j from i . Because probabilities are non-negative, and sum up to unity, the rule T_{ji} satisfies,

$$\begin{aligned} T_{ji} &\geq 0 \\ \sum_j T_{ji} &= 1. \end{aligned} \tag{86}$$

A matrix obeying these two restrictions is called a ‘stochastic matrix’. Its eigenvalues obey $|\lambda| \leq 1$. Also, there is an eigenvector with eigenvalue $\lambda = 1$. These facts are simple to prove.

Consider the eigenvector equation,

$$\sum_i T_{ji} v_i = \lambda v_j. \tag{87}$$

Take absolute values of both sides of the equation and use the fact that $T_{ji} \geq 0$ and the triangle inequality.

$$\sum_i T_{ji} \|v_i\| \geq \|\lambda\| \|v_j\|. \tag{88}$$

Now sum both sides of the equation over j and use the fact that $\sum_j T_{ji} = 1$,

$$\sum_i v_i \geq |\lambda| \sum_j v_j. \tag{89}$$

Thus $\lambda \leq 1$.

To show that a stochastic matrix has an eigenvalue of unity, consider the vector with all components the same, $v_j = 1$. Then, from the second line of Eq. 1,

$$\sum_j v_j T_{ji} = v_i. \quad (90)$$

So the constant vector is a left eigenvector of T of eigenvalue 1. Remember that the eigenvalues of a matrix are the same whether one considers left or right eigenvectors, but the eigenvectors themselves can be quite different unless the matrix is symmetric. This is important to keep in mind, because the right eigenvector of T is not the trivial constant vector. In fact, the right eigenvector of T is p_j .

That the eigenvalue $\lambda = 1$ is non-degenerate is a consequence of the Perron-Frobenius theorem.

Because T is the rule for generating one configuration from the next, we can view the generation of a long sequence of configurations in the Monte Carlo process [106] as the repeated application of the matrix T . When a matrix is applied repeatedly to a vector, the eigenvector of largest eigenvalue is projected out. Thus, because T is stochastic, the eigenvector of eigenvalue 1 is generated.

So now the goal is a little bit more precise: One wants to figure out T obeying Eq. 1 whose eigenvector of eigenvalue one is the vector of desired probabilities p_i . Then, repeatedly applying T will give us p and we're done.

It is easy to show that if T is constructed to obey 'detailed balance',

$$T_{ji} p_i = T_{ij} p_j \quad (91)$$

then p_i is an eigenvector of T of eigenvalue 1:

$$\sum_i T_{ji} p_i = \sum_i T_{ij} p_j = p_j \sum_i T_{ij} = p_j. \quad (92)$$

It is also easy to formulate T to obey detailed balance. The most famous prescription is due to Metropolis. The Metropolis algorithm says that one suggests a move from i to j and then accepts the move with probability one if j is more likely than i , that is, if $p_j/p_i > 1$. If j is less likely than i , accept j with probability p_j/p_i .

Exercise B1: Show that if you generate a random number r uniformly on $[0, 1]$ and accept the move when $r < p_j/p_i$, then the Metropolis algorithm is correctly implemented.

The argument presented above can be summarized as follows:

- [a] Metropolis ---> Detailed Balance ---> p is eigenvector of T of eigenvalue 1
- [b] T is stochastic ---> max eigenvalue of T is 1
- [a+b] p is eigenvector of T of largest eigenvalue
- [c] Repeated application of T yields eigenvector of largest eigenvalue
- [a+b+c] Repeated application of T gives p , as desired.

- (i.) Take an initial configuration i and propose a change to a new configuration j .
- (ii) Accept the new configuration with probability $\min(1, p_j/p_i)$.
- (iii) Measure quantities of interest.
- (iv) Repeat the process many times.

There are of course many subtleties: What sort of procedure is followed to "suggest changes"? How many configurations do you need to generate and do you, as in some experiments, need to allow the system time to equilibrate? Some of these issues are addressed below.

There are a number of useful analogies between Monte Carlo and experiment. Perhaps most importantly, when first encountering Monte Carlo it is natural to wonder how the relatively small sample of configurations that a computer generates could possibly replicate the behavior of physical systems which have incredibly huge numbers of states. A partial answer is provided by noting that the exact same question could be posed to any experimentalist, where, similarly, measurements are based on a very small subset of states which are generated by the time evolution during the course of the experiment.

Second, when one collects data in a Monte Carlo, one measures observables for each configuration generated and then does a simple average over all the configurations. There are no probabilities p_i put in the averaging. The reason,

of course, is that the computer is putting the p_i in for you, by generating the configurations with their correct p_i . This is just as in an experiment. No experimentalist weights her measurements with the Boltzmann factor!

In addition to averages, error bars are generated in Monte Carlo just as in experiments. (See Sec. XI.)

One often has to wait a little while after starting a simulation to allow the system to equilibrate, much as the experimentalist will not start recording data until some time has passed following perturbing the system in some way.

If you think about it, the transition matrix T actually has two pieces in its construction. The first is the suggestion of a new state j , and the second is the decision (e.g. Metropolis) whether to accept j or not. It is the *combination* of these two factors which determines T and which must obey detailed balance. Examples of how the method of suggesting states might go awry are given in the Exercises below.

Exercise B2: The Metropolis algorithm is not the only way to go. Show that the “heat bath” prescription

$$T_{ji} = p_j / (p_i + p_j) \quad (93)$$

obeys detailed balance.

Thus the starting point ‘Metropolis’ of [a] in Sec. III can be replaced by ‘Heat Bath’.

Exercise B3: Consider a system with two states and associated probabilities p_1, p_2 . Suppose the observable A has the values A_1 and A_2 in the two states. What will you get for $\langle A \rangle$ if you measure A only when a move is accepted? What is the correct value for $\langle A \rangle$? When should you measure A to get the right answer? Argue qualitatively that, if $p_1 \gg p_2$, the sequence of configurations generated gives a sensible answer when you put your measurement in the correct spot.

Exercise B4: Consider a system with three states and associated probabilities p_1, p_2, p_3 . Construct the 3×3 matrix for T assuming that if you are in a state i you suggest a change to one of the other two states with probability $\frac{1}{2}$ each, and then accept or reject with Metropolis. Verify that your T obeys Eq. 1 and that the vector $(p_1 p_2 p_3)$ is a right eigenvector of T of eigenvalue one. Verify the other two eigenvalues are less than one in absolute value.

Exercises B5 and B6 below emphasize that the rule T for generating states is not unique. The art of Monte Carlo is in finding the T which works best, that is, which moves you around in phase space most rapidly and generates the smallest error bars.

Exercise B5: Do Exercise B4 again, but use the heat bath algorithm.

Exercise B6: Again consider the same three state system as Exercise B4. Construct the 3×3 matrix for T assuming that if you are in a state i you suggest a new state (which could be the same as the one you are in) randomly, that is, with pick the new state to be 1 or 2 or 3, with probability $\frac{1}{3}$, and then do Metropolis. Verify that your T obeys Eq. 1 and that the vector $(p_1 p_2 p_3)$ is a right eigenvector of T of eigenvalue one. Verify the other two eigenvalues are less than one in absolute value. In which case is the next smallest eigenvalues closer to $\lambda = 1$, here, or in Ex. 5?

Exercise B7: Consider a system with an infinite number of states $E_i = \omega i$ for $i = 0, 1, 2, 3, \dots$, and associated probabilities $p_i \propto e^{-\beta E_i}$. Construct the matrix for T assuming that your suggestion of a move from state i is to one of the two immediately adjacent states $j = i \pm 1$, with probability $\frac{1}{2}$. Verify $(p_1 p_2 p_3 \dots)$ is a right eigenvector of T . Be especially careful with the state $i = 0$ which has no state beneath it! Should you suggest state $j = 1$ all the time, since there is no $j = -1$? This is an example of the subtlety mentioned in Sec. VI.

Exercise B8: Write a Monte Carlo code which computes $\langle E \rangle$ for the three state system of Exercise B4, using the T described in that exercise.

Exercise B9: Write a Monte Carlo code corresponding to the T of exercise 5.

Exercise B10: Write a Monte Carlo code corresponding to the T of exercise 6.

Exercise B11: Write a Monte Carlo simulation for an energy which has a continuous degree of freedom x with $E(x) = \frac{1}{2} kx^2$. Construct T by suggesting the new state $x' = x + \Delta(r - \frac{1}{2})$ where Δ is the ‘step-size’, and r is a random number uniformly distributed on $(0,1)$. Use Metropolis to accept/reject x' . What is the correct value for $\langle E \rangle$? Show your code gets it, for any value of Δ . What values of Δ are best? See also Sec. XI below.

Exercise B12: Do Exercise B11 again, except this time construct T by suggesting the new state $x' = x + \Delta(r - \frac{1}{3})$, and then use Metropolis. Show your code gets the wrong value for $\langle E \rangle$. Show that your T violates detailed balance, even though you use Metropolis after the move suggestion.

Many readers going through these notes have a particular (and presumably non-trivial) problem they wish to address with Monte Carlo. If, however, you do not, a standard Monte Carlo simulation to try is the two dimensional Ising

model. Many books on simulations contain descriptions [107, 108, 109].

As with all codes, tests are essential. Here three very useful ones are mentioned.

First, Monte Carlo simulation codes can often be tested on small lattices. That is, it is often possible to enumerate all the possible states of a small system (e.g. a 4x4 Ising lattice has 2^{16} configurations) and have the computer then generate the partition function and expectation values through an explicit enumeration of all the configurations.

Second, limits of the Hamiltonian in question are often soluble. At high and low temperatures, one often can figure out the values of the energy and other observables. Likewise, by turning off one or more terms in the Hamiltonian, it may become analytically soluble. Or, if you write your code so that the interactions are different in different directions, you can sometimes turn off one or more directions and reduce the dimensionality of the system to a point where analytic solutions are known.

Finally, while you will usually write your code so that it averages observable which should be equivalent by some symmetry, looking at the unaveraged values first is often useful: Many bugs in codes are fingered by measurements which should be equal by symmetry but are not.

My experience is that if your code checks out for the entire model on small lattices, and then individual pieces on different lattice sizes, and also the high and low T limits, then it is very likely correct.

The above discussion seems to rely very heavily on the fact that the system is classical. However, it turns out to be relatively easy to generalize classical Monte Carlo to Quantum Monte Carlo. To do this, one takes the operator $e^{-\beta\hat{H}}$ and writes its trace as a path integral. This sum over paths involves a *classical* action, which then can be attacked with classical Monte Carlo. A nice discussion of this for the quantum harmonic oscillator is given by Creutz [110]. Another particularly interesting example is the mapping of the $d = 1$ Ising model in a transverse magnetic field onto the classical $d = 2$ Ising model.[111] Of course, the determinant QMC algorithm described in the main body is also an example of such a mapping (with an obnoxiously complicated Boltzmann weight).

Relation to Molecular Dynamics and the Langevin Equation

At the beginning of these notes, Molecular Dynamics (MD) was mentioned as one way a computer might emulate nature. Since the equations of MD keep the energy constant (to within time step errors), one way to view MD is as a Monte Carlo where the proposed move does not change the energy, and is therefore accepted with unit probability according to the Metropolis prescription. Thus MD and Monte Carlo should give the same result, under the condition that the MD energy is initialized at the same value $\langle E \rangle$ as the average energy which comes out of the Monte Carlo. This is the usual equivalence of the canonical and microcanonical ensembles in statistical mechanics.

In practice, one might want to do MD at a particular temperature T instead of at fixed E . One way to accomplish this is to evolve the positions and velocities x_n and v_n using the MD equations, but then periodically ‘refresh’ the velocities by replacing their current values with new ones drawn from the Gaussian distribution $e^{-m_n v_n^2/2T}$. Here m_n is the mass of the n th particle. One chooses to ‘refresh’ the momenta, because usually the energy takes the form $E = \frac{1}{2} \sum_n m_n v_n^2 + V(\{x_n\})$. That is, the potential energy doesn’t depend on the velocities. So the probability distribution for the velocities is Gaussian, and it is known how to generate Gaussian distributed random numbers. The positions usually involve a more complicated V than Gaussian.

This sort of finite T molecular dynamics can be understood as a Monte Carlo with two types of moves. As remarked above, the conventional MD moves keep the energy constant and hence are always accepted. The momentum refreshment moves change the energy and hence are sometimes rejected according to the Metropolis prescription.

Exercise B13: Write a Molecular Dynamics code for $E = \frac{1}{2}kx^2 + \frac{1}{2}mv^2$. (That is, use $F = -kx$ and $a = F/m$ to update v .) Verify that you travel along an ellipse in phase space at constant energy, when dt is small. Here ‘ dt small’ really means dt is much less than the period $2\pi\sqrt{m/k}$. Compute $\langle x^2 \rangle$ and $\langle p^2 \rangle$ and show you get the correct answers (which only depend on x_0 and v_0). Note that the Molecular Dynamics integration of equation of motion introduces time step errors. In the Euler method, the accumulation of these errors will lead to an exponential increase in E . The “leap-frog” method is much more robust.

Exercise B14: Include steps which refresh the momentum. Compute $\langle x^2 \rangle$ and $\langle p^2 \rangle$ and show you get the correct answers (which now do not depend on the initial conditions as in Ex. 13 but only on temperature T .)

Monte Carlo can also be related to the Langevin Equation. Consider a system with an energy $E(x)$ which depends on the degree of freedom x . (For simplicity, consider a single degree of freedom.) Suppose a procedure is defined for updating x via

$$x' = x - \varepsilon \frac{\partial E}{\partial x} + \sqrt{4\varepsilon T} r \quad (94)$$

Here r is a Gaussian random number, $p(r) = e^{-r^2}/\sqrt{\pi}$, and T is the temperature. One can now show that this equation satisfies detailed balance with $p(x) \propto e^{-\beta E(x)}$.

The Langevin Equation amounts to a prescription T for getting a new state x' from an original state x . Given x' and x , the value of T is the probability of throwing the appropriate random number which will take you from x to x' .

$$T(x', x) = \frac{1}{\sqrt{\pi}} e^{-r^2} \quad (95)$$

$$r = \frac{1}{\sqrt{4\varepsilon T}} (x' - x + \varepsilon \frac{\partial E}{\partial x}) \quad (96)$$

Therefore, introducing the notation $dx = x' - x$,

$$T(x', x) = \frac{1}{\sqrt{\pi}} e^{-(dx + \varepsilon \frac{\partial E}{\partial x})^2 / (4\varepsilon T)} \quad (97)$$

Likewise,

$$T(x, x') = \frac{1}{\sqrt{\pi}} e^{-(-dx + \varepsilon \frac{\partial E}{\partial x})^2 / (4\varepsilon T)} \quad (98)$$

Note that actually the gradient of the energy in Eq. 99 should now be evaluated at x' , but because ε is small, dx will be small and x' close to x . Since the gradient is already multiplied by ε the difference is higher order and can be dropped.

Putting this together,

$$\frac{T(x', x)}{T(x, x')} = e^{-\frac{\partial E}{\partial x} dx / T} = e^{-dE/T} = e^{-(E(x') - E(x))/T} \quad (99)$$

$$T(x, x') e^{-E(x')/T} = T(x', x) e^{-E(x)/T}, \quad (100)$$

where again terms which are higher than linear order in ε are neglected. Eq. 15 completes the demonstration that the Langevin equation obeys detailed balance. Hence by the general theorems concerning Monte Carlo, it will generate configurations of the system according to the Boltzmann distribution.

A final comment: You will notice that the prefactors of the random force and the force which depends on E in the Langevin equation are not independent. This is an example of the fluctuation-dissipation theorem.

Exercise B15: In proving detailed balance higher order terms in ε were thrown away. Consider the energy $E(x) = \frac{1}{2}kx^2$ and go through the Langevin analysis retaining terms to all orders in ε . Show that detailed balance is obeyed with a k shifted by order ε . Will $\langle x^2 \rangle$ be overestimated or underestimated?

Exercise B16: Write a computer code to implement the Langevin equation for $E(x) = \frac{1}{2}kx^2$. Verify your results from Exercise B15.

Error Analysis in Monte Carlo

This final section is intended to review error analysis in Monte Carlo, and illustrate it with the very simple example of a simulation of $E(x) = \frac{1}{2}kx^2$. Begin with the definitions,

$$\langle x \rangle = \frac{1}{N} \sum_{i=1}^N x_i \quad (101)$$

$$\langle x^2 \rangle = \frac{1}{N} \sum_{i=1}^N x_i^2 \quad (102)$$

$$\sigma = \sqrt{\frac{\langle x^2 \rangle - \langle x \rangle^2}{N-1}}. \quad (103)$$

Here x_i is the i th measured value of x , and N is the number of measurements. The definitions of $\langle x \rangle$ and $\langle x^2 \rangle$ are unambiguous. The entire content of this note is to clarify the proper denominator of the definition of σ . Specifically, the formula for σ assumes that the N measurements are all independent. Since successive values of x are generated from each other, this is never true. The x values are more and more related the less time one waits between measurements.

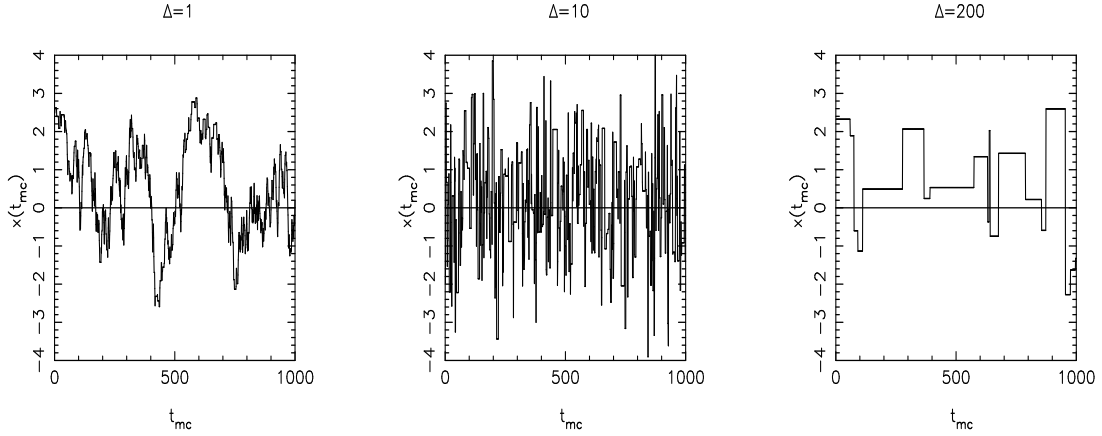


FIGURE 41. First 1000 steps in Monte Carlo time history of x for three different step sizes $\Delta = 1, 10, 200$. (Acceptance rates=0.70, 0.35, 0.02).

To quantify the correlations among successive x values, define the autocorrelation function,

$$c(l) = \frac{1}{N-l} \sum_{i=1}^{N-l} y_i y_{i+l} \quad (104)$$

Here $y(i) = x(i) - \langle x \rangle$ measures the fluctuation of x about its average value. $c(l)$ measures whether those fluctuations are related for x values l measurements apart. Saying x_i and x_{i+l} are independent means whether x_{i+l} is above or below $\langle x \rangle$ (the sign of y_{i+l}) is unrelated to the sign of y_i . If that is the case, $c(l) = 0$ (to within errors). Clearly $c(0)$ is never zero. In fact, $c(0) = \sigma^2$. It is conventional to redefine $c(0) \rightarrow c(0)/\sigma^2$ so that $c(0) = 1$.

Let's begin by looking at actual time histories of x . Choose $k = 1$ and $T = 2$ so that $\langle x^2 \rangle = 2$. The step size for suggested changes in x is Δ . Measure every Monte Carlo step and ran for $N = 400000$ sweeps. Here of course since $\langle x \rangle = 0$, $y_i = x_i$. The Monte Carlo time histories are given in Figure 1. That the data are correlated is immediately evident. If a value of x_i is positive, its successors tend to be positive and similarly if it is negative. The dependence on the step size Δ is easy to interpret.

If Δ is small you do not suggest much of a change, and successive values of x are highly correlated. Likewise, if Δ is large, most suggested Monte Carlo moves take you out of the part of phase space of low energy and are rejected. (This results in the long flat regions of the evolution of x .)

The plots of $c(l)$ resulting from the same data are given in Figure 2. $c(l)$ has a characteristic decaying exponential form. Define the correlation time τ to be the point when $c(l = \tau) = e^{-1}$ and say that measurements of x are independent when l exceeds τ . (Strictly speaking, one wants c to go to zero, but $c(\tau) = e^{-1}$ is an acceptable criterion.) Notice you can almost guess the values of τ given by Figure 2 directly from the time histories of Figure 1.

As mentioned earlier, in generating the above results x was measured at every Monte Carlo step. What happens if one instead measures only every m th step? Define $c_m(l)$ to be the correlation function when measurements are only every m th Monte Carlo step. It is easy to convince yourself that $c_m(l) = c_1(ml)$, so the correlation function rescales in a trivial fashion. The point is that if one choose $m > \tau$, then the measurements all become independent.

- So one way to ensure the value for the error bar σ is correct is to make sure measurements are separated by a waiting time $m > \tau$.

This approach has the advantage that one does not waste time making measurements when the measurements are not independent.

An alternate (and equivalent) approach to getting the correct σ is by "rebinning" the data. Take a file containing the complete time history of a measurement, for example the data for x which is partially shown in Figure 1. Choose a "bin size" M , and average the data for x over each of the $L = N/M$ bins (remember $N =$ total number of measurements) to create L "binned measurements" m_j .

$$m_j = \frac{1}{M} \sum_{i=M*(j-1)+1}^{M*j} x_i. \quad (105)$$

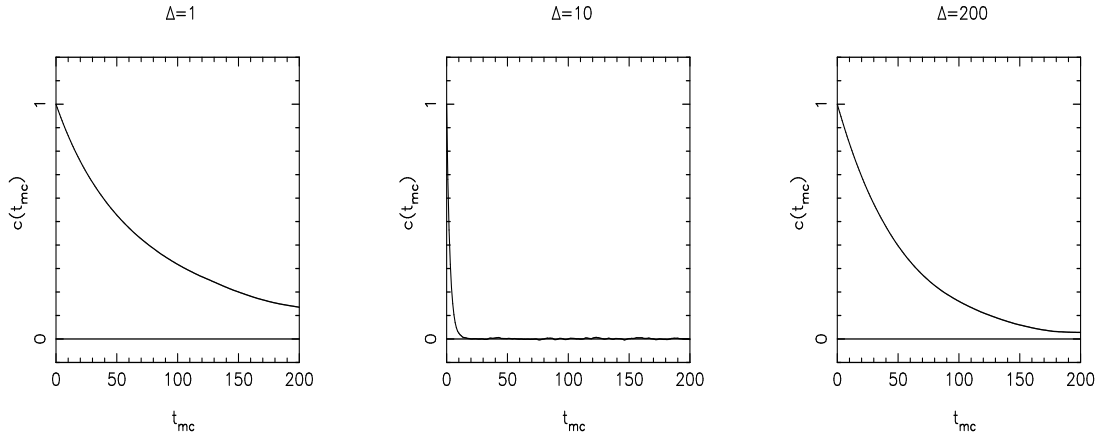


FIGURE 42. Autocorrelation functions for the complete data sets (400,000 steps) as in figure 1. (Step sizes $\Delta = 1, 10, 200$, Acceptance rates=0.70, 0.35, 0.02).

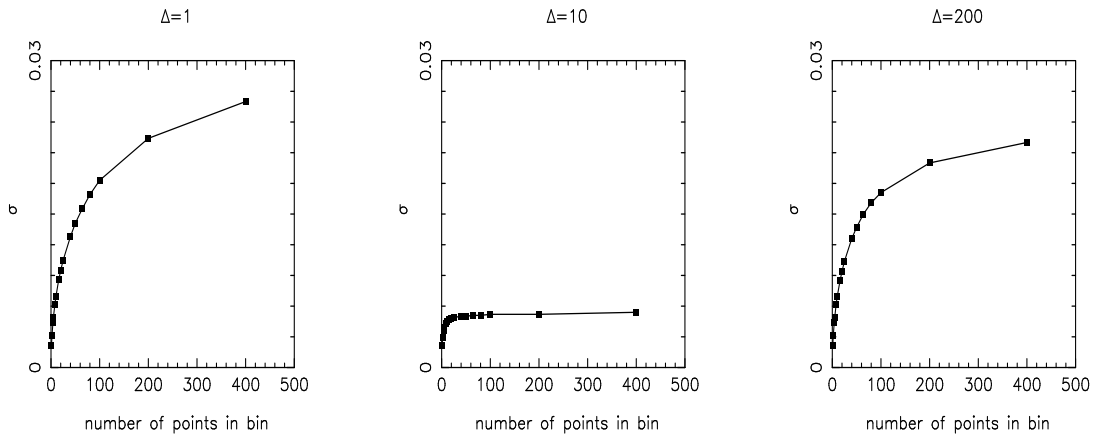


FIGURE 43. Error bars for different bin sizes M . Data is that of Figures 1,2: step sizes $\Delta = 1, 10, 200$. (Acceptance rates=0.70, 0.35, 0.02).

Treat these L values for m as your independent measurements. As seen in Equation 5, the values for m are already averages over M values of x . Define averages and error bars as in Equation 1, with L replacing N in the normalizations $1/N$ and $1/\sqrt{N-1}$. The average $\langle x \rangle$ is independent of M since all one is doing is reordering a linear sum. The average $\langle x^2 \rangle$ is however altered, and hence so is the error bar σ . Figure 3 shows values for σ as a function of the number of x values in each bin, M .

What is the interpretation of Figure 3? Consider $M = 1$. In this case only one value of x is put in each bin, so that in calculating σ it is assumed all x are independent. The error bar σ thus obtained is too small. As M becomes larger, more x values are put in each bin, the number of bins (independent measurements) decreases, and σ increases. Eventually σ goes to an asymptotic value which gives the correct error bar.

Why does σ not increase indefinitely as M increases? You might expect it to, since the denominator $\sqrt{L-1}$ is getting smaller and smaller. The answer is that as more measurements are put in each bin, the different bins fluctuate less and less. The numerator which measures these fluctuations decreases in exact compensation to the denominator. (However, to reiterate, initially for M small when you put more measurements in the bins the new values are not independent and so the numerator does *not* decrease.)

- So a second way to ensure the value for the error bar σ is correct is to consider different binnings of the data, and use the value obtained asymptotically as each bin contains a lot of data.

How does one see this result is consistent with the correlation function analysis? There are two checks. The first is to see that the value for M at which σ starts to flatten out should be roughly the same as the value of τ for which $c(l)$ gets small. Second, one can compare the values of σ_1 at $M = 1$, where one assumes all the x are independent, with the asymptotic value σ_∞ . The claim is that these should be related by $\sigma_\infty = \sqrt{\tau}\sigma_1$. You can see this is roughly true: For $\Delta = 1$ one obtains $\sigma_1 = 0.0022$ and $\sigma_\infty = 0.030$ from Figure 3. If you assume all the measurements are independent, you underestimate σ by more than an order of magnitude. Meanwhile, from figure 2, $\tau \approx 85$, and hence $\sqrt{\tau}$ similarly reflects this order of magnitude correction factor.

The acceptance rate provides a rough guide to the choice of a good step size. If the acceptance rate is too much greater than 0.5, then one is likely in the limit of Figures (1–3)a where the correlation time is unnecessarily large due to small suggested moves. Likewise, if the acceptance rate is too much less than 0.50, then one is likely in the limit of Figures (1–3)c where the correlation time is unnecessarily large due to multiple rejections.

Careful error analysis involves the procedure outlined above, calculation of correlation times, etc. However, in practice one often has (or develops) a good intuition about these things. A very simple approach to error bars, then is simply to bin the data from your run into a small number of bins, say ten (ie. $M = N/10$) and leave it at that. This strategy assumes that you were doing a reasonably long run, so that $N/10 > \tau$. My thinking is that if this is violated, you are in more serious trouble than just getting the wrong error bars: you will have less than 10 independent measurements (and perhaps have not even properly equilibrated) so it is likely your expectation values themselves are wrong. For the particular example considered here, the reported values from the simplistic approach for $\langle x^2 \rangle$ and σ were 1.973 ± 0.051 , 1.993 ± 0.010 , 1.995 ± 0.039 for $\Delta = 1, 10, 200$ respectively. These error bars should be the same as the asymptotic values of σ in Fig. 3.

Does it matter which measurement you look at? Here x_i has been the focus of the analysis. Would it matter x_i^2 or some other measurement had been examined? For this simple problem, no. In more complicated simulations it is often important to calculate correlation times separately for measurements of “local” quantities (observables for degrees of freedom that are close together spatially) and “global” quantities (observables for degrees of freedom that are far apart spatially). The spatial separation of the different degrees of freedom in an observable can affect the autocorrelation time. In particular, observables containing quantities which are widely spaced generally have longer correlation times.

More generally, the size of the system you are simulating (and hence the spatial separations of the degrees of freedom) can greatly affect the correlation time, especially in the vicinity of a phase transition. Just as physical quantities like the specific heat, susceptibility etc can diverge at a critical point, the correlation time can diverge too as the system size increases near a critical point. This of course makes Monte Carlo very difficult. There is a big literature on solving this problem.

APPENDIX C: DETERMINANT QUANTUM MONTE CARLO IN DETAIL

A Useful Analogy: Multidimensional Gaussian Integration

The equations involved in determinant QMC bear many similarities with multidimensional Gaussian integrals. Reviewing these identities will help provide an intuitive feel for the formulae of determinant QMC, within a familiar context.

The generalization of the one dimensional Gaussian integral,

$$\int_{-\infty}^{+\infty} dx e^{-ax^2} = \frac{\sqrt{\pi}}{a}, \quad (106)$$

to many dimensions is,

$$Z = \int_{-\infty}^{+\infty} \int_{-\infty}^{+\infty} \dots \int_{-\infty}^{+\infty} dx_1 dx_2 \dots dx_N e^{-\vec{x}A\vec{x}^T} = \frac{\pi^{n/2}}{\sqrt{\det A}}. \quad (107)$$

Here \vec{x} is an N dimensional vector of real numbers and A is a real, symmetric, N dimensional matrix. The notation Z has been used for the integral to emphasize that it would be the partition function for a set of classical variables whose action is given by the quadratic form $\vec{x}A\vec{x}^T$.

These integrals can also be done when the integrand includes factors of x_i .

$$\langle x_i x_j \rangle = Z^{-1} \int_{-\infty}^{+\infty} \int_{-\infty}^{+\infty} \dots \int_{-\infty}^{+\infty} dx_1 dx_2 \dots dx_N x_i x_j e^{-\vec{x}A\vec{x}^T} = \frac{1}{2} [A^{-1}]_{ij} \quad (108)$$

Again, the notation $\langle x_i x_j \rangle$ emphasizes a possible statistical mechanical interpretation of the ratio of integrals. Further factors of x_i in the integrand generate expressions like,

$$\begin{aligned}\langle x_i x_j x_k x_l \rangle &= Z^{-1} \int_{-\infty}^{+\infty} \int_{-\infty}^{+\infty} \dots \int_{-\infty}^{+\infty} dx_1 dx_2 \dots dx_N x_i x_j x_k x_l e^{-\bar{x} A \bar{x}^T} \\ &= \frac{1}{4} ([A^{-1}]_{ij} [A^{-1}]_{kl} + [A^{-1}]_{ik} [A^{-1}]_{jl} + [A^{-1}]_{il} [A^{-1}]_{jk}).\end{aligned}\quad (109)$$

These are similar in form to ‘Wick’s Theorem’, which tells us that contractions of products of many fermion operators can be expressed as sums of products of contractions taken two operators at a time, in all possible permutations. While it is possible to do these integrals with arbitrary polynomials as part of the integrand, they cannot be done when a quartic term appears in the exponential. The analogies of these various statements for traces over fermion Hamiltonians will be exhibited shortly.

Basic Formalism of Determinant QMC

In solving the Hubbard model it is necessary to evaluate expressions like

$$\begin{aligned}\langle \hat{A} \rangle &= Z^{-1} \text{Tr} [\hat{A} e^{-\beta \hat{H}}] \\ Z &= \text{Tr} e^{-\beta \hat{H}}\end{aligned}\quad (110)$$

The ‘Tr’ is a trace over the 4^N dimensional Hilbert space, where N is the number of sites.

In analogy with multidimensional Gaussian integration, we can do such traces if they are over *quadratic* forms of fermion operators. Suppose

$$\hat{H} = \sum_{ij} c_i^\dagger h_{ij} c_j \quad (111)$$

Here h is an $N \times N$ matrix. The identity is,

$$Z = \text{Tr} e^{-\beta \hat{H}} = \det [I + e^{-\beta h}]. \quad (112)$$

Note that while the original ‘Tr’ is over a quantum mechanical 4^N dimensional Hilbert space, the ‘det’ is a usual determinant of $N \times N$ matrices. ‘I’ is the N dimensional identity matrix and ‘h’ is the matrix of *numbers* entering the definition of \hat{H} . It is worth emphasizing that because one takes the trace over the full 4^N dimensional Hilbert space, states of all occupation numbers are included. The determinant QMC method, as formulated here, works in the grand canonical ensemble. Particle density is controlled by changing the chemical potential.

It is trivial to check that Eq. 113 holds for a single fermion degree of freedom, with Hamiltonian $\hat{H} = \epsilon c^\dagger c$. There are two states in the Hilbert space and

$$Z = \langle 0 | e^{-\beta \epsilon c^\dagger c} | 0 \rangle + \langle 1 | e^{-\beta \epsilon c^\dagger c} | 1 \rangle = 1 + e^{-\beta \epsilon}. \quad (113)$$

More generally (e.g. for more than one fermion degree of freedom) Eq. 113 can be verified by going to the basis where h is diagonal. The equations can also be derived by employing the techniques of Grassman integration.

There is a more general identity. If one has a *set* of quadratic Hamiltonians $l = 1, 2, \dots, L$

$$\hat{H}(l) = \sum_{ij} c_i^\dagger h_{ij}(l) c_j \quad (114)$$

then,

$$Z = \text{Tr} [e^{-\Delta\tau \hat{H}(1)} e^{-\Delta\tau \hat{H}(2)} \dots e^{-\Delta\tau \hat{H}(L)}] = \det [I + e^{-\Delta\tau h(1)} e^{-\Delta\tau h(2)} \dots e^{-\Delta\tau h(L)}]. \quad (115)$$

Here the prefactor in the exponential has been changed from β to $\Delta\tau$ for reasons which will soon be clear. It is also true that,

$$\begin{aligned}G_{ij} = \langle c_{i\sigma} c_{j\sigma}^\dagger \rangle &= Z^{-1} \text{Tr} [c_{i\sigma} c_{j\sigma}^\dagger e^{-\Delta\tau H(1)} e^{-\Delta\tau H(2)} \dots e^{-\Delta\tau H(L)}] \\ &= [I + e^{-\Delta\tau h(1)} e^{-\Delta\tau h(2)} \dots e^{-\Delta\tau h(L)}]_{ij}^{-1}.\end{aligned}\quad (116)$$

The “fermions Greens function” is just an appropriate matrix element of the inverse of the $N \times N$ matrix whose determinant gives the partition function.

The above formulae describe how to perform traces over quadratic forms of fermion degrees of freedom. Unfortunately, the Hubbard Hamiltonian has an interaction term $Un_{i\uparrow}n_{i\downarrow} = Uc_{i\uparrow}^\dagger c_{i\uparrow} c_{i\downarrow}^\dagger c_{i\downarrow}$ which is quartic in the fermion operators. To handle such terms, one employs the (discrete) Hubbard–Stratonovich transformation,

$$e^{-U\Delta\tau(n_{\uparrow}-\frac{1}{2})(n_{\downarrow}-\frac{1}{2})} = \frac{1}{2} e^{-\frac{U\Delta\tau}{4}} \sum_s e^{\lambda s(n_{\uparrow}-n_{\downarrow})} \quad (117)$$

Here $\cosh\lambda = e^{U\Delta\tau/2}$, and s is an Ising variable which can take on the two values $S = \pm 1$. This identity can be verified by explicitly enumerating the 4 possible choices for $n_{\uparrow}, n_{\downarrow}$.

Now divide $\beta = L\Delta\tau$ and employ the Trotter decomposition. This allows us to isolate different pieces of the Hamiltonian. Write $\hat{H} = \hat{K} + \hat{V}$ where \hat{K} contains all the one–body pieces and \hat{V} the on–site Hubbard interaction. Then,

$$Z = \text{Tr} e^{-\beta\hat{H}} = \text{Tr}[e^{-\Delta\tau\hat{H}}]^L \approx \text{Tr}[e^{-\Delta\tau\hat{K}} e^{-\Delta\tau\hat{V}} e^{-\Delta\tau\hat{K}} e^{-\Delta\tau\hat{V}} \dots]. \quad (118)$$

The final expression is only approximate since \hat{K} and \hat{V} do not commute. However, the approximation becomes better and better as L increases ($\Delta\tau$ decreases). As mentioned before, the errors should be pretty small if $tU(\Delta\tau)^2 \approx 1/10$.

The $e^{-\Delta\tau\hat{K}}$ are quadratic in the fermion operators. For each factor of the L terms $e^{-\Delta\tau\hat{V}}$ above, introduce N Hubbard–Stratonovich fields, one for each of the spatial sites where there is an on–site interaction to decouple. The Hubbard–Stratonovich field $s(i, l)$ therefore has two indices, space i and imaginary–time l . Now the $e^{-\Delta\tau\hat{V}(l)}$ are also quadratic in the fermion operators. The argument l on \hat{V} emphasizes that while the \hat{K} are all identical, the $\hat{V}(l)$ contain different Hubbard–Stratonovich fields on the different imaginary time slices.

Applying Eqs. 22-23 allows the analytic evaluation of the trace,

$$Z = \sum_{s(i,l)} \det M_{\uparrow} \det M_{\downarrow}, \quad (119)$$

with,

$$M_{\sigma} = I + e^{-k} e^{-v_{\sigma}(1)} e^{-k} e^{-v_{\sigma}(2)} \dots e^{-k} e^{-v_{\sigma}(L)}. \quad (120)$$

A determinant is obtained for each of the two spin species. The quantum partition function has now been expressed to a *classical* monte carlo problem: It is necessary to sum over the possible configurations of the real, classical, variables $s(i, l)$ with the “Boltzmann weight” which is the product of the two fermion determinants. Note that as in world-line QMC, the classical variable to be summed over has an additional index l labeling imaginary time.

Eqs. 2-4 can now be understood as coming from applying the general operator identity of Eqs. 22-23 to the specific problem of evaluating Eq. 26, with the interaction operators \hat{V} made into quadratic forms by using Eq. 25.

The algorithm, as stated, scales in CPU time as $N^4 L$. The reason is that re–evaluating the determinant of M' takes N^3 operations, and one must do that NL times to sweep through all the Hubbard–Stratonovich variables (if, as is typically done, just one at a time is changes). This scaling can be reduced to $N^3 L$. (In what follows the spin indices will be dropped.) The idea is to write $M' = M + dM$ and the ratio of determinants as,

$$\det M' / \det M = \det(M^{-1} M') = \det(M^{-1} (M + dM)) = \det(I + G dM), \quad (121)$$

with the definition $G = M^{-1}$. It turns out that dM is very simple because when a Hubbard–Stratonovich field is flipped, a single diagonal entry in $v(l)$ changes. Because dM is sparse, the evaluation of $\det(I + G dM)$ takes a cpu time independent of N and L ! In fact, a little bit of thought will convince you that Eq. 6 arises from Eq. 31 and the form for dM .

However, one needs $G = M^{-1}$ for this calculation, and once the Hubbard–Stratonovich field change is made, one needs to update G . This updating G does not take N^3 iterations, as one might expect of a matrix inversion, but can be done in only N^2 operations, again as a result of the simplicity of the change dM . The relevant identity which relates the new $G' = (M + dM)^{-1}$ to the old $G = M^{-1}$ is an application of the “Sherman–Morrison” formula given, for example, in Press’s ‘Numerical Recipes’. If you work through the Sherman–Morrison formula, as applied to the problem, you end up with Eqs. 7-8.

A final comment concerns the need for ‘wrapping’ Eq. 9. The use of Eq. 31 to derive Eq. 6, and the Serman–Morrison formula to derive Eqs. 7-8 require that the imaginary time slice of the Hubbard–Stratonovich variable being updated

be at the end of the product in Eq. 28. The process of wrapping moves the appropriate interaction matrix to the end of the product through a cyclic permutation. That is,

$$[e^{-k}e^{-v\sigma(L)}][I + e^{-k}e^{-v\sigma(1)}e^{-k}e^{-v\sigma(2)} \dots e^{-k}e^{-v\sigma(L)}]^{-1} [e^{-k}e^{-v\sigma(L)}]^{-1} \quad (122)$$

$$= [I + e^{-k}e^{-v\sigma(L)}e^{-k}e^{-v\sigma(1)} \dots e^{-k}e^{-v\sigma(L-1)}]^{-1} \quad (123)$$

Subtleties and “Tricks of the Trade”

While the above formulae allow you to write a “bare-bones” determinant QMC algorithm, there are a number of refinements which are important.

(1.) It is possible to measure correlation functions with non-zero imaginary time separation, but this requires considerably more work. Analytic continuation of such correlations is required to get the dynamical response. That is quite difficult.

(2.) The product of matrices required in constructing M and hence $G = M^{-1}$ (see Eq. 5 and Eq. 28) is numerically unstable at low temperatures and strong couplings. That is, the product has a very high ratio of largest to smallest eigenvalue. Special “stabilization” is required to do the matrix manipulations. While these add to the complexity of the code, they however have no content in the sense that all the above equations are valid, it is just a question of how best to multiply matrices on a machine of finite precision.

(3.) The determinants of the matrices can go negative. This is called the “fermion sign problem.” The sign problem does not occur for certain special cases. For example, if U is negative (the “attractive” Hubbard model), the individual determinants can go negative, but the matrices are always equal and hence the determinant appears as a perfect square. This is a consequence of the fact that the appropriate Hubbard–Stratonovich transformation couples S to the charge $n_{\uparrow} + n_{\downarrow}$ as opposed to the spin as given in Eq. 25 for the repulsive model. If U is positive but the chemical potential $\mu = U/2$ (“half-filling”) one is also okay. The matrices are not identical in this case, but the determinants are nevertheless related by a positive factor, that is, they again have the same sign, so their product is always positive. Some types of randomness are also acceptable. It is okay for the hoppings t and interactions U to depend on the link or site. These statements are demonstrated by various particle–hole transformations on the Hamiltonian.

(4.) Alternate Hubbard–Stratonovich transformations are possible. One can couple more symmetrically to the spin, that is not single out the z component. Or, one can couple to pair creation operators. So far, all such alternatives give a worse sign problem than the transformation Eq. 25. These more complicated transformations are needed to do ‘Hund’s rule terms’ in multi-orbital Hubbard models.

(5.) Very similar “ground state” determinant simulations exist which work at $T = 0$ and in the canonical ensemble.

What Determinant QMC Simulations Can Do and Concluding Remarks

The state of the art of determinant QMC simulations, in the absence of a sign problem, are studies of several hundred electrons down to temperatures of $\beta t = 10 - 20$. In terms of temperature and bandwidth, this means T of roughly $1/100$ of the bandwidth $W = 8t$ of the 2-d Hubbard model. This is plenty cold enough to see well developed magnetic correlations. For typical parameters, $t = 1, U = 4$ one chooses $\Delta\tau = 1/8$ so these beta values correspond to roughly $L = 100$, and the simulation involves approximately 10^4 Hubbard–Stratonovich variables.

In cases where one has a sign problem, βt is limited to 4–5. This is, unfortunately, not low enough in temperature to make conclusive statements about certain important problems, perhaps most prominently the question of the existence of long range d -wave superconducting correlations in the Hubbard model away from half-filling.

Determinant QMC is a powerful method for simulating interacting electron Hamiltonians in more than one dimension. One can easily study problems with several hundred particles, an order of magnitude greater than with exact diagonalization, and often large enough to make compelling finite size scaling analysis. The sign problem is a very significant limitation, however. For the repulsive Hubbard model, one can go to temperatures on the order of $W/30$ where W is the bandwidth. For special cases like the attractive Hubbard model or the repulsive model at half-filling, there is no sign problem, and the ground state properties can be obtained.

Algorithm development in determinant QMC currently focusses on applications to DMFT, where the Hubbard–Stratonovich field is allowed to fluctuate only in imaginary time. A number of questions are being actively explored in this field: How does one incorporate more complex (e.g. Hund’s rules) interactions into simulation which include multiple orbitals? Can one re-introduce some degree of spatial fluctuations?

APPENDIX D: SUPPLEMENTARY MATERIAL

Particle-Hole Symmetry

The Hubbard Hamiltonian has a fascinating ‘particle-hole’ symmetry which allows us to relate its properties for different values of the parameters. Particle-Hole symmetry also plays an important role in quantum monte carlo simulations. Consider the introduction of new operators which exchange the role of creation and destruction:

$$d_{i\sigma}^\dagger = (-1)^i c_{i\sigma} \quad (124)$$

The meaning of the $(-1)^i$ will be explained further below.

Exercise D1: Verify that the number operator for the d particles equals one minus the number operator for c particles: $d_{i\sigma}^\dagger d_{i\sigma} = 1 - c_{i\sigma}^\dagger c_{i\sigma}$. What happens to the interaction term in the Hubbard model $U(n_\uparrow - \frac{1}{2})(n_\downarrow - \frac{1}{2})$ under the particle-hole transformation?

Before seeing what happens to the kinetic energy term under a particle-hole transformation, one can introduce the idea of a bipartite lattice. A bipartite lattice is one which can be divided into two sublattices A and B in such a way that a site in A has neighbors which are all members of B and *vice-versa*. The $(-1)^i$ factor in the particle-hole transformation takes the value -1 on one sublattice and $+1$ on the other.

Exercise D2: Is a one dimensional chain a bipartite lattice? How about a two-dimensional square lattice?

Exercise D3: Is the triangular lattice bipartite? What about the honeycomb lattice?

The following Exercise determines what happens to the kinetic energy term when the particle-hole transformation is performed.

Exercise D4: Verify that the kinetic energy is unchanged under a particle-hole transformation. That is, it takes exactly the same form in terms of the d operators as it did in terms of the c operators. Where does the bipartite nature of the lattice come enter? What role do the $(-1)^i$ factors play?

What has been learned? The exercises above tell us that the Hubbard model, when the interaction term is written in the particle-hole symmetric form, is invariant under particle-hole transformations when $\mu = 0$. The condition $\mu = 0$ is necessary since the number operators which μ multiplies are not invariant but go into one minus themselves. Actually, a more precise statement is that the Hubbard model with a given μ maps into the Hubbard model with the sign of the chemical potential reversed, that is, with μ replaced by $-\mu$. In fact, this implies that the whole phase diagram of the Hubbard model on a bipartite lattice is symmetric about half-filling, as the following Exercises suggest.

Exercise D5: Show that the density of the Hubbard model on a bipartite lattice obeys the relation $\rho(\mu) = 2 - \rho(-\mu)$ by starting with $\rho = \langle n_\uparrow + n_\downarrow \rangle$ and making a particle-hole transformation.

Exercise D6: Show that the local moment of the Hubbard model on a bipartite lattice obeys the relation $\langle m^2 \rangle(\mu) = \langle m^2 \rangle(-\mu)$.

Exercise D7: Look back at you pictures of the density of states $N(E)$ obtained in the Exercises and explain their behavior when reflected about $E = 0$ in terms of particle-hole symmetry.

Relation between the Attractive and Repulsive Hubbard Models

It is also interesting to consider what happens when a particle-hole transformation is performed only on one of the spin species.

Exercise D8: Show that under the transformation,

$$d_{i\uparrow} = c_{i\uparrow} \quad d_{i\downarrow} = (-1)^i c_{i\downarrow}^\dagger$$

the sign of the interaction term reverses, while the kinetic energy remains unchanged.

The Hubbard model with $-U$ is called the attractive Hubbard model because a negative value of U represents an attraction between spin up and spin down electrons on the same site. By considering various operators one can show that magnetic order in the $+U$ Hubbard model is related to superconducting and charge order in the $-U$ Hubbard

model, so that an understanding of the phases of one model immediately implies considerable information about the other.

Exercise D9: Show that under a particle-hole transformation of just the down spin species, the following operator mappings occur. (Ignore constants.)

$$\begin{aligned}
 m_{z,i} &= n_{i\uparrow} - n_{i\downarrow} \leftrightarrow n_i = n_{i\uparrow} + n_{i\downarrow} \\
 m_{+,i} &= c_{i\uparrow}^\dagger c_{i\downarrow} \leftrightarrow c_{i\uparrow}^\dagger c_{i\downarrow}^\dagger \\
 m_{-,i} &= c_{i\downarrow}^\dagger c_{i\uparrow} \leftrightarrow c_{i\downarrow} c_{i\uparrow}
 \end{aligned}$$

The physical content of these results is that spin correlations along the z axis are interchanged with charge correlations, and spin correlations along the x and y axes (which are combinations of m_+ and m_-) are interchanged with pairing correlations.

Alternates to Determinant QMC

A discussion of the path integral formulation of quantum mechanics, starting with the harmonic oscillator and then moving to quantum spins, bosons, and fermions, with an emphasis on Quantum Monte Carlo, can be found at: <http://leopard.ucdavis.edu/rts/resproj6.html> by hitting the 'World-Line Quantum Monte Carlo' link (number 88). A shorter discussion which starts immediately with the Heisenberg model can be found at:

<http://leopard.ucdavis.edu/rts/boulder.html> by hitting the 'Lecture II (pdf file) link.

One of the reasons for the continued interest in the Hubbard model is because of a recently developed approach known as 'dynamical mean field theory' (DMFT). This new technique has allowed for very interesting solutions of the Hubbard model itself, and also, more importantly, has provided a framework for the inclusion of Hubbard-type interactions into density functional theory. A 'popular' introduction to DMFT is available in: while a much more complete technical review is in: "Strongly Correlated Materials: Insights From Dynamical Mean-Field Theory," Physics Today, March, 2004. A. Georges, G. Kotliar, W. Krauth, and M. Rozenberg, Rev. Mod. Phys. **68**, 13 (1996).

TUTORIAL ONE

On the machines in the computer laboratory, you will find three fortran codes:

hubvietri.f (determinant QMC code for $d = 2$ square lattice Hubbard model)
 ueq0vietri.f (analytic solution of $U = 0$ Hubbard model, $d = 2$ square lattice)
 teq0vietri.f (analytic solution of $t = 0$ Hubbard model)

I apologize that the codes are not very user-friendly and readable (eg well commented). You will also find one input file:

hubvietri.in (input for determinant QMC code)

The inputs for the other codes are simple enough just to enter while you run. The input file hubvietri.in contains comments explaining what all the parameters that you need to know about are. There are other parameters having to do with numerical stability that you should just leave alone. Two important notes: First, the name of the file which holds the output is specified as a character string in the input file (as is explained there). Second, the lattice sizes, both the linear spatial size n and the number of imaginary time slices l which determines β via $\beta = l\Delta\tau$ are set in parameter statements in the fortran code hubvietri.f. That is, they are *not* inputs. Note that when you change the settings for n and l you must change them globally. (They appear 31 times in the code!) An editor with a global replace feature is useful here. (This is one of the ways the code is not user friendly. At some point I will rewrite it so n and l are set globally at one location only.)

To compile the code

```
ifort hubvietri.f
```

(You might want to explore if ifort has any optimization switches.)

To run the code

```
a.out < hubvietri.in
```

Some information on the progress of the run will come to the screen. Specifically, every 10 sweeps through the lattice you will be told the acceptance rate for the Monte Carlo moves (should be around 0.5) and the "redo ratio" (should be small, like 0.0001). If you don't want this on your screen, use

```
a.out < hubvietri.in > outjunk
```

TO DO:

Your job is to verify the QMC code and the analytic codes agree.

For example, setting $n = 6, t = 0, U = 4, \mu = 1$ and $\Delta\tau = 0.125, l = 4$ so that $\beta = l\Delta\tau = 0.5$, I found that the QMC code run with $n_{\text{warm}}=500$ and $n_{\text{pass}}=5000$ gave: $\langle n_{\uparrow} \rangle = 0.5695 \pm 0.0009$ and $\langle n_{\downarrow} \rangle = 0.5659 \pm 0.0008$. The analytic answer is 0.56775. Likewise, for the QMC, $\langle n_{\uparrow} n_{\downarrow} \rangle = 0.2143 \pm 0.0002$, with an analytic answer 0.21435. Of course, since $t = 0$, the code should give the same answer (to within error bars) for all n . When $n = 6$ it was just running 36 single site simulations in parallel.

Similarly, setting $n = 6, t = 1, U = 0, \mu = -1$ and $\Delta\tau = 0.125, l = 4$ so that $\beta = l\Delta\tau = 0.5$, I found that the QMC code run with $n_{\text{warm}}=10$ and $n_{\text{pass}}=100$ gave: $\langle n_{\uparrow} \rangle = \langle n_{\downarrow} \rangle = 0.39906 \pm 0.00000$. The analytic answer is $\langle n_{\downarrow} \rangle = 0.39903$. Comments: (1) The QMC code should give the *exact* answers whenever $U = 0$ since it traces over the fermions analytically and there is no coupling to the Hubbard-Stratonovich field. That's why one could do such a short run ($n_{\text{warm}}=10, n_{\text{pass}}=100$.) The reason one does not just set $n_{\text{pass}}=1$, which should work in principle, is the way the code generates error bars. It assumes a certain minimal number of samples are taken. (2) The small disagreement between the codes is due to the Trotter error in the checkerboard breakup of the kinetic energy. (3) You will need to multiply the energy written by ueq0vietri.f by two, because it does a single spin species.

Exercise 1:

What do hubvietri.f and ueq0vietri.f give for the Green's function?

Exercise 2:

Can you show that when you reduce $\Delta\tau$ (at fixed β) that the agreement between the two codes becomes perfect? The Trotter errors associated with the checkerboard breakup can thus be eliminated.

Exercise 3:

Show (numerically) that for the special case of a 4x4 lattice there are no Trotter errors with the checkerboard breakup. That is, verify that the two codes agree perfectly in this case. Can you prove the result analytically?

Exercise 4:

Check that the results in hubvietri.f for $G(0, 1)$ are consistent with the results reported by the code for the kinetic energy. Although you do this check here at $U = 0$, the relation you will derive is perfectly general (true for any t, U, μ, β).

TUTORIAL ONE SOLUTIONS

Exercise 1:

What do hubvietri.f and ueq0vietri.f give for the Green's function?

| | |
|--------------|-------------------|
| hubvietri.f | $G(0,1)=-0.10272$ |
| ueq0vietri.f | $G(0,1)=-0.10246$ |
| hubvietri.f | $G(0,2)=-0.00410$ |
| ueq0vietri.f | $G(0,2)=-0.00411$ |

Exercise 2:

Can you show that when you reduce $\Delta\tau$ (at fixed β) that the agreement between the two codes becomes perfect? The Trotter errors associated with the checkerboard breakup can thus be eliminated.

| | |
|--|----------------------|
| hubvietri.f $L = 4, \Delta\tau = 0.12500$ | $G(0, 1) = -0.10272$ |
| hubvietri.f $L = 8, \Delta\tau = 0.06250$ | $G(0, 1) = -0.10252$ |
| hubvietri.f $L = 16, \Delta\tau = 0.03125$ | $G(0, 1) = -0.10247$ |
| teq0vietri.f | $G(0, 1) = -0.10246$ |

Exercise 3:

Show (numerically) that for the special case of a 4x4 lattice there are no Trotter errors with the checkerboard breakup. That is, verify that the two codes agree perfectly in this case. Can you prove the result analytically?

For a 4x4 lattice with $t = 1, U = 0, \mu = -1$ I find

| | |
|---|----------------------|
| hubvietri.f $L = 4, \Delta\tau = 0.12500$ | $G(0, 1) = -0.10136$ |
| hubvietri.f $L = 8, \Delta\tau = 0.06250$ | $G(0, 1) = -0.10136$ |

hubvietri.f $L = 16, \Delta\tau = 0.03125$
teq0vietri.f

$$G(0, 1) = -0.10136$$
$$G(0, 1) = -0.10136$$

I will leave the analytic proof of the vanishing to you. I suspect it might be related to the fact that the 4x4 lattice is topologically equivalent to the 2x2x2x2 lattice ($n=2$ hypercube in 4 dimensions). See also Tutorial 2 Solutions.

Exercise 4:

Check that the results in hubvietri.f for $G(0, 1)$ are consistent with the results reported by the code for the kinetic energy. The code reports $G(0, 1) = -0.10272$ and the kinetic energy as $KE = -0.82172$. The Green's function $\langle c_i c_j^\dagger \rangle$ contains only one of the two Hermitian conjugate terms in the kinetic energy. There are also two spatial directions (x, y) in the kinetic energy. Finally, there are two spin species. Thus one must multiply the near-neighbor Greens function by 8 to bring it into agreement with the kinetic energy. This relation is satisfied.

TUTORIAL TWO

Exercise 1:

Look for antiferromagnetism in the half-filled Hubbard model. Use $n = 4$ (a 4x4 lattice), $t = 1, U = 4, \mu = 0$, and $\Delta\tau = 0.125$. Run with $l = 4, 8, 16, 32, 48, 64$ so that so that $\beta = l\Delta\tau = 0.5, 1, 2, 4, 6, 8$. Use $n_{\text{warm}}=500$ and $n_{\text{pass}}=5000$. Look at the values for

zz Spin correlation function
xx Spin correlation function

The integers in the first two columns are the x and y separations between the two spins in the correlation function.

Questions:

- [1] Why are only six values listed? Aren't there 16 possible separations?
- [2] Is the pattern of signs in your low T data consistent with antiferromagnetism?
- [3] Why is the $(0,0)$ correlation function enhanced over its $T = \infty$ value of 0.500 even at the highest temperatures, $T = 2$ ($\beta = 0.5$) while the other separations only start to build up at much lower T ?
- [4] It looks like the correlation functions for $(0,2)$ and $(1,1)$ separations are the same to within error bars. Yet these are not the same separation in space. Or are they?!

Exercise 2:

If the computers are fast enough, try to redo Exercise 1 with $n = 6$ (a 6x6 lattice).

- [1] If you compare spin correlations at the same separation and same temperature for different lattice sizes, what happens? Why?

Exercise 3:

Look for the Mott plateau and encounter the sign problem! Use $n = 4$ (a 4x4 lattice), $t = 1, U = 4$, and $\Delta\tau = 0.125$. Run with $l = 32, 48, 64$ so that so that $\beta = l\Delta\tau = 4, 6, 8$. Sweep chemical potential $\mu = 0.0, -0.2, -0.4, -0.6, -0.8, -1.0, -1.2, -1.4$ for each l . Use $n_{\text{warm}}=500$ and $n_{\text{pass}}=5000$.

- [1] Why don't you need to get data at $\mu > 0$? Did you really need to run $\mu = 0$?
- [2] Make a plot of density versus μ for each β . Do you see a Mott plateau?
- [3] Make a plot of the error bars in the density as a function of the density. Also make a plot of the average sign versus density. Do these help you understand my claim that $\beta \approx 6$ is the temperature limit in these simulations?
- [4] It looks like some sort of plateau might also be developing around $\rho = 0.6$. Do you have any idea where that might come from?

TUTORIAL TWO SOLUTIONS

Exercise 1:

- [1] Why are only six values listed? Aren't there 16 possible separations?
On a 4x4 lattice with periodic boundary conditions, there are only six inequivalent lattice separations. The separations $(0,1)$ and $(1,0)$ are obviously equal by the x/y symmetry of the lattice. The separations $(0,3)$ and $(0,1)$ are equivalent through use of the periodic boundary conditions. One thus has to report correlation functions only for a small "wedge" of possible separations. The same is true in momentum space. The code automatically averages over the equivalent separations, just as it averages over the initial point j in any correlation function $\langle A(j+l)A(j) \rangle$.
- [2] Is the pattern of signs in your low T data consistent with antiferromagnetism?

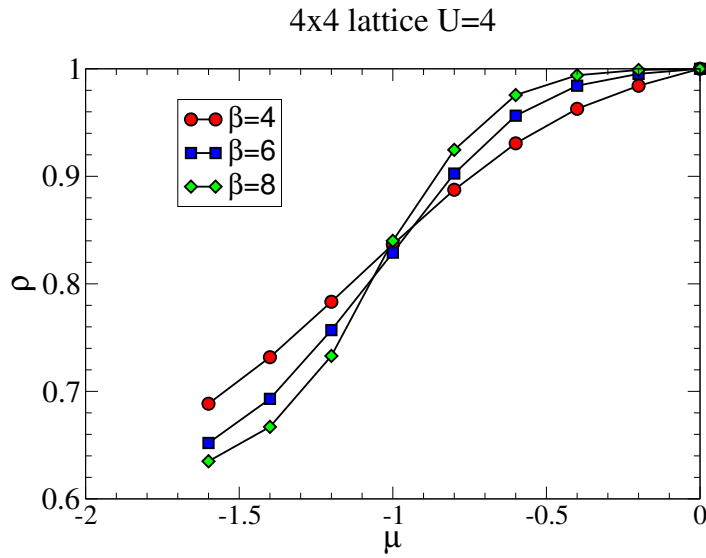


FIGURE 44. Density ρ vs chemical potential μ . As the temperature is lowered, the curve becomes increasingly flat near $\mu = 0, \rho = 1$.

You should find the spin correlations are negative for separations (0,1), (2,1) and positive for separations (0,0), (0,2), (1,1), and (2,2). It is easy to see that in the former case the spins are on different sublattices, while in the latter case they are on the same sublattice. Thus the signs are indeed consistent with AF order.

[3] Why is the (0,0) correlation function enhanced over its $T = \infty$ value of 0.500 even at the highest temperatures, $T = 2$ ($\beta = 0.5$) while the other separations only start to build up at much lower T ?

The (0,0) correlation function is the local moment, the correlation of a spin with itself. The energy scale of moment formation is the repulsion U , which suppresses double occupancy. On the other hand, the energy scale for spin order is $J = 4t^2/U$, a factor of four smaller.

[4] It looks like the correlation functions for (0,2) and (1,1) separations are the same to within error bars. Yet these are not the same separation in space. Or are they?!

This is not a coincidence. If you draw the lattice connections of a 4x4 square lattice with periodic boundary conditions, and those of a 2x2x2x2 (four dimensional hypercube of linear dimension 2 sites), you can see that all the lattice connections are equivalent. On the 2x2x2x2 hypercube you can see that the (0,2) and (1,1) separations on the 4x4 lattice are identical. (This especially high levels of artificial symmetry is a danger in interpreting data on 4x4 lattices.)

Exercise 2:

[1] If you compare spin correlations at the same separation and same temperature for different lattice sizes, what happens? Why?

The spin correlations on the smaller lattice are larger, when all other parameters are held fixed. The reason is that on small lattices the periodic boundary conditions provide additional paths connecting sites, enhancing their correlations. I am not sure of this, but perhaps in a frustrated system things could be different. For example if you ran the code on a 3x3 lattice with periodic boundary conditions, spin correlations might be reduced over those of larger lattices.

Exercise 3:

[1] Why don't you need to get data at $\mu > 0$? Did you really need to run $\mu = 0$?

From particle-hole symmetry it is clear that $\langle n \rangle(\mu) = 2 - \langle n \rangle(-\mu)$. This immediately also tells us that $\langle n \rangle(\mu = 0) = 1$, so it is not necessary to run that value.

[2] Make a plot of density versus μ for each β . Do you see a Mott plateau?

See attached figure and caption.

[3] Make a plot of the error bars in the density as a function of the density. Also make a plot of the average sign versus density. Do these help you understand my claim that $\beta \approx 6$ is the temperature limit in these simulations?

See attached figure and caption.

[4] It looks like some sort of plateau might also be developing around $\rho = 0.6$. Do you have any idea where that might come from?

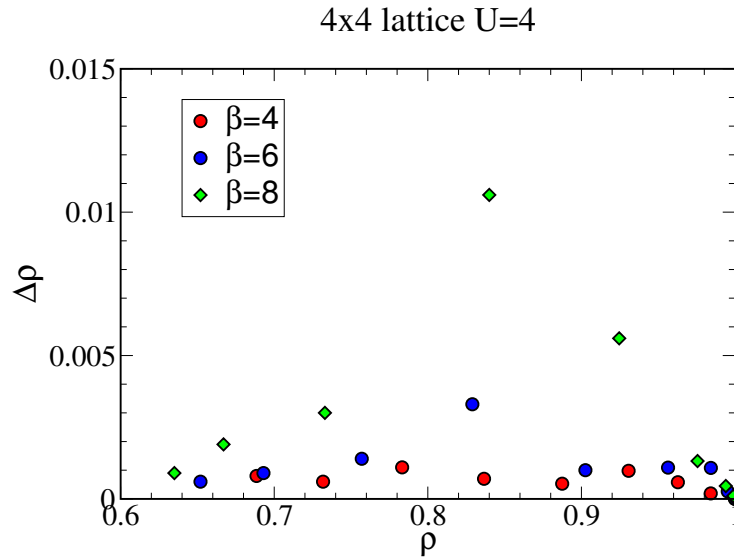


FIGURE 45. Error bars in the density as a function of the density for different temperatures. For $\beta = 8$ the error bar in the density is almost 2 percent of the density. While we can reduce the error bars by running longer (four times as long for a factor of two reduction in error bars), we also find the error bars at fixed run length grow exponentially with β . The origin is the sign problem. (See next plot.)

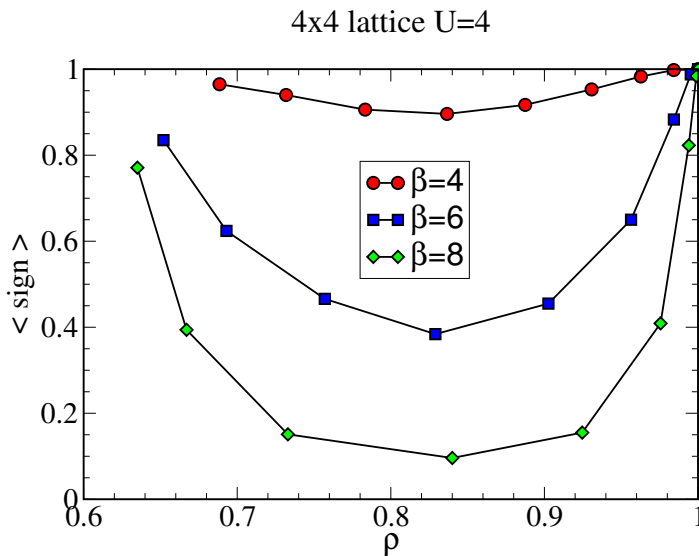


FIGURE 46. The average sign as a function of density for different inverse temperatures β . The sign begins to become quite small between $\beta = 6$ and $\beta = 8$.

This is a finite size effect. $\rho = 0.625$ is a special ‘shell’ filling. As the $U = 0$ Fermi surface expands from the origin, it encounters four new k points at $(\pm\pi/2, 0)$ and $(0, \pm\pi/2)$, and the filling jumps from $2/16$ (just the $k = (0, 0)$ point occupied by the two spin species) to $10/16 = 0.625$. $U = 4$ is not sufficiently strong coupling to wipe out this vestige of the discrete k points. Obviously as the lattice size increases, such effects become less evident. However, there is an important lesson here: weak couplings are often more subject to finite size effects than stronger ones.

TUTORIAL THREE

Computational:

Exercise 1:

Tutorial 2 demonstrated evidence for AF spin correlations in the half-filled Hubbard model. Here the goal is to use simple finite size scaling, to demonstrate that there is in fact *long range* AF order. [WARNING: Trying to get this data in just a one hour training section doesn't enable us to do a very good job. The error bars on the data will be a bit too big, and the largest lattice size will be 8x8. However, if you are willing to run for a couple of days (eg after you return home), you can both beat the error bars down and also do 10x10 and even 12x12 lattices.]

Run `hubvietri.f` for $t = 1, U = 4, \mu = 0, \beta = 8$, using ($L = 64$ and $\Delta\tau = 0.125$). Run length should be `nwarm=500` and `npass=5000`. Do $n = 4, 6, 8$ (lattices 4x4, 6x6, and 8x8). The 8x8 lattice took 45 minutes on my laptop to complete. Record the spin-spin correlations at maximal separation, ie the last value $(n/2, n/2)$ listed in

```
zz Spin correlation function
xx Spin correlation function
```

Average these two values. Also get the AF structure factors. They are called 'AF correlation function(xx)' and 'AF correlation function(zz)'. (These are not good names! One should label them the 'structure factor'!) Average them, and also divide by the volume n^2 . Plot these two averaged quantities versus $1/n$.

[1] Are the extrapolations to $1/n = 0$ (that is, $n = \infty$) nonzero?

[2] Do the extrapolations agree?

[3] Again, the data will not be so great. I suggest if you are serious, try running the code with `npass=20000` and also do 10x10 and 12x12 lattices. Actually, because the code can get stuck with the spin order in a particular direction, it is best to run `npass=5000` with ten or so random number seeds and average the results.

Analytic:

Try some of the analytic exercises in the notes and the morning meetings. E.g.

Exercise 1:

[1] Get the dispersion relation $E(k)$ for the triangular lattice Hubbard model at $U = 0$. Does it have a van-Hove singularity? Is it symmetric about $E = 0$?

Exercise 2:

Compute $A(\omega)$ for the $t = 0$ Hubbard model $H = U(n_{\uparrow} - \frac{1}{2})(n_{\downarrow} - \frac{1}{2}) + \epsilon(n_{\uparrow} + n_{\downarrow})$

Exercise 3:

Get the density of states for the honeycomb lattice and show it is a semi-metal.

Exercise 4:

Solve the four site $J_1 - J_2$ Heisenberg Hamiltonian. Show you get a level crossing.

Exercise 5:

Work out the Hubbard-Stratonovich transformation for the $U < 0$ Hubbard model. Why is there no sign problem in determinant QMC simulations?

...etc...

Note on Bibliography: This list of references is not intended to acknowledge all the papers in the field. Rather it is somewhat idiosyncratic, reflecting mainly papers that connected directly to the material of section V. These papers themselves contain a more formal and complete review of the literature for those who desire it.

REFERENCES

1. "Monte Carlo calculations of coupled boson-fermion systems. I," R. Blankenbecler, D.J. Scalapino, and R.L. Sugar, Phys. Rev. **D24**, 2278 (1981).
2. "Disordered Electronic Systems," P.A. Lee and T.V. Ramakrishnan, Rev. Mod. Phys, **57**, 287 (1985); "The Anderson-Mott transition," D. Belitz and T.R. Kirkpatrick, Rev. Mod. Phys, **66**, 261 (1994).

3. "Metallic behavior and related phenomena in two dimensions," E. Abrahams, S. V. Kravchenko, and M. P. Sarachik, *Rev. Mod. Phys.* **73**, 251 (2001); "Metal-insulator transition in two dimensional electron systems," S.V. Kravchenko and M.P. Sarachik, *Rep. Prog. Phys.* **67**, 1 (2004).
4. "Lecture Notes on Electron Correlation and Magnetism," P. Fazekas, World Scientific Series in Modern Condensed Matter Physics, Vol. 5, (1999).
5. E.Y. Loh, Jr., J.E. Gubernatis, D.J. Scalapino, R.L. Sugar, S.R. White, and R.T. Scalettar, in *Interacting Electrons in Reduced Dimensions*, ed. by D. Baeriswyl and D.K. Campbell, Plenum, New York (1989).
6. "A Numerical Study of the Two-D Hubbard Model with Repulsive Coulomb Interaction," S.R. White, D.J. Scalapino, R.L. Sugar, E.Y. Loh, Jr., J.E. Gubernatis, and R.T. Scalettar, *Phys. Rev.* **B40**, 506 (1989).
7. E.Y. Loh, Jr. and J.E. Gubernatis, in *Electronic Phase Transitions*, ed. by W. Hanke and Yu. V. Kopaev, North-Holland, Amsterdam (1992).
8. www.ccmr.cornell.edu/~cyrus/book/muramatsu.ps.gz (This includes also a discussion of the 'world-line' method for the Hubbard Hamiltonian.)
9. "Scaling Theory of Localization– Absence of Quantum Diffusion in 2 Dimensions," E. Abrahams, P.W. Anderson, D.C. Licciardello, and T.V. Ramakrishnan, *Phys. Rev. Lett.* **42**, 673 (1979).
10. "Inverse participation ratio in 2+ epsilon dimensions," F. Wegner, *Z. Phys.* **B 36**, 209 (1980).
11. "Interaction between diffusion modes in localization theory," *Zh. Eksp. Teor. Fiz.* **79**, 1120 (1980). K.B. Efetov, A.I. Larkin, and D.E. Khmel'nitskii, *Sov. Phys. JETP* **52**, 568 (1980).
12. "Disordered Electronic Systems," P.A. Lee and T.V. Ramakrishnan, *Rev. Mod. Phys.* **57**, 287 (1985).
13. "Weak localization and Coulomb interaction in disordered systems," A.M. Finkelstein, *Zeit. fur Physik* **B56** 189 (1984).
14. "Interaction-driven metal-insulator transitions in disordered fermion systems," C. Castellani, C. Di Castro, P. A. Lee, and M. Ma, *Phys. Rev. B* **30**, 527 (1984).
15. "The Anderson-Mott transition," D. Belitz and T. R. Kirkpatrick, *Rev. Mod. Phys.* **66**, 261 (1994).
16. "Possible metal-insulator transition at B=0 in two dimensions," S. V. Kravchenko, G. V. Kravchenko, J. E. Furneaux, V. M. Pudalov, and M. D'Iorio, *Phys. Rev. B* **50**, 8039 (1994).
17. "Scaling of an anomalous metal-insulator transition in a two-dimensional system in silicon at B=0," S. V. Kravchenko, W. E. Mason, G. E. Bowker, J. E. Furneaux, V. M. Pudalov, and M. D'Iorio, *Phys. Rev. B* **51**, 7038 (1995).
18. "Electric Field Scaling at a B = 0 Metal-Insulator Transition in Two Dimensions," S. V. Kravchenko, D. Simonian, M. P. Sarachik, W. Mason, and J. E. Furneaux, *Phys. Rev. Lett.* **77**, 4938 (1996).
19. "Metal-Insulator Transition in Two Dimensions: Effects of Disorder and Magnetic Field," D. Popović, A. B. Fowler, and S. Washburn, *Phys. Rev. Lett.* **79**, 1543 (1997).
20. "Reflection symmetry at a B=0 metal-insulator transition in two dimensions," D. Simonian, S. V. Kravchenko, and M. P. Sarachik, *Phys. Rev. B* **55**, R13421 (1997).
21. "The Metallic-like Conductivity of a Two-Dimensional Hole System," Y. Hanien, U. Meirav, D. Shahar, C. C. Li, D. C. Tsui, and Hadas Shtrikman, *Phys. Rev. Lett.* **80**, 1288 (1998).
22. "Metal-Insulator Transition at B = 0 in a Dilute Two Dimensional GaAs-AlGaAs Hole Gas," M. Y. Simmons, A. R. Hamilton, M. Pepper, E. H. Linfield, P. D. Rose, D. A. Ritchie, A. K. Savchenko and T. G. Griffiths, *Phys. Rev. Lett.* **80**, 1292 (1998).
23. "Scaling Theory of Two-Dimensional Metal-Insulator Transitions," V. Dobrosavljević, E. Abrahams, E. Miranda, and S. Chakravarty, *Phys. Rev. Lett.* **79**, 455 (1997).
24. "Metallic phase and metal-insulator transition in two-dimensional electronic systems," C. Castellani, C. Di Castro, and P. A. Lee, *Phys. Rev. B* **57**, R9381 (1998).
25. "Interactions and scaling in a disordered two-dimensional metal," S. Chakravarty, L. Yin, and E. Abrahams, *Phys. Rev. B* **58**, R559 (1998).
26. "Wigner glass, spin liquids and the metal-insulator transition," S. Chakravarty, S. Kivelson, C. Nayak, and K. Voelker, *Phil. Mag.* **B79**, 859 (1999).
27. "Superconductivity in a two-dimensional electron gas," P. Phillips, Y. Wan, I. Martin, S. Knysh, and D. Dalidovich, *Nature* **395**, 253 (1998).
28. "Possible triplet superconductivity in MOSFETs," D. Belitz and T. R. Kirkpatrick, *Phys. Rev. B* **58**, 8214 (1998).
29. "Theory of Metal-Insulator Transitions in Gated Semiconductors," B. L. Altshuler and D. Maslov, *Phys. Rev. Lett.* **82**, 145 (1999).
30. "A few electrons per ion scenario for the B=0 metal-insulator transition in two dimensions," T. M. Klapwijk and S. Das Sarma, *Solid State Comm.* **110**, 581 (1999).
31. "Coherent Propagation of Two Interacting Particles in a Random Potential," D. L. Shepelyansky, *Phys. Rev. Lett.* **73**, 2607 (1994).
32. "Do Interactions Increase or Reduce the Conductance of Disordered Electrons? It Depends!," T. Vojta, F. Epperlein, and M. Schreiber, *Phys. Rev. Lett.* **81**, 4212 (1998); "Delocalized Coulomb phase in two dimensions," X. Waintal, G. Benenti, and J.-L. Pichard, *Europhys. Lett.* **49**, 466 (2000).
33. "Consistent description of high-Tc superconductors with the three-band Hubbard model," G. Dopf, A. Muramatsu, and W. Hanke, *Phys. Rev. Lett.* **68**, 353 (1992).
34. "Two-dimensional Hubbard model-metal insulator transition studied by Monte Carlo calculation," N. Furukawa and M. Imada, *J. Phys. Soc. Japan* **61**, 3331 (1992).
35. "Numerical simulation of the 1D and 2D Hubbard models: Fermi liquid behavior and its breakdown," S. Sorella, E. Tosatti, S. Baroni, R. Car, and M. Parinello, *Int. J. Mod. Phys.* **B1**, 993 (1988).

36. "Two Dimensional Hubbard Model: Numerical Simulation Study," J.E. Hirsch, Phys. Rev. **B31**, 4403 (1985).
37. "Boson Localization and the Superfluid–Insulator Transition," M.P.A. Fisher, P.B. Weichman, G. Grinstein, and D.S. Fisher, Phys. Rev. **B40**, 546 (1989).
38. "Onset of superconductivity in the two-dimensional limit," D.B. Haviland, Y.Liu, and A.M. Goldman, Phys. Rev. Lett. **62** 2180, (1989).
39. "Tunneling Study of Superconductivity near the Metal-Insulator Transition," R.C. Dynes *et al*, Phys. Rev. Lett. **53**, 2437 (1984); "Destruction of Superconductivity in Quenched Condensed Two Dimensional Films," A.E. White, R.C. Dynes, and J.P. Garno, Phys. Rev. **B33**, 3549 (1986).
40. "Magnetic Field Tuned Superconductor–Insulator Transition in Two Dimensional Films," A.F. Hebard and M.A. Paalanen, Phys. Rev. Lett. **65**, 927 (1990); and "Global phase coherence in two-dimensional granular superconductors," B.G. Orr, H.M. Jaeger, A.M. Goldman and C.G. Kuper, Phys. Rev. Lett. **56**, 378 (1986).
41. "Electron tunneling determination of the order-parameter amplitude at the superconductor-insulator transition in 2D," J.M. Valles, R.C. Dynes, and J.P. Garno, Phys. Rev. Lett. **69**, 3567 (1992).
42. "Superconducting-insulating transition in two-dimensional a-MoGe thin films," A. Yazdani and A. Kapitulnik, Phys. Rev. Lett. **74**, 3037 (1995).
43. "Pairing and Spin Gap in the Normal State of Short Coherence Length Superconductors," M. Randeria, N. Trivedi, A. Moreo, and R.T. Scalettar, Phys. Rev. Lett. **69**, 2001 (1992).
44. "Superconductor–Insulator Transition in a Disordered Electronic System," N. Trivedi, R.T. Scalettar, and M. Randeria, Phys. Rev. **B54**, 3756 (1996).
45. "Localization: Theory and Experiment," B. Kramer and A. MacKinnon, Rep. Prog. Phys. **56**, 1469 (1993).
46. J. Tinka Gammel, D.K. Campbell, and E.Y. Loh, Jr., Synthetic Metals **57**, 4437 (1993).
47. C. Lin, F.H. Zong, and D.M. Ceperley, Phys. Rev. E **64**, 016702 (2001), and references cited therein.
48. "Localization Transitions in Non-Hermitian Quantum Mechanics", N. Hatano and D.R. Nelson, Phys. Rev. Lett. **77**, 570 (1996); "Vortex pinning and non-Hermitian quantum mechanics," Phys. Rev. B **56**, 8651 (1997).
49. "Statistics of complex levels of random matrices for decaying systems," F. Haake, F. Izrailev, N. Lehmann, D. Saher, and H.J. Sommers, Zeit. Phys. B **88**, 359 (1992).
50. "Spectrum of Large Random Asymmetric Matrices", H.J. Sommers, A. Crisanti, H. Sompolinsky, and Y. Stein, Phys. Rev. Lett. **60**, 1895 (1988).
51. "Random Matrix Model of QCD at Finite Density and the Nature of the Quenched Limit," M.A. Stephanov, Phys. Rev. Lett. **76**, 4472 (1996).
52. "Nonhermitian Random Matrix Models," R.A. Janik, M.A. Nowak, G. Papp, and I. Zahed, Nucl. Phys. B **501**, 603 (1997) and "Macroscopic Universality: Why QCD in Matter is Subtle," Phys. Rev. Lett. **77**, 4876 (1996).
53. "Two-level system with noise: Blue's function approach," E. Gudowska-Nowak, G. Papp and J. Brickmann, J. Chem. Phys. **220**, 125 (1997).
54. "Almost-Hermitian Random Matrices: Eigenvalue Density in the Complex Plane," Y.V. Fyodorov, B.A. Khoruzhenko and H.J. Sommers, Phys. Lett. A **226** 46 (1997).
55. "Fermion determinants in matrix models of QCD at nonzero chemical potential," M.A. Halasz, A.D. Jackson, and J.J.M. Verbaarschot, Phys. Rev. D **56**, 5140 (1997).
56. "Non-hermitian random matrix theory: Method of hermitian reduction," J. Feinberg and A. Zee, Nucl. Phys. B **504**, 579 (1997).
57. "Non-gaussian non-hermitian random matrix theory: Phase transition and addition formalism," J. Feinberg and A. Zee, Nucl. Phys. B **501**, 643 (1997).
58. B. Zickel, unpublished.
59. "Cold Bosonic Atoms in Optical Lattices," D. Jaksch, C. Bruder, J.I. Cirac, C.W. Gardiner, and P. Zoller, Phys. Rev. Lett. **81**, 3108 (1998).
60. "Phase diagram for ultracold bosons in optical lattices and superlattices," P. Buonsante and A. Vezzani, Phys. Rev. A **70**, 033608 (2004).
61. "Fractional-filling loophole insulator domains for ultracold bosons in optical superlattices," P. Buonsante, V. Penna, and A. Vezzani, Phys. Rev. A **70**, 061603 (2004).
62. "Cell strong-coupling perturbative approach to the phase diagram of ultracold bosons in optical superlattices," P. Buonsante, A. Vezzani, Phys. Rev. A **72**, 013614 (2005).
63. J.B. Sokoloff, Phys. Rep. **126**, 189 (1985).
64. Y. Last, Proc. of XIth Int. Congress of Math. Phys. 366, 1994); S. Jitomirskaya, *ibid*, 373.
65. "Cold Atom Optical Lattices as Quantum Analog Simulators for Aperiodic One-Dimensional Localization Without Disorder," V.W. Scarola and S. Das Sarma, Phys. Rev. **A73**, 041609(R) (2006).
66. N. Trefethen and M. Embree, "Spectra and Pseudospectra - the behavior of nonnormal matrices and operators", Princeton University Press.
67. "Exact study of the one-dimensional boson Hubbard model with a superlattice potential," V.G. Rousseau, D.P. Arovas, M. Rigol, F. Hébert, G.G. Batrouni, and R.T. Scalettar, Phys. Rev. **B73**, 174516 (2006).
68. "Constrained Path Quantum Monte Carlo Method for Fermion Ground States", S. Zhang, J. Carlson, and J. E. Gubernatis Phys. Rev. Lett. **74**, 3652 (1995); "Constrained path Monte Carlo method for fermion ground states", S. Zhang, J. Carlson, and J. E. Gubernatis Phys. Rev. B **55**, 7464 (1997).

69. "Dynamical mean-field theory of strongly correlated fermion systems and the limit of infinite dimensions," A. Georges, G. Kotliar, W. Krauth, and M. Rozenberg, *Rev. Mod. Phys.* **68**, 13 (1996).
70. "Investigation of correlated electron systems using the limit of high dimensions," D. Vollhardt, in *Correlated Electron Systems*, edited by V. J. Emery (World Scientific, Singapore) 57 (1993).
71. "Quantum Cluster Theories," Th. Maier, M. Jarrell, Th. Pruschke, and M. Hettler, *Rev. Mod. Phys.* **77**, 1027 (2005).
72. "Monte Carlo Method for Magnetic Impurities in Metals," J.E. Hirsch and R.M. Fye, *Phys. Rev. Lett.* **56**, 2521 (1986).
73. "Insulator, metal, or superconductor: The criteria," D. J. Scalapino, S. R. White, and S. C. Zhang, *Phys. Rev. B* **47**, 7995 (1993).
74. Consider lower temperatures and average over larger numbers of disorder realizations: for the higher temperatures generally 4 realizations are sufficient, for the lowest temperatures the fluctuations are larger and up to 20 (72) realizations are used for $U = 4$ ($U = 0$).
75. For a related enhancement of the superfluid density by interactions in a disordered Bose system, see "Superfluid-insulator transition in disordered boson systems," W. Krauth, N. Trivedi, and D. M. Ceperley, *Phys. Rev. Lett.* **67**, 2307 (1991).
76. For $\Delta = 1.2$ and $\beta = 5$, $\sigma_{dc} = 0.88(1), 0.76(1)$ for $U = 0, 4$, respectively. For $\Delta = 2.0$ and $\beta = 6$, $\sigma_{dc} = 0.45(2), 0.49(3), 0.52(4)$ for $U = 0, 2, 4$, respectively. Numbers between brackets represent the error bar in the last digit shown.
77. "Spin Dynamics of Nearly Localized Electrons," M. A. Paalanen, S. Sachdev, R. N. Bhatt, and A. E. Ruckenstein, *Phys. Rev. Lett.* **57**, 2061 (1986).
78. "Spin Degree of Freedom in a Two-Dimensional Electron Liquid," T. Okamoto, K. Hosoya, S. Kawaji, and A. Yagi, *Phys. Rev. Lett.* **82**, 3875 (1999).
79. "Parallel Magnetic Field Induced Transition in Transport in the Dilute Two-Dimensional Hole System in GaAs," J. Yoon, C. C. Li, D. Shahar, D. C. Tsui, and M. Shayegan, *Phys. Rev. Lett.* **84**, 4421 (2000).
80. "Metal-Insulator Transition in a 2D Electron Gas: Equivalence of Two Approaches for Determining the Critical Point," A. A. Shashkin, S. V. Kravchenko, and T. M. Klapwijk, *Phys. Rev. Lett.* **87**, 266402 (2000).
81. "Effects of a Parallel Magnetic Field on the Metal-Insulator Transition in a Dilute Two-Dimensional Electron System," K. V. Eng, X. G. Feng, D. Popović, and S. Washburn, *Phys. Rev. Lett.* **88**, 136402 (2002).
82. "Spin polarization and transition from metallic to insulating behavior in 2D systems," E. Tutuc, E. P. De Poortere, S. J. Papadakis, and M. Shayegan, *Physica E* **2-4**, 748 (2002).
83. "Magnetic Field Induced Spin Polarization of AlAs Two-dimensional Electrons," E. P. De Poortere, E. Tutuc, Y. P. Shkolnikov, K. Vakili, and M. Shayegan, *Phys. Rev.* **B66**, 161308 (2002).
84. "Ground-state properties of the two-dimensional disordered Hubbard model," G. Caldara, B. Srinivasan, and D. L. Shepelyansky, *Phys. Rev. B* **62**, 10680 (2000).
85. "Disorder and Interaction in 2D: Exact Diagonalization Study of the Anderson-Hubbard-Mott Model," R. Kotlyar and S. Das Sarma, *Phys. Rev. Lett.* **86**, 2388 (2001).
86. "Role of a parallel magnetic field upon a few correlated electrons trapped in 2d mesoscopic disordered clusters," F. Selva and J.-L. Pichard, *Europhys. Lett.* **55**, 518 (2001).
87. "Parallel magnetoconductance of interacting electrons in a two-dimensional disordered system," R. Berkovits and J. W. Kantelhardt, *Phys. Rev. B* **65**, 125308 (2002).
88. "The effect of parallel magnetic field on the Boltzmann conductivity and the Hall coefficient of a disordered two-dimensional Fermi liquid," I. F. Herbut, *Phys. Rev. B* **63**, 113102 (2001).
89. "Interaction corrections at intermediate temperatures: Magnetoresistance in a parallel field," G. Zala, B. N. Narozhny, and I. L. Aleiner, *Phys. Rev. B* **65**, 020201 (2002).
90. "Conducting phase in the two-dimensional disordered Hubbard model," P. J. H. Denteneer, R. T. Scalettar, and N. T. Trivedi, *Phys. Rev. Lett.* **83**, 4610 (1999).
91. This point of view of the effect of B_{\parallel} in the experiments is substantiated in: "Fate of the extended states in a vanishing magnetic field: The role of spins in strongly interacting two-dimensional electron systems," M. R. Sakr, M. Rahimi, and S. V. Kravchenko, *Phys. Rev. B* **65**, 041303 (2002).
92. "R.C. Magnetic field induced insulator to metal transition in amorphous-Gd_xSi_{1-x}," W. Teizer, F. Hellman, and R. C. Dynes, *Solid State Comm.* **114**, 81 (2000).
93. "The mobility edge problem: Continuous symmetry and a conjecture," F. J. Wegner, *Z. Phys. B* **35**, 207 (1979).
94. "Transport Properties and Density of States of Quantum Wires with Off-diagonal Disorder," P. W. Brouwer, C. Mudry, and A. Furusaki, *Physica E* **9**, 333 (2001).
95. "Quasiparticle localization in superconductors with spin-orbit scattering," T. Senthil and M. P. A. Fisher, *Phys. Rev. B* **61**, 9690 (2000).
96. "Localization and Delocalization in Dirty Superconducting Wires," P. W. Brouwer, A. Furusaki, I. A. Gruzberg, and C. Mudry, *Phys. Rev. Lett.* **85**, 1064 (2000), and cited references.
97. "Deviations from Fermi-Liquid Behavior above T_c in 2D Short Coherence Length Superconductors," N. Trivedi and M. Randeria, *Phys. Rev. Lett.* **75**, 312 (1995). As in the case of Equation 2, this expression for the density of states is valid at temperatures below characteristic frequency scales of structures in $N(\omega)$.
98. "Magnetic correlations in the two-dimensional Anderson-Hubbard model," M. Ulmke and R. T. Scalettar, *Phys. Rev. B* **55**, 4149 (1997), M. Ulmke, P. J. H. Denteneer, R. T. Scalettar, and G. T. Zimanyi, *Europhys. Lett.* **42**, 655 (1998).
99. One can verify that beyond a certain large site disorder ($\Delta_{\mu} \geq 4t$) σ_{dc} decreases again.
100. "Collapse of the charge gap in random Mott insulators," Y. Otsuka, Y. Morita, and Y. Hatsugai, *Phys. Rev. B* **58**, 15314 (1998).

101. "Can correlations drive a band insulator metallic?," A. Garg, H.R. Krishnamurthy, and M. Randeria, *Phys. Rev. Lett.* **97**, 046403 (2006).
102. "Model of the Neutral-Ionic Phase Transformation," J. Hubbard and J.B. Torrance, *Phys. Rev. Lett.* **47**, 1750 (1981); "Lattice Effect of Strong Electron Correlation: Implication for Ferroelectricity and Superconductivity," T. Egami, S. Ishihara and M. Tachiki, *Science* **261**, 130 (1994); "Macroscopic polarization as a geometric quantum phase: Many-body formulation," G. Ortiz and R. Martin, *Phys. Rev. B* **49**, 14202 (1994); "Many-Body Effects on Polarization and Dynamical Charges in a Partly Covalent Polar Insulator," R. Resta and S. Sorella, *Phys. Rev. Lett.* **74**, 4738 (1995) and "Electron Localization in the Insulating State," *Phys. Rev. Lett.* **82**, 370 (1999); "From Band Insulator to Mott Insulator in One Dimension," M. Fabrizio, A.O. Gogolin, and A.A. Nersisyan, *Phys. Rev. Lett.* **83**, 2014 (1999); "Quantum Monte Carlo study of the one-dimensional ionic Hubbard model," T. Wilkens and R.M. Martin, *Phys. Rev. B* **63**, 235108 (2001); and "Exact Bond Ordered Ground State for the Transition between the Band and the Mott Insulator," C.D. Batista and A.A. Aligia, *Phys. Rev. Lett.* **92**, 246405 (2004).
103. "Ferromagnetism and Metal-Insulator Transition in the Disordered Hubbard Model," K. Byczuk, M. Ulmke, and D. Vollhardt, *Phys. Rev. Lett.* **90**, 196403 (2003).
104. "Mott-Hubbard metal-insulator transition at noninteger filling," K. Byczuk, W. Hofstetter, and D. Vollhardt, *Phys. Rev. B* **69**, 045112 (2004).
105. "Anomalous normal-state properties of high- T_c superconductors: intrinsic properties of strongly correlated electron systems?," Th. Pruschke, M. Jarrell, and J.K. Freericks, *Adv. Phys.* **44**, 187 (1995).
106. There is one slightly confusing point here. From the description provided, one might think that in a Monte Carlo simulation one stores a vector p_i and applies T to it. This is completely impractical because the number of one configurations i of the system is incredibly huge and one could never allocate enough memory to hold p_i . Instead, generally only one configuration i at a time is stored, and T_{ji} gives us a probabilistic rule to get the (single) configuration j from i . The probability p_i appears through the average of all the single configurations over a long simulation.
107. "Computational Physics," R.H. Landau and M.J. Páez, Wiley, 1997.
108. "Computational Physics," N. Giordano, Prentice-Hall, 1997.
109. "Statistical Mechanics of Phase Transitions," J. Yeomans, Oxford, 1992.
110. "A statistical approach to quantum mechanics," M. Creutz and J. Freedman, *Annals of Phys.* **132**, 427 (1981).
111. See, <http://leopard.physics.ucdavis.edu/rts/nato.html> Sec. 3 of the article nato2.pdf.